Review

Iron as modifier of Pd and Pt-based catalysts for sustainable and green processes

Sofia Capelli [1], Stefano Cattaneo [1], Marta Stucchi [1], Alberto Villa [1], and Laura Prati [1,*]

[1] Università degli Studi di Milano; Chemistry Department, Via C. Golgi 19, 20133, Milan (Italy).

* Correspondence: laura.prati@unimi.it ; Tel.: +39- 02503-14357

Dedication:

Abstract: This review provides an overview of the synthetic methods used for the preparation of monometallic Pd and Pt metal nanoparticles (NPs) supported on iron oxide and bimetallic Pd-Fe and Pt-Fe systems. The use of iron as a support or as a modifier leads to a change in electronic density on the noble metal, which in turn affects the catalyst activity. In particular, when iron oxide is used as a support the noble metal tends to donate electrons to the support. On the contrary, bimetallic noble metal-Fe NPs show a charge transfer from iron to the noble metal. This behavior occurs both when iron is in contact or strictly closed to the noble metal NPs. The synthetic approach used for the synthesis influences the physico-chemical properties of the final material, thus a focus on the synthetic procedures and the catalyst characterization are provided to elucidate the key factors that influence the exceptional catalytic performances of these materials. Pd-Fe, Pt-Fe bimetallic NPs were selected as representative systems due to their broad use in heterogeneous oxidation and hydrogenation catalytic reactions.

Keywords: iron; palladium; platinum; gold; nanomaterials, bimetallic catalysts, heterogeneous catalysis, reduction, oxidation, material characterization

1. Introduction

Iron is the fourth most abundant element (5.63 %) in Earth's crust, after Oxygen (46.1 %), Silicon (28.2 %) and Aluminum (8.23 %)[1], and the second most abundant metal on our planet. Iron is mostly obtained from minerals called magnetite (Fe_3O_4) and hematite (Fe_2O_3), and in small amount from limonite ($FeO(OH)\cdot nH_2O$), siderite ($FeCO_3$), and taconite. The chemistry of iron has been exploited since 1500 B.C., when it was used to fabricate tools and weapons with a superior resistance than their bronze equivalents[2]. Subsequently, iron modification with silicon or carbon led to the synthesis of alloys (steel) with tunable properties[3]. Iron and steel are nowadays key components of buildings[4], machinery and automotive industries[5,6], and they are commonly used also in the construction of railways, roads and pipelines[7]. Furthermore, stainless steel is used to produce cutlery, watches, surgical instruments, jewelry and components of spacecraft and space stations.

Iron, has an important role in catalysis as well, although it has been traditionally eclipsed by other noble and transition metals. The two main industrial processes that use iron as catalytic material are the Haber-Bosch process[8] for the synthesis of ammonia and the Fischer-Tropsch process for the production of hydrocarbons from CO and H_2[9]. The Haber-Bosch process uses a K_2O or Al_2O_3-promoted iron catalyst which are prepared by reduction of high-purity magnetite[10]. On the other hand, the Fischer-Tropsch synthesis takes advantage of iron carbide as the active species[11], with the addition of promoters such as potassium and copper to increase the catalytic performance and stability[12][13]. These two well-known industrial processes are based on iron as bulk material; during the last 20 years, however, the use of iron as catalytic support or active metal (i.e. iron nanoparticles) supported on carbonaceous materials or metal oxides has attracted the attention of the scientific community. It is commonly known that hydrogenation[14–16] and oxidation[17–

19] reactions are facilitated by the presence of a noble metal-based catalysts. However, the high costs and the low availability of noble metals lead to the transition to available and environmentally friendly metals.

In this perspective iron can play a key role due to its unique physical-chemical properties. Iron has three different oxidation states (Fe^0, Fe^{II}, and Fe^{III}) and it is possible to modify the crystallinity, the oxidation state and its allotropic form by annealing processes[20–23] or during the synthesis itself[24–27]. Moreover, the magnetic properties of iron oxide make this material very suitable for catalysis due to its simple recovery after the use[28]. Many researchers studied the synthesis of iron-based nanomaterials for several applications, such as water treatment[29–31], biomedical applications[32–34], photocatalytic[35–37], electrochemical[38–40] and cross-coupling[41–43] reactions, pollutants degradation[38,44] and dehalogenation processes[45–47]. Figure 1 shows the VOSviewer[48,49] map visualization based on the Scopus research for the keyword "iron based material". VOSviewer software, based on co-occurrence, organizes the topic keywords into four main categories: magnetic properties (yellow), adsorption and waste-water treatment (red), iron alloy (green), and iron compounds in catalysis (blue). The size of the circles reveals the strength of the co-occurrence linking with other keywords. Iron based materials are used in a wide range of applications, but the research about their application in catalysis is still at the beginning, as can be inferred by Figure 1.

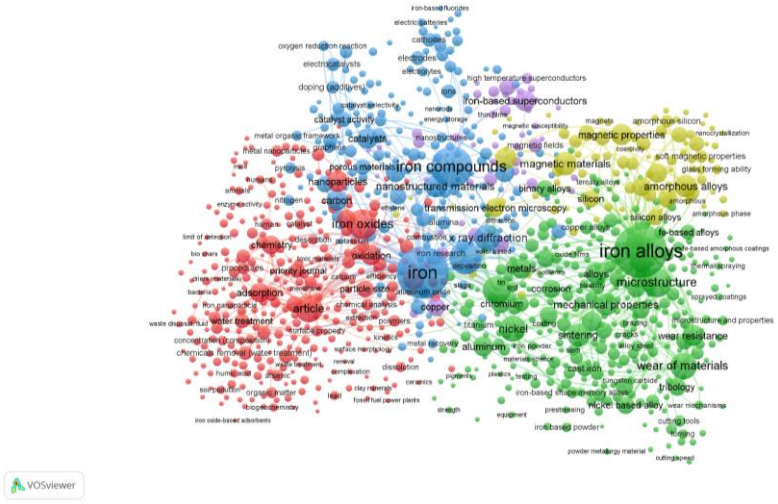

Figure 1. VOSviewer generated map for "Iron based material" Scopus research. Adsorption and waste-water treatment (red), catalytic applications (blue), magnetic properties (yellow), and iron alloy (green).

Iron can be used in heterogeneous catalysis as a support for its unique magnetic properties and the possibility to synthesize mesoporous or nano-scale supports in different oxidation states. Fe, in fact, has shown in the last few decades to be extremely versatile as a support for noble metal NPs (such as Pd and Pt) when present in one of its many oxidized ~~form~~forms (commonly referred as FeOx). Another way to implement the use of Fe into active catalysts is by adding Fe to the active noble metal (Pd and Pt) in a similar molar amount in order to create bimetallic systems that are mainly composed of M-Fe or M-FeOx entities (where M is either Pd or Pt) present as small NPs and supported on a wide range of materials such as metal oxides or carbonaceous materials.

The synthetic approaches used for the preparation of iron-based materials are different, from the classical impregnation and precipitation methods, to biosynthesis, continuous synthesis, microemulsion assisted

protocol, and strong adsorption method. These protocols allow to synthesize a broad range of iron/iron oxide NPs size and bimetallic iron-metal NPs in the form of alloy[50–54], core-shell[55–58], and more complicated structures[59,60]. The current literature studied the use of these materials for biomedical applications, for studying mechanical and magnetic properties, for adsorption and waste-water treatment, but recent reviews about the preparation methods and utilization of iron-based materials in heterogeneous catalysis are missing. Due to the increase of publications about this subject and the wide variety of the synthetic approaches, this review aims to summarize the methods used for the preparation of noble metal (specifically Pd and Pt) NPs supported on iron oxides (M/FeOx) materials and noble metal-iron supported bimetallic NPs (MFe/support) for heterogeneous catalytic applications, more specifically for hydrogenation and oxidation reactions. It should be pointed out that there is often a thin line dividing what is considered Fe as a support or as a co-active metal. For sake of clarity, in this review we consider Fe as a support when it is present in much larger amount compared to the active metal, and there is only minimal contact between the two entities (i.e. metal nanoparticles anchored on FeOx). On the other hand, we consider Fe as a co-active metal when present in similar molar amount compared to the active metal and intimately mixed with it, regardless of its oxidation state. For this reason, NPs consisting of an homogeneous mix of M and Fe in a zero valent oxidation state will be discussed along with NPs composed of a mixture of M and FeOx species. Moreover, since the different synthetic approaches influence the physical-chemical properties of the final catalysts, a wide description about the characterization results of the material will be provided in order to understand the role of the iron species in the modification of the noble metal electronic properties. Pd and Pt have been chosen as reference noble metal due to their wide use in heterogeneously catalyzed oxidation and hydrogenation reactions. Beyond these systems, Au-Fe catalysts can be used for heterogeneous catalytic reactions. In this case the iron does not modify the electronic properties of the gold, but it provides reactive oxygen species[61,62]. Since iron in Au-Fe system is not an electronic modifier, the discussion of these catalytic materials falls outside the scope of this review.

2. Synthesis, characterization and catalytic application of Pd-Fe and Pt-Fe systems

2.1. Pd-Fe systems

Pd supported NPs are excellent catalysts for the hydrogenation of the C=C double bond[63–67], therefore when a substrate possesses both C=O and C=C bonds, the selectivity towards the reduction of the carbonyl bond is often difficult[68–70]. For this reason, the use of specific catalytic materials able to decrease the activity of Pd and tune the selectivity towards the C=O hydrogenation is a matter of interest. The influence of iron oxide NPs on catalytic hydrogenation of various substrate has been verified in several occasions for Pd NPs[71]. Pd-Fe systems proved to have exceptional performance in promoting the C-C and C-O cleavage as well as selective hydrogenation of C=O double bonds, opening the way to produce added value chemicals from biomass derived compounds[72].

The main peculiarity of Pd-Fe systems is the possibility to have intimate contact and interaction between Pd and Fe, which allows modification of the electronic density of Pd thus promoting unpredicted catalytic reactions under mild reaction conditions. The electronic modification of the metals is often studied using X-ray photoelectron spectroscopy (XPS). Using XPS analysis, a positive (or negative) shift in the binding energy of Pd indicates a partially positive (or negative) charge due to the electron transfer between Pd and Fe. Spontaneous support reduction is observed when Fe is used as a support (in the form of iron oxides), but the mechanism of support reduction is not uniquely recognized. Liu et al. suggested that the promoting effect of Pd in the reduction of hematite to magnetite directly originates from the catalysts preparation protocol[73]. Therefore, when Pd-Fe based materials are prepared with an in situ formation of Pd NPs on the iron oxide support their promoting effect is more emphasized than when they are synthesized with a two-steps protocol[74,75]. On the other hand, other researchers agree that even when Pd NPs are not directly attached

to the iron oxide (i.e. multilayer catalyst) their proximity can result in collision, leading to interactions and electron transfer between iron oxide support (or NPs) and the Pd surface. This behavior results in the activation of the functional groups thus helping the hydrogenation[71,74].

In many cases Fe NPs are used to prepare bimetallic alloyed systems supported on carbonaceous materials or metal oxides. In some cases, when Fe is present in large amount, it is useful to isolate Fe NPs from the catalytic centers using carbon (graphene) or silica coating. The coating of magnetic NPs is suitable to isolate NPs thus preventing the oxidation and to impart functional groups. The carbon shell provides protection due to its high thermal and chemical stability, while silica shell does not fully block the oxygen diffusion[76]. The peculiarity of bimetallic systems is the possibility to tune electronic and chemical properties of the alloy[77] or to enhance the synergic effect of non-competitive adsorptions[78]. Moreover, the Fe can improve the catalyst stability against Pd leaching, even in acidic environment[79]. Fe can be used as support in the form of Fe_2O_3, Fe_3O_4 or zero valent iron (ZVI), and in bimetallic systems such as alloy or core-shell NPs. The multiple forms of the iron oxides are of a great interest since the reducibility of the support can influence the activity and the selectivity to unsaturated alcohols[80]. Pd-Fe bimetallic catalyst have been reported to be effective in nitrocompounds reduction[81] and hydrogenolysis reactions[72], while for hydrogenation reactions they have shown divergent results. In the following sections, iron as support (Pd/FeOx) and iron in bimetallic systems (PdFe/support) will be described.

2.1.1 Pd nanoparticles supported on FeOx

Pd NPs supported on iron or iron oxides can be prepared using the classical impregnation, deposition and co-precipitation methods[82], as well as the more recent continuous synthesis[83] and bio-synthesis[84].

- Impregnation

Pd/FeOx materials can be easily synthesized by impregnation (wet impregnation (WI) and incipient wetness impregnation (IWI))[85]. WI leads to the formation of very small Pd NPs (1-3 nm)[86,87] while with IWI it is possible to synthesize a wide range of particle size[88,89]. Pélisson et al. and Farrag reported the synthesis of Pd/Fe_2O_3 by wet impregnation with different approaches. Farrag prepared atomically precise monodisperse palladium nanoclusters protected by N-acetyl-L-cysteine ($Pd_n(NALC)_m$) ligand[87]. Firstly, he prepared Pd^0 clusters protected by NALC and chemically reduced by $NaBH_4$. Then, after their recovery, he impregnated them on commercial α-Fe_2O_3. The removal of the ligand was performed using microwaves, allowing to obtain a highly dispersed 1 nm Pd^0 clusters onto commercial α-Fe_2O_3. The material proved to be very active in the hydrogenation of cinnamaldehyde (75 % conversion after 3 h at 80 °C and H_2 bubbling), with selectivity > 90 % to cinnamyl alcohol and stability over 4 repeated cycles. Using this procedure, the surface area of the support was increased one and a half times and the microwave treatment allowed to completely remove the organic ligand, thus increasing the catalyst activity. Pélisson et al.,[86] on the other hand, synthesized magnetically recoverable Pd^0/γ-Fe_2O_3 nanocomposite by impregnating magnetic iron oxide NPs with Pd precursor salt and without the use of organic modifier. Magnetic iron oxide NPs were synthesized through a typical co-precipitation method using aqueous Fe^{2+}/Fe^{3+} salt solution.[90] The support was then impregnated with Pd precursor and subsequently reduced with $NaBH_4$. The obtained magnetic material was characterized using TEM, XPS, XRD, and Mossabuer spectrometry. Relatively uniform superparamagnetic iron oxide NPs (11 nm) were present mainly in the form of γ-Fe_2O_3. The prepared 3 nm Pd NPs supported on γ-Fe_2O_3 exhibited excellent activities towards the reduction of olefinic compounds and nitro derivatives leading to the design of an attractive catalyst in terms of activity, selectivity, and recyclability.

Similar approach was used by Caparrós et al.[91] who loaded and reduced different amount of Pd on commercial magnetite (49 m^2 g^{-1}, 40 nm) functionalized with N-(3,4-dihydroxyphenethyl)-4-(diphenylphosphino)benzamide. Using low amount of Pd (0.11 %wt) they obtained Pd single atom, while small Pd clusters (1.2 nm) and small Pd NPs (4.3 nm) were obtained for loading of 0.4 %wt and 3 %wt,

respectively. The single atom catalyst proved to be particularly effective in the hydrogenation of CO_2 to ethanol, although the single atoms progressively evolved into NPs under high reaction temperature (250-300 °C), which as a consequence decreased the selectivity to ethanol.

Likewise, Li et. al impregnated and reduced Pd NPs on Fe_3O_4 prepared by hydrothermal protocol[92]. Briefly, a mixture of iron chloride, sodium acetate and polyvinylpyrrolidone dissolved in ethylene glycol was heated at 200 °C. The as synthesized magnetic support was covered with a shell of carbon, SiO_2, polypyrrole(PPy), polyaniline (PANI), polydopamine (PDA), and chitosan (CHI), thus creating a core-shell structure. XRD analysis of Fe_3O_4 and supported Pd NPs showed that no changes of the support structure occurred during the coating process. The bare support and the supported Pd core-shell catalysts were also characterized by TEM. Fe_3O_4 magnetic support showed spherical clusters with a size in the range of 400-500 nm, and shells with different thickness were clearly observed for the core-shell supports (Figure 2). The Pd particle sizes varied from 3.3 to 4.6 nm, depending on the composition and surface moieties of the shell. Moreover, XPS analyses revealed that Pd NPs were both in the metallic and oxidized form. The presence of $Pd^{\delta+}$ was due to the strong interaction between surface functionalities of the shell and Pd NPs, resulting in electrons transfer from Pd^0 to the support[65,93]. The higher the $Pd^{\delta+}$ amount, the stronger the metal-support interaction and the smaller the Pd NPs size. The actual deposition of the shell on the Fe_3O_4 was also verified by IR spectroscopy and the magnetization of the sample was determined by vibrating sample magnetometer, where a reduction of the magnetic properties was found for all the coating samples respect to the bare support. From a catalytic point of view, the presence of a carbon or SiO_2 shell resulted in low activity towards bromate reduction, due to their low points of zero charge, which invoke electrostatic repulsive interaction with anionic bromate and suppress bromate adsorption. On the other hand, CHI, PDA and PANI shells displayed high catalytic activities due to their high points of zero charge, resulting in enhanced bromate adsorption; PPy shell, despite having a high point of zero charge, exhibited low catalytic activity due to its strong surface hydrophobicity, which according to the authors inhibits the access of bromate to Pd sites of the catalysts.

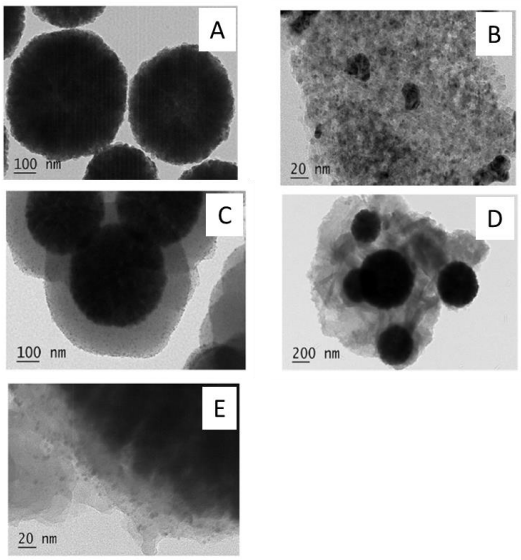

Figure 2. TEM images of **A**) Fe_3O_4 **B**) Pd/Fe_3O_4@CHI **C**) Pd/Fe_3O_4@PDA **D**) Pd/Fe_3O_4@PPy, and **E**) Pd/Fe_3O_4@PANI. Adapted from [92] Copyright 2019 Elsevier.

Hajdu et al. adopted a different strategy regarding both the support synthesis and the impregnation technique. Maghemite NPs were synthesized by a combustion method by calcining iron(III) citrate dispersed in polyethylene glycol at 500 °C for 2 h. The Pd was loaded by impregnation in ethanol using a homogenizer to sonicate the dispersion. The energy in the "hot spot" created by ultrasonic cavitation can cover the needs of the reduction of metal cations to metal in the presence of a reducing agent[94]. No phase-change in the support was observed after the homogenizer assisted Pd deposition. The palladium loading on maghemite support led to the aggregation of the magnetic particles whose size increased from 22 nm to 70-200 nm. Pd NPs mean size was 4.5 nm and XRD analyses showed that all the particles were in the form of metallic Pd. The catalyst was used for the hydrogenation of nitrobenzene to aniline, obtaining full conversion and 97 % selectivity at 293 K.

IWI synthesis is one of the most commonly used method to prepare Pd/Fe systems, since it allows to obtain a wide range of Pd NPs using a very simple technique. Hensley et al. reported the synthesis of Pd/Fe_2O_3 catalysts with different Pd loadings (0.1-5 %wt)[95]. They firstly prepared Fe_2O_3 support by aqueous phase precipitation of ferric nitrate in ammonium carbonate. After the recovery and drying of the support, they impregnated the support with a $Pd(NH_3)(NO_3)_2$ aqueous solution and they dried the material at 80 °C overnight. The authors obtained well dispersed Pd NPs with an average size of about 5 nm. Moreover, from TPR analyses, a strong interaction between Pd NPs and Fe_2O_3 support was highlighted by a shift of the Fe_2O_3 reduction peak at lower temperature (Figure 3A). Computational studies, supported by experimental characterization (TPR and XPS analyses), revealed the synergistic effect of Pd-Fe system in the hydrodeoxygenation of phenolic compounds. In particular, they demonstrated that the addition of Pd onto the Fe_2O_3 protects the active metallic Fe from oxygen poisoning through donation of Pd electrons to the topmost surface of Fe, which allowed the oxide surface electrons to become more delocalized.

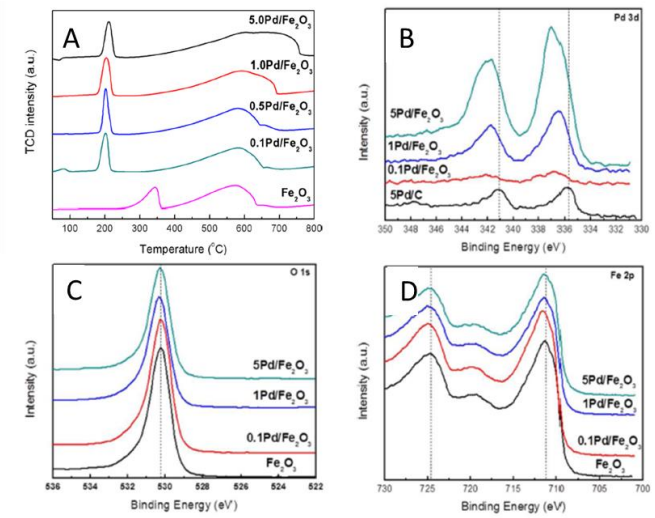

Figure 3. **A**) TPR profiles and XPS spectra of fresh Pd/Fe_2O_3 samples in the **B**) Pd 3d, **C**) O 1s, and **D**) Fe 2p regions. Adapted with the permission of Hensley et al.[95] Copyright 2014 American Chemical Society.

The same approach for catalysts preparation was followed by Jiang et al.[75] who prepared a Pd/meso-γ-Fe_2O_3 catalyst by synthesizing a mesoporous γ-Fe_2O_3 starting from iron nitrate, 1-butanol, nitric acid, and poly(ethylene glycol) solution. The prepared mesoporous support had a spherical shape with "hedgehog-like" aggregates which consisted of radially oriented NPs (Figure 4A). Moreover, the impregnation of Pd on mesoporous γ-Fe_2O_3 led to an observable change of peaks shape in XRD patterns ascribable to structure modifications of the support by Pd deposition (Figure 4B). This catalyst showed excellent activity in hydrogenation of nitrobenzene, with a TOF two times higher than Pd/Fe_2O_3 prepared using commercial iron oxide. Therefore, the choice of the physical-chemical properties of the support plays a key role in the hydrogenation reaction of nitro compounds.

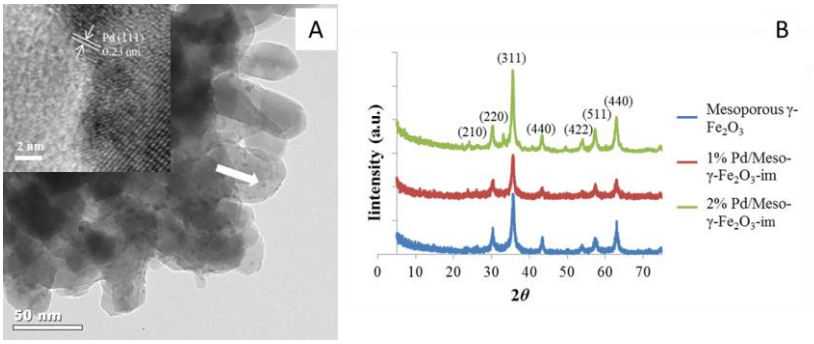

Figure 4. A) TEM images of 1% Pd/meso-γ-Fe_2O_3-im catalyst and **B**) High-angle XRD patterns of mesoporous γ-Fe_2O_3, 1%, and 2% Pd/meso-γ-Fe_2O_3-im catalysts. Adapted from [75] Copyright © 2015 Elsevier B.V.

A different approach was used by Neri et al. who impregnated palladium(II)acetylacetonate on Fe_2O_3 prepared by precipitation of iron nitrate[89]. From TEM, TPR and XRD analyses a strong interaction between Pd and iron oxide was found. Matching TEM and XRD results they hypothesized an intimate contact between Pd NPs and the support which leads to a strong metal-support interaction that hinders the crystal growth and the crystallization of both support and Pd NPs. Moreover, from TPR analyses no clear peak of the reduction of Pd NPs was observed, while a broad peak at higher temperature appeared. This meant that both Pd NPs and iron oxide support were simultaneously reduced, indicating a strong interaction between them and a stabilization of Pd(II) species[96]. The catalyst was applied in the selective hydrogenation of an unsaturated aldehyde (campholenic aldehyde), showing a remarkable activity compared to several other similar catalysts (Pd deposited on metal oxides such as SiO_2, TiO_2, ZnO, NiO and Co_3O_4), although the Fe_2O_3-based catalyst displayed poor selectivity to either the product of hydrogenation of the C=O bond or the C=C bond. The different behavior of the Pd catalysts was attributed to a modification of the noble metal electronic properties which consequently change the interaction of surface Pd atoms with adsorbed reactant species. Specifically, this effect occurs when a strong Pd interaction is established with the support, leading to new surface sites created at the Pd–support interface and/or formation of mixed ensembles or bimetallic Pd-based alloys.

- Co-precipitation

Pd/FeOx catalysts can be also prepared by the co-precipitation method, where one or more metal precursors are mixed within a solution containing a precipitation agent (hydroxides, oxalates, formats, carbonates). Liu et al. [73] prepared Pd/Fe_3O_4 catalysts by co-precipitation of iron nitrate and palladium chloride with sodium carbonate. The obtained catalysts were calcined (Pd/Fe(OH)x) and reduced at 200 °C under a flow of hydrogen. The XRD patterns of Pd/Fe(OH)x precursor indicated that iron hydroxide was present in its amorphous state, while PdO is highly dispersed with a crystallite size under the detection limit. The surface

area of Fe(OH)x and Pd/Fe(OH)x was 110 m^2 g^{-1} and 229 m^2 g^{-1}, respectively; this indicated that $PdCl_2$ efficiently improves the dispersion of Fe(OH)x. Moreover, the TPR profile (Figure 5B) showed a peak centered at 157 °C indicating the simultaneous reduction of Pd^{2+} to Pd^0, and Fe(OH)x to magnetite, while the peak at 87 °C was ascribed to the reduction of Pd^{2+} to Pd^0 and Fe^{3+} to Fe_3O_4. After the reduction step, the final Pd/Fe_3O_4 catalysts was obtained. The XRD analyses revealed the presence of Fe_3O_4 with an average crystallite size of about 11 nm (Figure 5A). The N_2 adsorption isotherms showed that, after the reduction step, the surface area of Pd/Fe_3O_4 was a little bit lower than that of Pd/Fe(OH)x, and a type IV isotherm identified a mesoporous structure. The corresponding pore size distribution indicated a relatively uniform pore size centered at about 3.4 nm. Moreover, the active surface area determined by CO chemisorption was 4.0 m^2 g^{-1}, while average Pd particle size determined by TEM was < 3 nm. For comparison, the authors synthesized a Pd/Fe_2O_3 catalyst by incipient wetness impregnation method, which displayed active surface area of 2.1 m^2 g^{-1} and average Pd particle size of 10 nm. The authors ascribed the higher H_2 TOF observed in the aqueous-phase reforming of ethylene glycol obtained with the Pd/Fe_3O_4 catalyst to a synergistic mechanism involving small Pd NPs and magnetite, which effectively promotes the water-gas-shift reaction. In addition, the catalyst produced by co-precipitation retained 80 % of its initial activity after reaching the steady-state.

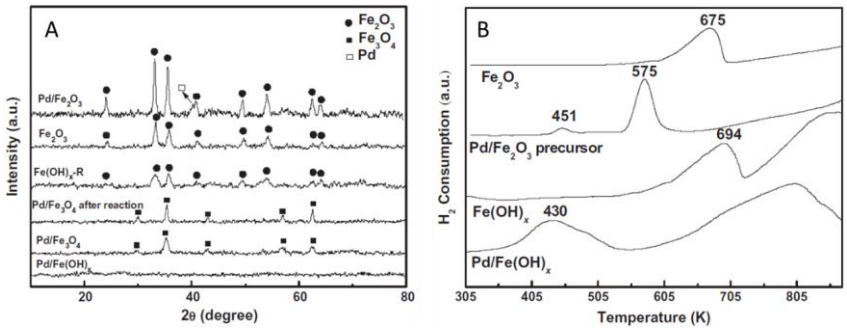

Figure 5. A) XRD pattern and **B**) TPR curves of $Pd/Fe(OH)_x$ and Pd/Fe_2O_3. Adapted from ref [73] Copyright © 2010 Elsevier Inc

Similar results were obtained by Mauriello et al.[88], who synthesized Pd/Fe_3O_4 by both co-precipitation and incipient wetness impregnation. The catalysts displayed significant differences in their physico-chemical properties. The co-precipitation catalyst showed higher surface area (170 m^2 g^{-1} versus 60 m^2 g^{-1}), higher active surface area (2.51 m^2 g^{-1} versus 0.23 m^2 g^{-1}) and smaller average Pd particle size (1.8 nm versus 8.8 nm). As expected, these differences had a strong impact on the catalysis, where the co-precipitated palladium catalyst allowed a complete conversion of glycerol to 1,2-propanediol and ethylene glycol under mild reaction conditions by using 2-propanol as hydrogen donor. In addition, the physico-chemical characterization of the co-precipitated palladium catalyst suggested that a strong interaction between Pd and the support leading to formation of bimetallic ensembles which positively promote the glycerol catalytic transfer hydrogenolysis reaction.

Gumina et al. used palladium nitrate as metal precursor instead of palladium chloride[97]. The Pd NPs size and TPR profile were similar to the one obtained by Liu et al. and Mauriello et al[73,88]. Extended x-ray adsorption fine structure (EXAFS) characterization confirmed the formation of Pd-Fe cluster since a Fe-Pd distance (0.259 nm) was observed, which is shorter than the length of Pd-Pd bond (0.266 nm)[98]. Finally, XPS analysis showed the presence of Pd-Fe ensembles/alloy due to the shift of the Pd $3d_{5/2}$ peak (+0.5 eV); this was assigned to the presence of partial positively charged $Pd^{\delta+}$ species. The catalyst was used for the hydrogenolysis of sorbitol as well as in the hydrogenolysis of C5-C3 polyols, where it showed excellent activity respect to a Pd/C catalyst. In particular, 91 % of conversion was obtained with Pd/Fe_3O_4 after 24 h at 180 °C

and 5 bar of H_2, compared to only 14 % obtained with a commercial Pd/C in the same reaction conditions. In addition, gas phase analysis at the end of the reaction showed the absence of CO, thus confirming the excellent performance of the co-precipitated Pd/Fe_3O_4 catalyst in promoting the water-gas-shift reaction.

Co-precipitation method was also used to prepare Pd/Fe_2O_3 catalysts. Musolino et al. co-precipitated palladium chloride and iron(III) nitrate with sodium carbonate and they dried the obtained material at 80 °C under vacuum. Finally they reduced the catalyst at 200 °C for 2 h under hydrogen flow[99,100]. The method is similar to the one described above, but the phase of the support changed due to the different temperatures and times used during the drying and the calcination step. The synthesized catalysts showed a mean particle size of 2.4 nm and TPR analysis revealed a strong interaction between Pd and Fe. The absence of the satellite peak of Fe 2p in the XPS analysis denoted a magnetite structure of the support[101,102]. The shift of Pd 3d peak towards higher values was ascribed to a change in the Pd electronic density as a consequence of the metal-support interaction or metal-metal interactions[103]. The Pd/Fe_2O_3 catalyst was tested in glycerol hydrogenolysis and aliphatic carbonyl reduction giving better results than the respective catalysts prepared by incipient wetness impregnation. Therefore, the enhancement of the activity of this catalyst respect to that prepared by impregnation is due to the modification of the electronic properties of the Pd NPs. In particular, in the absence of any alloy, the carbonyl reduction mechanism implied and oxidative approach by Fe^{3+} on the oxygen moiety of the carbonyl molecule and its reduction to Fe^{2+}. This implied a decrease of the π^*_{CO}, preferring the activation of the carbonyl bond on the Pd surface.

For the transfer hydrogenation/hydrogenolysis of furfural an analogous synthetic protocol was followed by Scholz and co-workers using $PdCl_2$ as metal precursor[104]. In this case, however, the catalyst was reduced in-situ in the reaction mixture under the reaction condition used (25 bar of N_2 and 150 °C). The Pd/Fe_2O_3 catalyst was compared with materials prepared in a similar way by only changing the active metal (Cu and Ni). The authors demonstrated that only the Pd-based catalyst accomplished complete metal reduction under the reaction conditions used. In addition, the Pd/Fe_2O_3 catalyst proved to be the most active, achieving 68 % of furfural conversion after 7.5h versus 37 % and 46 % of the Cu/Fe_2O_3 and Ni/Fe_2O_3 catalysts respectively. The reactivity of Pd/Fe_2O_3 in C-O cleavage reactions was attributed to a strong metal–support interaction. The authors extended the study of the Pd/Fe_2O_3 catalyst to the continuous hydrogenation/hydrogenolysis of 5-hydroxymethyl furfural (HMF), showing a high selectivity towards either 2,5-bis(hydroxymethyl)furan or 2,5-dimethylfuran depending on the residence time and the temperature. Additionally, after an initial decrease in conversion, the activity of Pd/Fe_2O_3 remained stable over 47 h.

Wu et al. prepared $5\%Pd/Fe_2O_3$ catalyst by precipitation of iron nitrate and palladium nitrate[98]. The $Pd/Fe(OH)_x$ catalysts was calcined in air at 300 °C for 2 h and then pre-reduced in a flowing stream of H_2/N_2 at 200 °C for 1-72 h. XRD pattern confirmed the presence of Fe_2O_3 phases but no Pd peaks were observed due to the extremely small Pd particles on the surface of the reduced iron oxide. TPR profile showed just one peak at about 130 °C owing to the strong interaction of Pd with iron, which led also to the formation of PdFe clusters under the pre-reduction conditions. The direct observation of the PdFe clusters was extrapolated from EXAFS characterization, where a Pd-Fe distance (2.59 Å) was acquired. Moreover, XPS analyses revealed a shifting in the binding energies of Pd and Fe to higher values indicating the formation of a PdFe alloy-like structure[102,105,106]. Furthermore, TEM images confirmed the presence of small clusters and metal particles (0.5-2.5 nm), and even single atoms around the edges of the clusters were found. This catalyst was effectively applied in the catalytic production of methanol through a non-syn-gas route, using ethylene glycol as substrate. The catalyst was compared to other Pd-based catalysts such as Pd/ZnO, Pd/Ga_2O_3, Pd/CeO_2 and Pd/Al_2O_3, proving to be the most active with conversion over 2 times higher as well as the most selective to the desired product methanol.

- Deposition-precipitation

Besides impregnation and co-precipitation technique, Pd/FeOx systems can be prepared by deposition-precipitation (DP) method. The objective of the precipitation technique is to obtain a well-dispersed metal hydroxide (or carbonate) phase on the support through its precipitation from an aqueous metal solution by adding a base (urea, ammonia, sodium hydroxide, hydrazine, triethanolamine, carbonate, sodium borohydride…).

Shukla et al. prepared Pd/Fe_2O_3 catalysts by deposition method using triethanolamine (TA) and hydrazine (HZ) as precipitating and mild reducing agents[107]. Fe_2O_3 support was prepared by hydrothermal method using iron chloride as metal precursor and polyvinylpyrrolidone as stabilizer. This solution was heated at 180 °C for 48 h in an autoclave. Palladium precursor was then added by deposition with TA or HZ. The particle size of 1%Pd/Fe_2O_3 evaluated with TEM analyses was 18.4 nm and 5.2 nm for 1%Pd/$Fe_2O_3^{HZ}$ and 1%Pd/$Fe_2O_3^{TA}$, respectively. Moreover, different amount of Pd was loaded on Pd/$Fe_2O_3^{TA}$ and TEM images revealed that the higher the loading, the larger the Pd NPs sizes (Figure 6A-C). The crystallinity of the obtained materials was determined by XRD analyses. XRD pattern of 1%Pd/$Fe_2O_3^{TA}$ did not show the Pd^0 and PdOx peaks due to the small crystallite size and the low loading. However, increasing the Pd loading from 1 to 5 %wt, PdO peak appeared indicating the existence of bigger palladium oxide crystals. SEM images of 1%Pd/$Fe_2O_3^{TA}$ revealed the spherical and somewhat oval-shaped morphology of the iron oxide NPs with a size in the range of 60-120 nm. XPS analyses of 1%Pd/$Fe_2O_3^{TA}$ showed the presence of metallic Pd, PdO, and $Pd(OH)_2$, while after hydrogen pre-treatment the last peak disappeared. Interestingly, after hydrogen pre-treatment no variation in the oxidation state of the support was observed. UV-Visible diffuse reflectance spectra were recorded to confirm the interaction between Pd and Fe_2O_3 particles (Figure 6D). Moreover, TPR analyses of 1%Pd/$Fe_2O_3^{TA}$ catalysts revealed the presence of stronger metal-support interaction than 1%Pd/$Fe_2O_3^{HZ}$ due to the presence of highly dispersed and smaller Pd NPs (Figure 6E). The prepared support displayed a broad band in the range of 300-620 nm at the absorption edge of 608 nm[108]. After the deposition of Pd, 1%Pd/$Fe_2O_3^{TA}$ catalyst showed a red shift at the absorption edge of 613 nm which was due to the charge transfer between the Pd NPs and the Fe_2O_3 support. Finally, EXAFS analysis was performed to explore the local and electronic environment of 1%Pd/$Fe_2O_3^{TA}$. Pd-O bond distance and some long distance related Pd-Pd interactions were observed. The prepared catalysts were used for the selective hydrogenation of nitro compounds and Suzuki coupling reactions in aqueous medium. The authors showed that both catalyst preparation method as well as size of active metal played a significant role in catalysis. In particular, smaller Pd NPs obtained using TA as reducing agent led to a general increase in activity compared to the catalyst synthesized with HZ as well as an increase in stability. The authors further demonstrated the particle size effect by synthesizing a 1%Pd/Fe_2O_3 catalyst by incipient wetness impregnation having average Pd particle size of 22 nm; the activity towards p-nitrophenol reduction and Suzuki coupling decreased by a factor of 4 compared to the most active 1%Pd/$Fe_2O_3^{TA}$ catalyst.

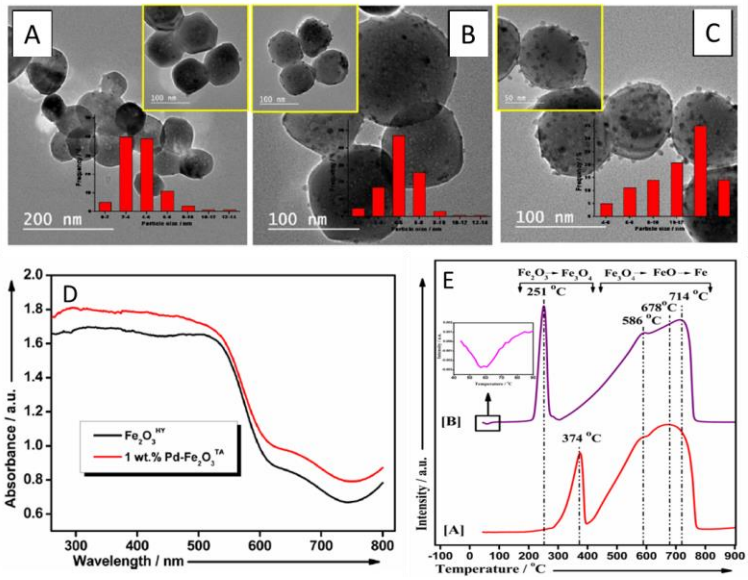

Figure 6. TEM images of **A**) 0.5%Pd/$Fe_2O_3^{TA}$, **B**) 1.5%Pd/$Fe_2O_3^{TA}$, **C**) 3%Pd/$Fe_2O_3^{TA}$ catalysts; **D**) UV-Vis Diffuse reflectance spectra of Fe_2O_3 (black line) and 1%Pd/$Fe_2O_3^{TA}$ (red line), and **E**) TPR profile of pure $Fe_2O_3^{HY}$ (red line) and 1%Pd/$Fe_2O_3^{TA}$ (purple line) Adapted from ref [107] © 2019 Wiley-VCH Verlag GmbH & Co. KGaA, Weinheim

Je at al.[82] prepared rod-like and plate-like iron oxides by a modified precipitation method[109] and a modified hydrothermal approach[110], respectively. For the rod-like support, iron sulphate aqueous solution was heated to 78 °C and urea solution was then added dropwise. Therefore, the obtained material was dried and calcined at 350 °C for 2 h. Instead, the plate-like iron oxide was synthesized starting from an aqueous solution of $FeCl_3$ and NaH_2PO_4. The solution was transferred into an autoclave and maintained at 220 °C for 8 h. Pd deposition was performed using DP technique from an alkaline solution of NaOH and Na_2PdCl_4. XRD analyses of the support showed the presence of only α-Fe_2O_3 phase and a different contribution of <110> plane. Rod-like nanocrystal preferred <110> plane direction, while plate-like support the <001>. TEM images of the rod-like iron oxide displayed a diameter of about 150 nm while the plate-like support had a width of 10 nm and a length of 150 nm. Pd NPs with a particle size distribution within 2-4 nm were uniformly dispersed on the different supports. The Pd/plate-like catalysts showed better activity in the hydrogenolysis of glycerol compared to the Pd/rod-like due to a combination of a higher Pd dispersion on the support and to a higher quantity of surface oxygen vacancies (presumably due to the dominant polar but unstable (001) surface on the plate-like iron oxide).

- Other techniques

Beside these common procedures for the synthesis of the catalysts, Pd/FeOx materials can also be obtained by solvothermal method, biosynthetic route, post coating technique and continuous synthesis.

Cappelletti et al. prepared Fe_3O_4@Pd core-shell NPs using solvothermal procedure[111]. Superparamagnetic NPs of Fe_3O_4 were obtained from a Fe-urea complex synthesized starting from iron nitrate and urea. The Fe-urea complex was dispersed in oleylamine (OA) and dibenzyl ether (DBE) and this suspension was heated at 155 °C for 1 h, and at 300 °C for another 1 h. Pd^0 shell was obtained using a similar methodology mixing Fe_3O_4-OA powder with palladium acetate in OA or DBE. This synthetic procedure allowed obtaining well-defined

core-shell structure with a Pd shell thickness of 1.3 nm and a particle size of 7 nm. FT-IR spectra showed the typical signal of Fe-O in magnetite structure[112] and the signal of OA which remained on the superparamagnetic NPs despite the washing. XRD patterns displayed the typical diffraction peaks of the *fcc* Pd phase and Fe_3O_4, while no PdO signals were observed. The as synthesized catalyst displayed high chemical stability against oxidation to maghemite for several months due to the Pd shell, as well as a very good catalytic activity for the Suzuki–Miyaura coupling reaction (80 % yield in the coupling reaction between p-iodoanisole and boronic acid at 115 °C and N_2 atmosphere after 5h). The catalyst proved also to be reusable for at least for four reaction cycles by simple magnetic separation, showing only a small decrease in activity.

A similar procedure was followed by Biglione et al. who prepared the Fe_3O_4@Pd core-shell superparamagnetic NPs using either triphenylamine or triphenylphosphine as stabilizer[113]. The authors detected additional peaks belonging to PdO phase in the XRD pattern, as well as the presence of amorphous shape particles with larger particle size and polydispersity (9 ± 6 nm) compared to a similar catalyst synthesized using OA as stabilizer (7 ± 1nm). The OA-stabilized Fe_3O_4@Pd catalyst was tested in the hydrogenation of p-chloronitrobenze, showing almost full conversion after only 1 minute of reaction.

Pd supported on mesoporous γ-Fe_2O_3 can be also synthesized by one-step sol-gel method. Jiang et al. mixed palladium nitrate with iron nitrate, poly-ethylene glycol (P123), nitric acid, and 1-butanol[75]. The phase of the support was checked by XRD and both 1%Pd/meso-γ-Fe_2O_3 and 2%Pd/meso-γ-Fe_2O_3 showed the characteristic peaks of γ-Fe_2O_3. Moreover, BET analysis confirmed the mesoporosity of the support and the catalysts prepared by sol-gel method exhibited a higher surface area than the one synthesized by impregnation as a reference. The one-step sol-gel catalyst was applied in the nitrobenzene hydrogenation reaction, where it showed lower TOF compared to the one prepared by impregnation due to less accessible Pd NPs on the surface of the mesoporous Fe_2O_3 support; higher stability over Pd leaching was however achieved, making the one-step sol-gel Pd/meso-γ-Fe_2O_3 catalyst a good candidate for the selective hydrogenation of nitrobenzene to aniline.

Besides the Pd/iron oxide catalysts, interesting Pd NPs supported on zerovalent iron (ZVI) can be prepared by post-coating method. This method uses spontaneous redox reaction occurring between Fe^0 and Pd^{2+} leading to the formation of Pd/ZVI NPs [114]. Pd NPs were deposited on nanoscale zero ZVI NPs synthesized by reduction with $NaBH_4$. The overall process can be described with the following reactions:

$$2Fe(OH)_2 + 2BH_4^- + 2H_2O \rightarrow 2Fe^0 \downarrow + 2B(OH)_3 + 5H_2 \uparrow$$

$$Pd^{2+} + Fe^0 \rightarrow Pd^0 + Fe^{2+}$$

The Pd/ZVI NPs had a surface area of 27 $m^2 g^{-1}$ which was independent from the Pd loading. Characterization analyses showed that individual particles had a size of 5-80 nm with a core/shell structure. In particular, the iron core was composed by ZVI enclosed within a thin layer of iron oxide, while the shell was only composed by metallic Pd. TEM images showed that no obvious change of particle morphology and size occurred after the deposition of Pd, while SEM revealed a heterogeneous distribution of Pd NPs on iron surface[114]. The catalyst was applied to the dechlorination of mono-, di- and tri-clorobenzenes in water, reaching full conversion in less than 60 minutes. The system, however, proved to be rather unstable, as the Pd/ZVI NPs exhibited significant decrease in dechlorination reactivity after a 24 h ageing step, possibly due to Pd dislodgment from the aged Pd/Fe particles and Pd islets encapsulation by the iron oxides film developed over aging period. The reactivity of the aged Pd/ZVI could be only partially restored after HCl treatment, while regeneration with $NaBH_4$ could not restore the initial activity, although zerovalent state of the iron was reinstated.

Similarly, Elliott et al. performed a field demonstration gravity-feeding 100-200 nm Pd/ZVI NPs into ground-water contaminated by thrichloroethene and other chlorinated aliphatic hydrocarbons at a manufacturing site[115]. The study showed trichloroethene reduction efficiencies of up to 96 % on a 4-week monitoring period with injection of approximately 1.7 kg of the NPs into the test area over a 2-day period. The data gathered from the field assessment were consistent with the results of pre-injection laboratory studies, showing that Pd-Fe systems can be appealing for industrial applications as well.

Huang and colleagues synthesized Pd/ZVI by reductive deposition of Pd^{2+} ions onto freshly prepared Fe^0 NPs, using $Fe_2(SO_4)_3 \bullet 6H_2O$ and $Pd(OAC)_2$ as metal precursors[116]. The NPs were found in homogeneous spherical shape with diameter between 40 and 100 nm. XPS analysis revealed the presence of Fe(III) oxides and oxyhydrides, as well as the presence of zerovalent Fe, suggesting a typical structure composed of a thin Fe oxides layer with metallic Fe core and Pd reductively deposited on the shell. The catalyst was ~~succesfully~~successfully applied in the selective hydrogenation of acetylene to ethylene in dimethylformamide at room temperature, achieving simultaneous isolation and *in-situ* conversion of acetylene. The performance was compared with other metal/ZVI catalysts (transition metal tested: Pt, Au, Ag, Cu and Ni) prepared with the same technique, as well as a bimetallic Pd-Ag industrial catalyst. The Pd/ZVI catalyst attained a remarkable catalytic activity higher by a factor of 2.2 orders of magnitude than that of the currently used industrial method. In addition, reusability tests indicated a very good reactivity and stability, with no loss in either conversion or selectivity after 5 recycles.

A recent paper by Elazab et al. reported the continuous flow synthesis of Pd supported on Fe_3O_4 NPs[83]. The continuous flow synthesis allows preparing large amount of catalyst compared to the small amount that can be prepared with the standard lab-scale methods. Moreover, due to the use of a flow reactor (Figure 7), all the reagents flows are well controlled by flowmeters, avoiding human errors in the operations. An aqueous solution containing iron nitrate and palladium nitrate and a separate solution of hydrazine were prepared. By using a pump, these two solutions were injected into the T-Mixer and then mixed and pumped together to the microwave applicator. Different catalysts were synthesized varying the metal/hydrazine ratio, the flows of the solutions and the temperature. XRD and XPS analyses revealed that the catalysts were enriched of Fe_3O_4 and Pd^0. Interestingly, the lower the temperature used during the synthesis, the higher the Pd^0 content. Moreover, TEM images showed that increasing the temperature the particles size increased from 4 to 9 nm. In all the cases, Pd NPs supported on magnetite prepared under flow reaction conditions were smaller than those synthesized under batch reaction conditions, although they showed lower Pd(0) content. This resulted in a slightly lower activity in the CO hydrogenation reaction, where 100 % conversion was obtained at 137 °C, compared to a reaction temperature of 128 °C of the catalyst prepared in batch.

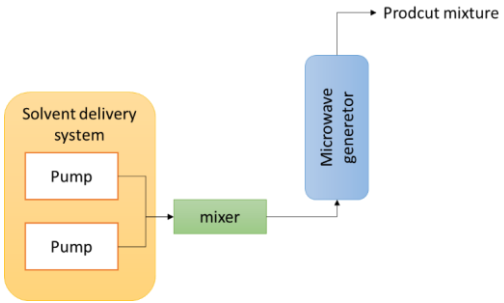

Figure 7. Schematic representation of the continuous flow micro-reactors.

Finally, Pd/Fe_3O_4 catalysts can be prepared with an innovative and green method based on the biosynthesis of Pd/Fe_3O_4 nanocomposites. These types of nanocomposite are produced under ambient and physiological

conditions by *Shewanella oneidensis* MR-1 microbes. Tuo et al. demonstrated that monometallic Pd NPs can be produced on bio-synthesized magnetite giving high catalytic activity towards the hydrogenation of nitroarene compounds[84]. Fe_3O_4 support was prepared by *Shewanella oneidensis* MR-1 microbes starting from akageneite[117] and lactate suspended in an anaerobic PIPES buffer. Akagenite was added as electron acceptor, while lactate as electron donor. This bio-reduction system was incubated at anaerobic conditions at 30 °C in darkness. Then, the recovered and washed bio-synthesized Fe_3O_4 NPs were suspended again in a serum bottle, and Na_2PdCl_4 and lactate were added. The suspension was anaerobically incubated at 30 °C in the dark for 2 days. Finally, the nanocomposites were recovered with the help of a magnet. Microbial extracellular polymeric substances binding on the surfaces of biogenic Fe_3O_4 participate in the appearance of rod-like Fe_3O_4. The Fe_3O_4 nano-roads exhibited a length of 100-200 nm and a width of 7-17 nm, while Pd particles showed a mean particle size diameter of 5.5 nm with a crystal phase assigned to the <111> lattice spacing of the fcc Pd, also confirmed by XRD analysis. Similar catalysts were produced in order to obtain monometallic Au/Fe_3O_4 and bimetallic AuPd/Fe_3O_4. The materials were tested in the reduction of different nitroaromatic compounds, showing excellent catalytic activities. In particular, the bimetallic AuPd/Fe_3O_4 catalyst achieved 94 % of 4-nitrophenol conversion after 8 minutes of reaction, compared to 76 % and 24 % of the Pd/Fe_3O_4 and Au/Fe_3O_4 respectively. The improved catalytic activity of alloyed PdAu NPs compared to that of monometallic Pd NPs was attributed to geometric and electronic effects after the introduction of Au, which can cause a contraction of the lattice and withdraw electron density from Pd (as further suggested by XPS data). In addition, the catalysts displayed satisfying stability over multiple reaction cycles, retaining most of its initial activity after over 8 cycles.

Catalyst	Preparation Method	Pd Precursors	Fe Precursor	Particle Size [nm]	Catalytic Application	Ref.
$Pd/\alpha\text{-}Fe_2O_3$	WI	$Pd(NO_3)_2 \bullet 2H_2O$	$\alpha\text{-}Fe_2O_3$	1-2	Cinnamaldehyde hydrogenation	[87]

2.1.2 PdFe and PdFeOx nanoparticles supported on metal oxides and carbonaceous materials

Similarly to what reported for monometallic Pd NPs supported on Fe oxides, the procedures to prepare bimetallic PdFe NPs are impregnation, galvanic replacement and chemical co-reduction.

- Impregnation

Both incipient-wetness impregnation and wet impregnation are reported to be effective in the preparation of PdFe NPs via co-impregnation or a two-step process[50,118]. With these techniques, it is possible to obtain bimetallic alloy or mix-oxide NPs with a size range of 1-13 nm. γ-Al_2O_3, SiO_2, activated carbon (AC), carbon nanotube (CN) and carbon-coated silica can be used as support. Pino et al. reported the synthesis of PdFe/γ-Al_2O_3 and PdFe/SiO_2 by co-impregnation[50,118]. Aqueous solution of $Pd(NO_3)_2$ and $Fe(NO_3)_3$ was used to impregnate the commercial support. Low surface area γ-Al_2O_3 (90 m^2 g^{-1}) and SiO_2 (130 m^2 g^{-1}) were used as support. The obtained catalytic materials were dried, calcined at 500 °C in air and finally pre-reduced at 250 °C in hydrogen. The XRD pattern showed the peaks associated to SiO_2 along with two new peaks at around 41.2° and 47.2°, which can be ascribed to the formation of a Pd-Fe alloy. When Fe atoms are incorporated in the *fcc* structure of the Pd, in fact, they cause a positive shift of the diffraction angle[79,81] and the low intensity indicated a good dispersion of Pd-Fe NPs. On the other hand, no peaks of Pd or Pd-Fe alloy were visible in the alumina-based catalyst. The absence of alloy was also confirmed by TEM-EDX and XPS analyses, where no shift in biding energy of Pd 3d species was observed. Therefore, no evidences about the interaction between iron and palladium was found for the PdFe/γ-Al_2O_3 catalyst. On the contrary, the PdFe/SiO_2 catalyst showed a clear shift of 0.4 eV towards higher binding energies of the Pd 3d peak, indicating that the formation of Pd-Fe alloys is favorable on the SiO_2 support but much less so on γ-Al_2O_3. The shift at higher binding energies of the Pd 3d peak led to the conclusion that Pd-Fe NPs are in the form of alloy, although the fundamental cause of this behavior is a matter of debate. Some authors stated that the binding energy shift is due to the electron transfer from Pd to Fe, which would be the opposite if we considered the electronegativity of the two metals (Pd=2.2 and Fe=1.83)[118]. Felicissimo et al., on the other hand, proposed that the shift is due to the simultaneous contribution of both electron transfer and orbital rehybridization[119]. This hypothesis was confirmed by Pino et. al by DFT calculation, which clearly showed that alloying Pd with Fe led to a core-level shift of Pd 3d. TEM images showed homogeneous metal NPs distribution for both samples, with an average particle size of 2.5 nm and 4.1 nm for the alumina- and silica-based catalysts respectively. The materials were used in the furfural hydrogenation reaction. The change of the support affected the formation of Pd-Fe alloy and consequently the selectivity toward 2-methylfuran. When using γ-Al_2O_3 as a support, the selectivity greatly shifted from 2-methylfuran to furan, showing a behavior that was much more like a monometallic Pd/SiO_2 used as comparison than the bimetallic Pd-Fe/SiO_2. These results suggest that the intrinsic properties of support have significant influence on the catalytic performance of Pd-Fe catalysts, with the contrasting behavior of the two supports explained in terms of a segregation of the metals induced by a higher interaction with the support in the case of alumina that does not occur on silica. In addition, DFT calculations showed that furfural, furfuryl alcohol, furan and methylfuran favorably adsorb via the furanic ring on Pd(111) surface, while the addition of Fe clearly weakens these adsorption energies. The stronger binding of the carbonyl group (strongly bound to the oxophilic Fe) and -OH group on Pd-Fe alloy surface promotes the furfural hydrogenation and furfuryl alcohol hydrogenolysis towards 2-methylfuran.

Similarly, Dimas-Rivera et al. prepared bimetallic PdFe NPs supported on high surface area γ-Al_2O_3 (244 m^2 g^{-1}), along with the monometallic Pd catalyst[50]. The materials were in this case calcined at 620 °C in air and pre-reduction in H_2 flow at 450 °C. Thermogravimetric analysis (TGA) and differential thermal analysis (DTA) of the PdFe/γ-Al_2O_3 revealed a maximum exothermic peak at 517 °C and another endothermic peak at 916 °C; these thermal events were related to the formation of PdO and PdO decomposition to Pd^0 respectively

[120,121]. The TPR profile showed two peaks for both monometallic and bimetallic catalysts: an intense signal at 220 °C and a broader peak at 370 °C. The peaks were assigned to the reduction of PdO particles weakly and strongly interacting with the support. In the bimetallic catalyst, both peaks were shifted at lower temperatures (200 and 360 °C respectively) as a result of co-reduction of Pd and Fe species due to their intimate contact. This suggested the presence of alloyed NPs. As found for Pd/FeOx catalysts, Pd can reduce Fe^{3+} to Fe^{2+} without the presence of a reducing atmosphere. The synthesized PdFe bimetallic NPs were characterized by HRTEM (Figure 8) and a calculation of the interplanar distances (IDs) was performed. The evaluation led to measure four different IDs related to the presence of $O_4Pd_{3.5}$ crystalline phase (zone A), Pd_3Fe alloy (zone B), magnetite and maghemite iron oxides (zone C), and crystalline Pd^0 (zone D). The catalysts were used in the ring-opening hydrogenolysis of 4-methylfuran to alcohols. The bimetallic PdFe/γ-Al_2O_3 presented the highest conversion, with an activity 6 times higher than the monometallic counterpart and a production of a mixture of 1-pentanol, 2-pentanol and 1-butanol. The authors ascribed this greater activity to the enhanced hydrogenation efficiency of the surface $FePd_3$ species.

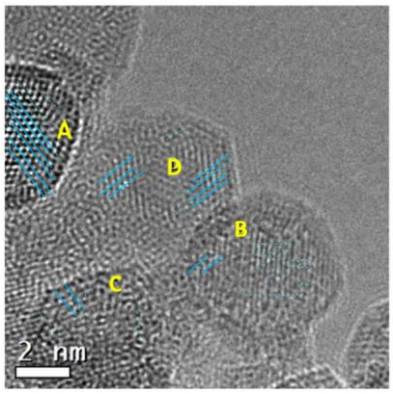

Figure 8. HRTEM image over a group of NPs of PdFe/ γ-Al_2O_3. Reproduced from ref [50]. © 2017 Elsevier B.V.

Another method to obtain PdFe/γ-Al_2O_3 is a two steps impregnation synthesis where the loading of the two metals is performed sequentially. Stytsenko et al. prepared PdFe/γ-Al_2O_3 with different Pd:Fe molar ratios for the selective hydrogenation of acetylene[122]. Palladium chloride was dissolved in an ammonia solution and the commercial support was added. The solvent was then removed by vacuum distillation and the catalyst was dried and reduced in hydrogen flow for 1 h at either 250 or 500 °C. Then, Pd/γ-Al_2O_3 was added in a solution of ferrocene and *n*-hexane and left overnight at room temperature. Finally, the catalyst was dried and reduced at the previous conditions. DRIFT analysis was performed using CO as probe molecule. The high-temperature reduced catalysts prepared with the highest amount of Pd and Fe showed characteristic adsorption peaks at 1990-2160 cm^{-1}. The bands at 2127 cm^{-1} and 2102-2084 cm^{-1} were attributed to the linear Pd^{2+}-CO and Pd^0-CO, respectively, whereas the presence of intense bands at 1991-1985 cm^{-1} suggested the presence of large Pd^0 NPs. The band at 2150-2153 cm^{-1} was instead attributed to the presence of Fe^{2+} species. On the contrary, the catalysts reduced at 250 °C did not show any characteristic bands suggesting that the metals or the unsaturated cations are not accessible to the CO. TEM confirmed the large particle size (10 nm) and EDX analysis revealed that the catalyst surface is simultaneously enriched with Pd and Fe. From a catalytic point of view, both mono- and bimetallic catalysts were comparable in activity, but the PdFe/Al_2O_3 catalyst proved to be more selective towards ethylene. The author ascribed this effect to the modification of the Pd surface with iron, which changed the character of the interaction of H_2 with the active sites of the catalyst.

A two-step impregnation method was applied also by Shesterkina et al.[57] and Cheng and co-workers[51]. The former synthesized PdFe/SiO_2 using high (HS) and low (LS) surface area SiO_2, while the latter produced PdFe NPs loaded on carbon coated SiO_2 (PdFe/SiO_2@C). PdFe/SiO_2 were synthesized by incipient wetness impregnation (IWI) starting from tetraamminepalladium(II) and ammonium iron(III) oxalate and using commercial SiO_2 with a surface area of 300 $m^2\ g^{-1}$ (HS) and 30 $m^2\ g^{-1}$ (LS). After the impregnation the samples were dried and, in some cases, calcined at 250-400 °C in air. The dried only or calcined samples were then reduced for 3 h at 400 °C in hydrogen flow. The phase composition was determined by XRD (Figure 9). The prepared samples showed different crystalline phases depending on the surface area of the support and the temperature used during the heat treatments. Pd^0, α-Fe_2O_3 and Fe_3O_4 phases were detected after the calcination at about 250 °C and the Pd^0 crystallite size was 10 nm and 20 nm for PdFe/SiO_2^{HS} and PdFe/SiO_2^{LS}, respectively. Fe^0 phase, on the other hand, appeared after the reduction. TPR analyses exhibited several overlapped peaks, which confirmed the presence of many phases. In particular, peaks below 350 °C (i.e. before reaching the temperature of the reduction of iron oxide) were detected indicating a strong interaction between Pd and Fe. Therefore, a Pd-Fe alloy phases was hypothesized. The authors found that the catalytic activity in phenylacetylene hydrogenation and the selectivity to styrene depended on the composition and thermal treatment conditions. In particular, the formation of the amorphous Pd–Fe alloy in the reduced sample caused a significant ~~drop in~~drop in activity of the sample compared to the monometallic one. However, recrystallization caused by NPs sintering during annealing in argon at 550 °C significantly increased the activity and selectivity (93 %) of styrene formation, which is higher than that in the case of monometallic Pd catalyst (77 %). It is likely that an increase in ~~the selectivity~~the selectivity of bimetallic PdFe catalysts reduced in hydrogen after calcination is associated with the reduction of iron oxides and the formation of alloys. As a result, the obtained bimetallic PdFe/SiO_2 catalyst was more effective than the monometallic Pd/SiO_2.

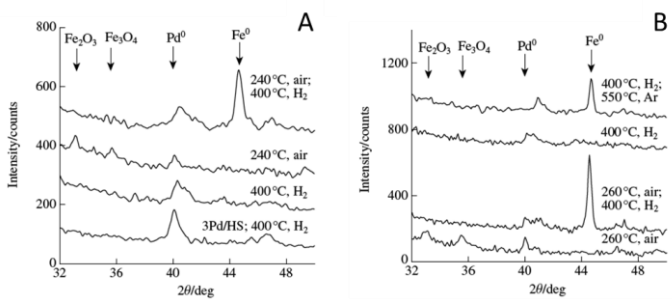

Figure 9. XRD patterns of the **A**) PdFe/SiO_2^{HS} and **B**) PdFe/SiO_2^{LS} catalysts after thermal treatment under different conditions. Adapted from ref [57] © 2016 Published by Elsevier España, S.L.U.

As reported in the introduction, PdFe NPs can be loaded on oxides covered with a layer of carbon and silica. SiO_2 allows oxygen diffusion while carbon provides protection against thermal sintering due to its high thermal and chemical stability. Cheng and co-workers coated SiO_2 with a thin film of carbon created by impregnation ad calcination of furfuryl alcohol (SiO_2@C)[51]. Then, Fe and Pd were loaded in different relative amounts by sequential IWI using acetone solutions of ferrous acetate and palladium acetate. After the drying, the impregnated support was reduced at 200 °C in hydrogen flow. EDS/HAADF-STEM revealed that the particles were enriched in Pd with a molar percentage higher than the calculated one. Therefore, they hypothesized that Fe was present within the particles and covered by Pd. Moreover, some Fe species formed segregated particles, although HRTEM and EDS images indicated that Pd and Fe were mainly in alloy form. CO chemisorption measurements showed that adsorbed CO was only detected on Pd surfaces and its dispersion decreased increasing the Fe amount. STEM images showed that monometallic Pd/SiO_2@C had NPs

in a 1-2 nm size range, while for bimetallic catalysts a wider range of NPs size was detected: while particle sizes between 1–2 nm dominated, both smaller particles down to 0.5 nm and larger particles up to 5.5–6 nm were also observed. Moreover, increasing the Fe content, the fraction of smaller and larger particle slightly increased. To confirm the presence of alloy phase, HRTEM, XRD, XPS, and TPD analyses were performed. HRTEM images showed lattice fringes of 0.213 nm and 0.202 nm which corresponded to Pd-Fe alloy and Fe phase, respectively. Unfortunately, XRD and XPS analyses did not give any useful information due to the very small size of Pd and Fe NPs and the low metal content. More effective results were obtained with H_2-TPD analyses where a shift in the peak of hydrogen desorption at higher temperature was detected. No desorption peak was observed for the monometallic Fe catalyst. This indicated a strong interaction between Pd and adsorbed hydrogen when Fe was present. Bimetallic PdFe catalysts were found to have significantly increased TOFs for the condensed-phase hydrogenation of carbonyl, C=C and aromatics compared to monometallic Pd catalyst. The extent of the activity enhancement varied by the moiety being hydrogenated as well as the Pd-to-Fe molar ratio, with an optimal value being 45 mol% of Fe relative to Pd. The enhanced activity was ascribed to Pd modification by Fe, leading to formation of $Pd^{\delta-}$, as Fe was found to have no reactivity under the reaction conditions used. This was hypothesized due to the much greater increase in carbonyl hydrogenation activity than for C=C and aromatic hydrogenation, which is consistent with the formation of $Pd^{\delta-}$ species.

The impregnation method can be also used for the loading of Pd and Fe on carbon-based supports. Sun et al. used a two-steps sequential IWI for the synthesis of 2 wt% Pd–10 wt% Fe on carbon (2Pd10Fe/C) catalyst for the vapor-phase hydrodeoxygenation of guaiacol[55]. Firstly, iron precursor was impregnated on coconut shell activated carbon and calcined at 350 °C for 2 h in flowing Ar. The Pd precursor was then impregnated and a second calcination step was performed. Before characterization and catalytic test, the material was reduced *in-situ* in H_2 flow at 450 °C for 2 h. XRD analysis clearly showed the peak of metallic Fe and its calculated crystallite size was 32 nm. No diffraction peaks corresponding to Pd or PdFe alloy phase were resolved. STEM-EDS analyses revealed the presence of small NPs which were present in a much higher number than larger ones. EDS showed also that either Fe-enriched Pd NPs and Pd-enriched Fe NPs were present. A more detailed single-spot EDS analyses clearly evidenced that the particles consisted of a Pd core and a FeOx shell, suggesting that Fe and Pd were in close contact. However, for small NPs (1-2 nm) the Fe segregation at the surface was probably due to air exposure during TEM sample preparation. TPR profile (Figure 10A) confirmed the presence of the PdFe alloy, since a H_2 consumption peak between -15 °C and 100 °C was observed. To further prove the presence of PdFe alloy, EXAFS spectrum (Figure 10B) was collected. The recorded spectrum significantly differed from that of monometallic Pd: a peak at 2.15 Å suggested the formation of PdFe alloy. Furthermore, a short Pd-Pd bond distance was calculated (2.726 Å) besides a Pd-Fe bond distance of 2.608 Å with a coordination number of 2.7. This clearly demonstrated the presence of alloyed Pd-Fe NPs. Furthermore, DFT calculations were used to better understand the interaction between Pd and Fe. Nilekar et al. reported that when Pd is used as atom impurity within a Fe host, a strong surface segregation is preferred. On the contrary, when Pd hosts Fe impurities a strong anti-segregation behavior was observed[123]. Therefore, Sun et al. hypothesized different scenarios and the results suggested that Pd atoms prefer to form a pure layer on Fe <110> surface rather than mixing with Fe (Figure 10C,D). These results agreed with STEM-EDS observations. Analogous calculations were performed using Pd as host and Fe as impurity. In this case, it was found that Fe atoms preferred to form a pure layer in the second layer of Pd <111> structure. From a catalytic point of view, the bimetallic PdFe catalyst was compared with other monometallic (Fe, Pd, Cu, Pt and Ru) carbon-supported catalysts. Phenol was found to be the major intermediate on all the metal-supported catalysts studied. Precious metal catalysts showed higher activity, although saturation of aromatic ring and C–C bond cleavage also took place, leading to the formation of cyclohexanone, cyclohexanol, and gaseous C_1 products. Base metal catalysts, on the other hand, were found to be less active but they exhibited higher hydrodeoxygenation selectivity without ring opening and ring saturation with benzene, toluene, phenol, and cresol being the major products. The bimetallic PdFe/C

catalyst, however, was found to exhibit a significantly enhanced hydrodeoxygenation activity with 83.2 % yield to benzene/toluene/TMB at 450 °C, which was ascribed to the modification of Fe by Pd.

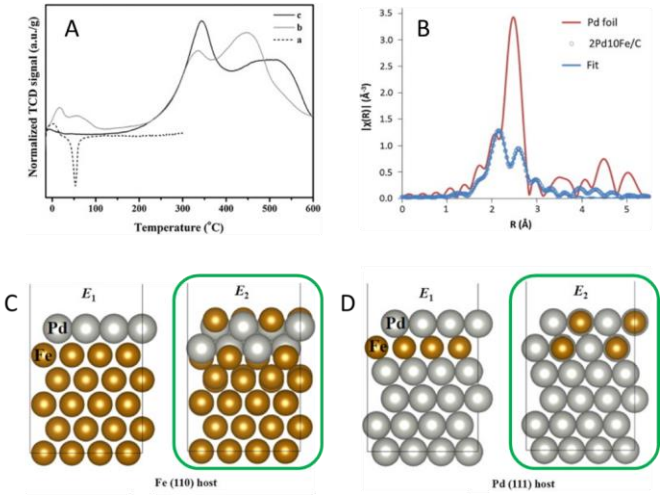

Figure 10. A) H_2-TPR profiles of: (a) 5Pd/C, (b) 2Pd10Fe/C and (c) 10Fe/C. **B**) Magnitude of k2-weighted Fourier transform of Pd K-edge EXAFS data for the 2Pd10Fe/C (blue, open circles), fit (blue line) and Pd foil (red line). Structures of a **C**) Pd layer in the Fe (110) surface host, and **D**) Fe layer within the Pd (111) surface host. The bottom layer is fixed in its bulk position. The most stable configurations are highlighted by the green rectangle Adapted from ref [55] Copyright © 2013 Elsevier Inc.

Similar catalyst was used also for the chemo selective hydrogenation of bioactive carbohydrates[124]. Protected O-aryl-β-D-glycopyranosides from protected glycosyl bromides were obtained through a biphasic reaction in alkaline media with very good yield and high β-selectivity. The use of the bimetallic PdFe catalyst in the reduction of carbonyl and nitro moieties of protected O-aryl-β-glycosides led to hydrolysis and hydrogenolysis of these aromatic groups. A comparison with Ni-based catalysts showed that even after long reaction times, poor yields were achieved with these latter catalysts. Gastrodin synthesis was achieved successfully after 3 simple reaction steps, with a 92 % yield after 24 h.

Finally, Wang and co-workers prepared PdFe confined in the interface of carbon nanotubes (CNT) and N-doped carbon (NC) by impregnation-reduction technique (Figure 11A)[125]. Co-impregnation of K_2PdCl_4 and $FeCl_3$ on hydroxylated carbon nanotubes was performed under ultrasonication. Then, sodium borohydride was added to reduce the metal precursors forming CNT/PdFe. The obtained material was coated with a polydopamine layer (CNT/PdFe/PDA) which was transformed into NC due to carbonization at 600 °C. TEM images of the CNT/PdFe/CN catalyst (Figure 6B) showed a double-shell tubular structure where bimetallic PdFe NPs (6 nm) were confined between the two carbon layers. In addition, dark-field (DF)-STEM images and EDS analyses demonstrated a homogeneous element distribution (Figure 11C). The oxidation state of the elements was evaluated with XPS analyses. Pd 3d HR spectra showed the presence of only Pd^0 (335.9 eV and 341.2 eV) while the signal of Fe 2p (711.6 eV and 725.5 eV) was assigned to Fe^{3+} species. Moreover, recorded spectra of monometallic Pd and Fe demonstrated that Fe can reduce the 3d electron density of Pd at the Fermi's level, which avoids the PdOx formation. Finally, a mesoporous support structure was revealed from N_2 adsorption-desorption isotherms, and a pore size of 2 nm and 25 nm was found to belong to the outer NC and inner CNT diameters, respectively. The bimetallic catalyst exhibited a superior catalytic activity compared to corresponding monometallic counterparts towards nitroarene reduction, thus showing an enhanced

synergetic effect for the dual-metal component. The authors reported TOF for 4-nitrophenol reduction higher than that of many noble-metal based catalysts reported within recent literature. In addition, owing to the particular configuration of the catalyst and strong MSI, the encapsulated dual-metal PdFe NPs showed only slight leaching after repeated catalytic tests, with minimal loss of activity after 7 reaction cycles.

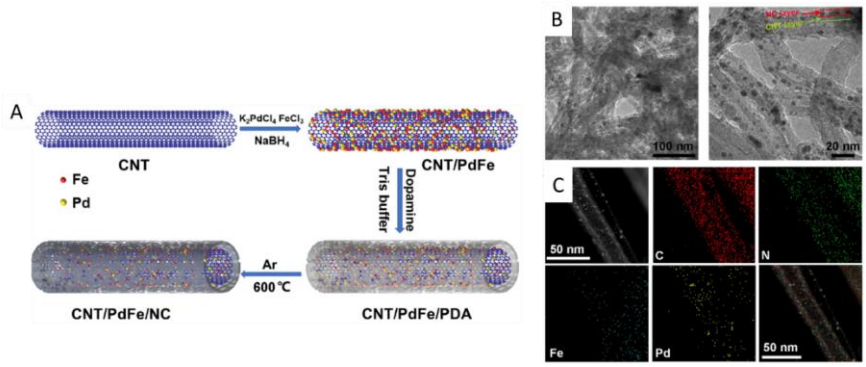

Figure 11. A) Scheme of the preparation, **B**) TEM analysis and **C**) STEM image with corresponding EDS elemental mapping of the CNT/PdFe/NC catalyst. Adapted from ref [125] Pd-Fe dual-metal NPs confined in the interface of carbon nanotubes/N-doped carbon for excellent catalytic performance.

- Galvanic replacement

Besides the impregnation technique, supported PdFe NPs can be prepared by spontaneous displacement. With this method, a metal can be replaced with another one considering the spontaneous reaction between the two metals which have different redox potential. The Fe atoms act as sacrificing component for the reduction of Pd^{2+} to Pd^0, allowing the deposition of a layer of Pd on the Fe NPs. Liao et. al firstly immobilized iron sulphate on commercial activated carbon[126]. Then, the iron precursor was reduced with $NaBH_4$ to Fe^0. A solution of potassium tetrachloropalladate was then added dropwise allowing the displacement reaction. The catalyst was finally recovered, washed and dried. TEM images showed a highly dispersion of bimetallic NPs with an average size of 3.8 nm. XRD patterns revealed the presence of Pd <111>, <200>, and <220> at about 40.23°, 46.66° and 68.30°, respectively. The absence of any peak related to Fe suggested a core-shell structure with Pd layers that coated the Fe core; the core-shell structure was also confirmed by XPS analyses; the Pd:Fe relative amount obtained from the survey spectra was 3.92:1, thus there was a higher concentration of Pd on the particle surface despite the atomic ratio of Pd and Fe was 1:3.94 from ICP-AES analysis. Furthermore, Pd 3d region revealed the presence of both Pd^{2+} and Pd^0. These finding corroborated the hypothesis of a pseudo core-shell structure. The catalyst was applied in the electrooxidation of formic acid, showing enhanced stability and activity up to 11 times higher compared to a reference monometallic Pd/C catalyst.

Analogous protocol was used by Feng and co-workers who prepared PdFe/RGO (reduced graphene oxide) starting from graphene oxide[56]. Also in this case, a pseudo-core shell structure was obtained and the average size of PdFe NPs was 3.9 nm. Electrochemical studies showed that the optimized PdFe/RGO with a Pd:Fe molar ratio of 1:5 possessed excellent electrocatalytic activity and stability towards the formic acid oxidation. The doping of Fe ~~increase~~increases the ratio of surface Pd atoms, leading to a high atom utilization efficiency, and modified the microscopic electron structure on the surface of NPs due to the bimetal synergistic effect.

- Co-reduction

PdFe/C catalyst can be also prepared by co-reduction[127]. Iron and palladium precursor were dissolved in a water/ethanol mixture and added to the functionalized carbon (NC). The dispersion was sonicated for 1 h and stirred for 24 h at room temperature. The solid was then recovered and reduced in a H_2/N_2 flow at 450 °C for 2 h. XRD patterns revealed a *fcc* structure of Pd and the <111> peak of Pd in the PdFe/NC shifted to higher values compared to the same peak in the monometallic Pd/NC catalyst. The shift indicated that some PdFe alloys were created with Fe embedded into the Pd lattice. On the other hand, no peaks of Fe were detected indicating a completely amorphous structure. HAADF-STEM images showed a good dispersion of Fe with some aggregations of Pd (Figure 12A,B). Moreover, XPS analysis of Pd 3d regions confirmed the completely reduction of Pd^{2+} species to Pd^0 and a shift to higher binding energy than monometallic Pd, confirming the formation of a Pd-Fe alloy (Figure 12C). The bimetallic PdFe/C catalyst exhibited good catalytic performance for the semihydrogenation of phenylacetylene to styrene, showing a conversion twofold higher than similar Pd-based bimetallic catalysts (PdNi/C and PdCo/C) after 30 min of reaction and comparable selectivity (> 95 %). The modification of Pd with Fe promoted the selectivity of the catalyst, especially when the Pd:Fe mass ratio was optimized (1:1).

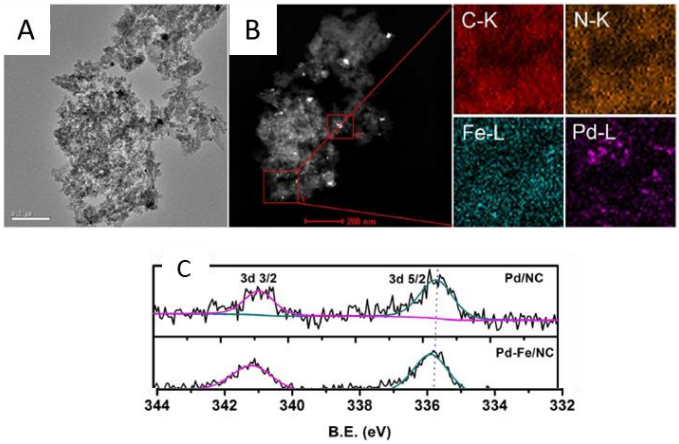

Figure 12. A) TEM images of PdFe/NC, **B**) HAADF-STEM and element mapping analysis of PdFe/NC, and **C**) high-resolution XPS spectra of Pd 3d Adapted from ref [127] © 2019 Wiley-VCH Verlag GmbH & Co. KGaA, Weinheim.

2.2 Pt-Fe systems

Pt supported NPs are widely used for hydrogenation[128–130] and oxidation reactions[131,132]. However, when Pt NPs are used for CO oxidation reaction, the noble metal can be easily poisoned by CO due to its strong adsorption on the NPs[133]. The catalyst activity can be increased by adding a transition metal oxide (i.e. iron oxide), whose role is to provide lattice oxygen[134]. For these reasons, Pt-Fe systems are acquiring high scientific interest due to their good chemical stability[135], as well as large uniaxial magnetocrystalline anisotropy[136–138] and high saturation magnetization and coercivity[139,140]. The addition of Fe to Pt can modify the electronic structure of Pt, thus modifying the electron density and therefore the catalyst activity[141,142].

These characteristics make Pt-Fe materials suitable for many different applications such as biomedical imaging[143], advanced permanent magnets[143], and ultrahigh density magnetic recording[143]. Beyond these applications, Pt-Fe systems have been proven to have exceptional activity in both hydrogenation and

oxidation reactions. The selective hydrogenation of carbonyl groups in α,β-unsaturated aldehydes, ketones or carboxylic acid is an important step in the synthesis of various fine chemicals. From an industrial point of view, the most important products are unsaturated alcohols and therefore the hydrogenation reaction must be selective towards the reduction of C=O[144,145]. Many researchers have been devoted to enhancing the selectivity of heterogeneous supported metal catalysts for these reactions. It was demonstrated that the use of reducible supports, cationic promoters and the effect of the metal particle size have a positive effect in hydrogenation reactions[135].

Pt-Fe systems can be also used in oxidation reactions. Pt/FeOx catalysts are characterized by a strong metal support interaction which leads to an electron transfer from Pt to the iron oxide support[142,146]. These catalysts showed enhanced catalytic performance in glycerol oxidation to tartronic acid[147], preferential oxidation of CO[148], and formaldehyde oxidation[146].

Fe can also be used as modifier and the peculiarity of the bimetallic PtFe system is the facile phase transformation of bimetallic NPs from one crystallinity to another which led to atomic, structure reconstruction and electronic modification which modifies the physical and chemical properties[147]. It is largely established that the morphology and the catalytic properties of bimetallic materials can be finely tuned by controlling the atoms arrangements during the synthesis[149]. However, a good control in the synthesis of these materials via bottom up methods is seldom obtained due to the differences in the reduction kinetics of the metal precursors[150]. Recent works demonstrated that phase transformation of magneto crystals, via interdiffusion from *fcc* disordered morphology to an ordered *fct* structure, can occur in a simple one-pot annealing process[151,152]. Moreover, anisotropic transformation led to significant structure evolution of bimetallic nanocomposites. The mechanism that regulates phase transformations and its impact on the catalytic properties of these bimetallic systems are largely unexplored. The variation of cohesive properties, moment-stabilizing mechanism and chemical bonding is due to a continuous transition from itinerant to local-moment magnetism. This transition occurs due an interplay of scalar relativistic effects, electronegativity, covalent bonding, and charge transfer[153]. Ji et al. found that structural modification in the PtFe alloy from a *fcc* to *fct* structure results in higher durability of the materials under acidic conditions[154]. In the case of PtFe bimetallic systems the electronic properties of the two metals can be varied carefully changing the synthetic method. The use of a stabilizer often leads to electron density modification of the noble metal as well.

Pt-Fe systems can be divided in Pt NPs supported on iron oxides and bimetallic PtFe NPs supported on carbonaceous materials or metal oxides. These catalysts can be prepared by the classical impregnation, precipitation, sol-immobilization, colloidal deposition, and solvothermal synthesis, or via metal vapour synthesis and strong electrostatic adsorption (SAD).

2.2.1 Pt nanoparticles supported on FeOx

Pt/FeOx catalysts are commonly prepared by impregnation, colloid deposition and solvothermal method. Most recent publications reported the synthesis of this material via co-precipitation, sol-immobilization, SAD, and redox reaction as well.

- Impregnation

Impregnation method allows the loading of Pt on pure iron oxides or mixed materials, such as iron oxide-coated Al_2O_3 and multi-walled carbon nanotube (MWCN). Fan et al. reported the synthesis of Pt/Fe_3O_4-MWCNTs by WI[155]. The Fe_3O_4/MWCNTs composite was synthesized by hydrothermal method by dispersing MWCNTs in a solution of $FeCl_3$ and ethylene glycol. The mixture was sealed in an autoclave and heated at 200 °C for 12 h. The final Pt/MWCNTs-Fe_3O_4 catalyst was then prepared impregnating the prepared support with an aqueous solution of H_2PtCl_4. The Pt precursor was later reduced with $NaBH_4$ under vigorous stirring and the obtained catalysts was recovered, washed and dried. TEM images showed that Fe_3O_4 loaded on

MWCNTs had an average particle size of about 200 nm but no Pt NPs were detected, despite EDS spectrum revealed the presence of Pt. Similarly, XRD analysis was able to detect Pt while crystal planes of cubic Fe_3O_4 clearly appeared. FTIR spectra revealed the presence of interaction between Fe_3O_4 and MWCNTs due to a shift of the characteristic peaks of C-O stretching modes (1584-1649 cm^{-1}) to higher wavenumbers. This catalyst was used for the solvent-free reduction of a variety of aromatic nitro compounds to their corresponding amines at 60 °C and a hydrogen pressure of 40 bar. The yield was > 99 % with ~~all of~~all the substrates tested, and the Pt/Fe_3O_4-MWCNTs catalyst proved to be quite stable and could be reused four times without significant deactivation.

Kobayashi et al. synthesized Pt/Fe_2O_3-Al_2O_3 catalyst for isobutene dehydrogenation[142]. The support was prepared by co-precipitation method varying the amount of Fe, while Pt was loaded by wet impregnation using hexachloroplatinic acid as metal precursor. The catalysts were calcined at 500 °C for 3 h and reduced for 5 h at 500 °C in hydrogen flow before the reaction. The surface area was almost constant for low Fe loading, while decreased when Fe_2O_3 amount was higher than 12 %wt. From CO chemisorption analysis the authors observed that the amount of adsorbed CO drastically decreased with the addition of only 1 %wt Fe_2O_3. On the other hand, further Fe_2O_3 additions up to 7 %wt caused only a gradual decrease in CO adsorption. FTIR of adsorbed CO showed three characteristic peaks (Figure 13C): 1) CO species adsorbed on the edge, corner sites, or step of Pt (F1), 2) CO species adsorbed on the terrace of Pt<100> (F2), and 3) CO species adsorbed on the terrace of Pt<111>[156,157]. By adding Fe_2O_3 a red shift was observed, suggesting an increase of Pt electron density. XRD analyses (Figure 13A,D) were able to detect α-Al_2O_3 and α-Fe_2O_3 only in the sample with high iron oxide loadings. Reduced Pt/Fe_2O_3-Al_2O_3 catalyst with an iron oxide content > 34 %wt showed clear diffraction peaks of Fe, while this signal was absent for lower content of Fe_2O_3. No Pt^0 peaks were observed due to the small particle size. The Fe amount influenced the electronic properties of the catalysts and as a consequence the activity towards isobutane dehydrogenation was affected as well. The addition of Fe_2O_3 increased the electron density of surface Pt atoms by the formation of PtFe NPs. This facilitated the hydride elimination and consequently enhanced the catalytic activity of the materials. The catalyst with a 7 %wt Fe_2O_3 showed the highest conversion rate and selectivity to isobutene. The authors reported lower deactivation phenomena in the catalysts containing Fe_2O_3 as well.

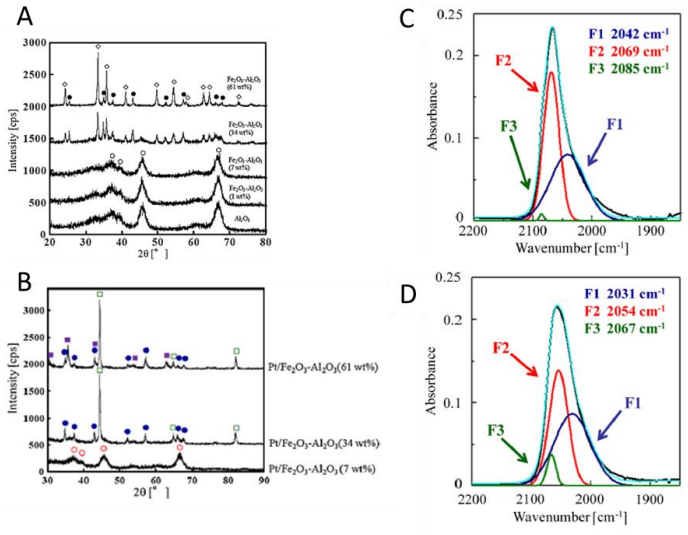

Figure 13. A) XRD of Al_2O_3 and Fe_2O_3-Al_2O_3 mixed-oxide supports: (◌) γ-Al_2O_3, (●) α-Al_2O_3 (corundum), (◊): α-Fe_2O_3 (hematite), **B**) XRD of Pt/Fe_2O_3-Al_2O_3 catalysts after H_2 reduction at 500 °C for 1 h: (◌) γ-Al_2O_3, (●) α-Al_2O_3, (□) Fe^0, (▪) Fe_3O_4. Deconvolution of IR spectra of CO adsorbed onto Pt catalysts: (**C**) Pt/Al_2O_3, (**D**) Pt/Fe_2O_3-Al_2O_3 (7 wt%) Adapted from ref [142] Copyright © 2012 Elsevier B.V.

Finally, Rachmady et al. studied the catalytic behavior of acetic acid hydrogenation over Pt NPs supported on different metal oxides, such as TiO_2, SiO_2, η-Al_2O_3, and Fe_2O_3 prepared by IWI[158]. The catalysts were reduced *in-situ* under H_2 atmosphere prior chemisorption characterization and reaction. Pt crystallite size was measured by H_2 chemisorption and it was in all the samples lower than 2.5 nm. The Pt size in the Pt/Fe_2O_3 sample, however, could not be calculated due to the unusually low H_2 uptake. From kinetic results, the authors found strong evidence that the reaction involved the participation of both metal and metal oxide support. In particular, the conversion of acetic acid takes place at sites on the oxide surface, with Pt that has the principal role to serve as a source of mobile activated hydrogen atoms. Among the metal oxides studied as support, TiO_2 was the most active for acetic acid hydrogenation, with the sample reduced at high temperature (500 °C) having a TOF 7-8 times greater than the catalyst reduced at low temperature (200 °C) and more than 100-fold times higher than the other Pt catalysts; the Pt/TiO_2 catalyst showed the highest selectivity to ethanol (up to 70 %) as well. The Pt/Fe_2O_3 catalyst was also active for the hydrogenation of acetic ~~acid, and~~acid and displayed a particularly high selectivity towards acetaldehyde (up to 80 %), although it required a much higher temperature of operation than Pt/TiO_2.

- Colloidal method

Pt NPs supported on iron oxide are often prepared by colloidal method. The use of a surfactant (i.e. protecting agent or stabilizer) helps to limit the growth and the aggregation of the NPs by forming a monolayer on the particle surface. The preparation of the colloid can be divided in two main steps: the first is the formation of the colloid and the second is the immobilization or deposition of the colloid on the support[159]. The colloidal methods can be divided in solvothermal process and sol-immobilization on the basis of the solvent, the temperature used for the synthesis and how the metal precursor is reduced. The solvothermal methods involves the use of a glycol or ethylene glycol (EG) solution in which the metal precursor is dissolved. The subsequent reduction process is activated increasing the temperature of the system above 90 °C. When polyols are used instead of EG the method is called polyol process.

An et al.[160] synthesized Pt/Fe_2O_3 preparing a Pt colloid by heating a glycol solution of NaOH and H_2PtCl_6 at 140 °C for 3 h. $Fe(OH)_3$ was synthesized by precipitation method using iron nitrate and sodium carbonate as precipitating agent. The mixed solution of colloidal Pt and iron hydroxide was heated at 80 °C to allow the deposition process. Finally, the obtained catalyst was dried and calcined at 200-500 °C in O_2/Ar flow to obtain the final Pt/Fe_2O_3 material. In the XRD pattern the characteristic peaks of α-Fe_2O_3 appeared, while no peaks associated to Pt were detected (Figure 14A). This suggested that Pt NPs were highly dispersed on Fe_2O_3 support. Moreover, increasing the calcination temperature the crystallinity of the support increased, despite the diffraction peaks of the iron oxide in Pt/Fe_2O_3 were always weaker than those of the bare support. These results indicated that the addition of Pt NPs influenced the Fe_2O_3 crystallinity and that an interaction between Pt NPs and the support was present. This hypothesis was also confirmed by TG-DTA analysis where the loading of Pt NPs shifted the peak of the support phase transformation at higher temperature. TEM images showed that no particle aggregation occurred during the calcination step, even at high temperature (500 °C). The images showed highly dispersed Pt NPs with a mean size diameter of 1.9 nm. The study of the surface redox properties was performed by XPS analyses. Pt 4f region showed the presence of three different contributions related to Pt^{4+}, Pt^{2+} and Pt^0. The catalyst calcined at 300 °C presented only Pt^{2+} and Pt^0 species with a higher fraction of Pt^{2+} than the sample calcined at 200 °C. This meant that Pt can be oxidized in higher valence states increasing the calcination temperature. Pt^{2+} and Pt^{4+} species were found at 72.1 eV and 74.5 eV, respectively in the catalyst calcined at 400 °C. The main species detected was Pt^{2+}, while Pt^{4+} peak appeared in the sample calcined at 500 °C. Therefore, increasing the calcination temperature, the amount of

platinum oxide species increased. H_2-TPR analyses (Figure 14B) displayed a strong and broad reduction peak at 600 °C which was attributed to the transformation of Fe_3O_4 to FeO[161]. The catalyst calcined at 200 °C exhibited a peak at 90 °C with a calculated hydrogen consumption much higher than the one required for the reduction of PtOx. This meant that a partial reduction of iron oxide occurred simultaneously with the reduction of PtOx and the low temperature indicated that Pt species were introduced in the lattice of iron oxide. Increasing the calcination temperature to 300 °C the peaks at 90 °C shifted to 105 °C and a new peak (270 °C) related to the reduction of bulk Fe_2O_3 appeared. For higher calcination temperatures the peaks intensity at low temperature decreased and a further peak associated to the reduction of Pt^{4+} species appeared. The presence of a suitable interaction between Pt NPs and iron oxide support proved to play a positive role in influencing the physicochemical property as well as the catalytic performance in the complete oxidation of formaldehyde. All the catalysts achieved full conversion at low temperature (lower than 60 °C). In particular, the samples calcined at 200 and 300 °C exhibited high catalytic activity and stability even at room temperature.

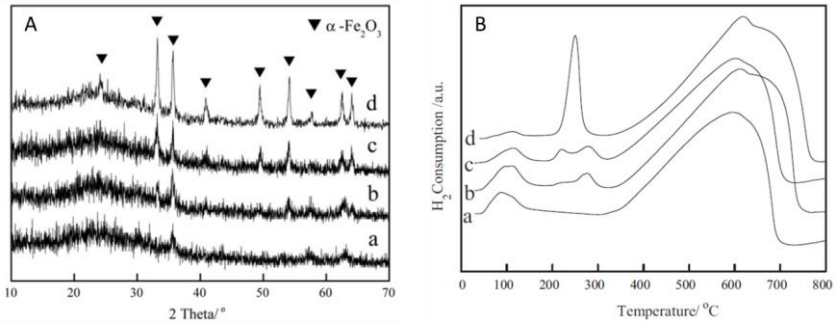

Figure 14. A) XRD patterns of Pt/Fe_2O_3 catalysts calcined at different temperatures (a): 200 °C, (b): 300 °C, (c): 400 °C, and (d): 500 °C; **B**) H2-TPR profiles of 1%Pt/Fe_2O_3 calcined at different temperatures: (a) 200 °C; (b) 300 °C; (c) 400 °C; (d) 500 °C. Adapted from ref [160] Copyright © 2010 Elsevier B.V.

In a later study, the same authors compared the Pt/Fe_2O_3 catalyst prepared by colloidal method (calcined at 200 °C) with a similar materials prepared by wet impregnation and co-precipitation[146]. The catalyst prepared by impregnation used Fe_2O_3 support synthesized by precipitation method using iron nitrate and sodium carbonate as metal precursor and precipitating agent, respectively. The as synthesized support was then impregnated with a solution of H_2PtCl_6 and the excessive water was removed at 80 °C. The obtained catalyst was finally dried and calcined at 200 °C in a flow of oxygen and argon. The Pt/Fe_2O_3 catalyst synthesized by co-precipitation was prepared starting from chloroplatinic acid and iron nitrate as metal precursors, and sodium carbonate as precipitating agent. The obtained catalyst was then dried at 100 °C and calcined at 200 °C in a flow of O_2/Ar. In both samples, XRD pattern showed the presence of α-Fe_2O_3 phase, while no peaks associated to Pt were found. This suggested that Pt NPs were highly dispersed on the surface of the support. Moreover, the low peaks intensity indicated the presence of an interaction between Pt NPs and iron oxide which also modified the crystallinity of FeOx. TEM images revealed that Pt NPs were homogeneously dispersed on the support and with an average particle size of 2.6 nm and 2.3 nm for the impregnated and co-precipitated catalysts respectively. TPR profiles were collected to study the oxidation states. For the catalyst prepared by impregnation two peaks at 140 °C and 260 °C were found, which were assigned to the reduction of Pt^{2+} and crystalline Fe_2O_3 + Pt^{4+}, respectively. For the co-precipitated catalyst, the same peaks were shifted at 170 °C and 200 °C. No intermediate peaks were detected, indicating a low interaction between Pt and iron. From a catalytic point of view, the sample prepared by colloidal method exhibited higher catalytic activity in the oxidation of formaldehyde compared to the other catalysts. The preparation method, in fact, significantly influenced the structure of the support and the redox properties of

the Pt/Fe_2O_3 catalyst, in particular through the presence of suitable interactions between the Pt particles and the support (Pt-O-Fe). Through these interactions, highly dispersed Pt could weaken the Fe-O bond located at the Pt/FeOx interface thus increasing the mobility of the active oxygen which is involved in the oxidation of formaldehyde.

The colloidal procedure used by An et al. was further optimized varying the colloid concentration (from 1.0 to 9.8 g L^{-1}) and the solvent (EG and a mixture of EG/H_2O 1:5 v/v)[162]. Even though the XRD patterns were similar to those reported in Figure 14A, different peaks intensities were observed changing the solvent and colloid concentration. It was demonstrated that these two parameters influenced the Pt NPs size. Pt mean diameter of 1.1 nm was observed for the lowest colloid concentration in pure EG (Figure 15A), while increasing the colloid concentration, the average particle diameter increased to 1.9 (Figure 15B). Moreover, when EG/H_2O solution was used, larger NPs were obtained (2.7 nm) (Figure 15C). Despite no Pt was observed in XRD analyses, the changes in peaks intensity were attributed to the creation of different metal-support interactions with different strengths, thus resulting in a change of Fe_2O_3 crystallinity. Different Pt particle size affected the overall catalytic activity in the low-temperature oxidation of CO. The presence of suitable metal−support interactions in the Pt/Fe_2O_3 catalysts played a crucial role in adjusting the redox properties of the catalysts, thus being beneficial to the formation of neighboring Pt and Fe active sites for the activation of CO and O_2, respectively. The Pt/Fe_2O_3 catalysts with stronger O_2-activation abilities were found to be more efficient in the oxidation of CO at low temperature.

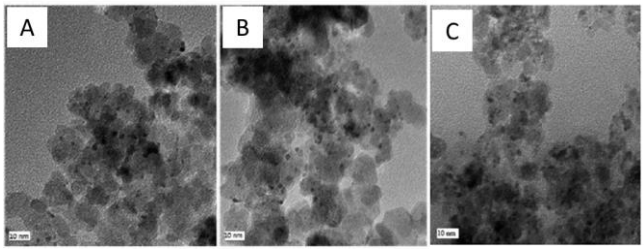

Figure 15. TEM images of the three Pt/Fe_2O_3 catalysts synthesized with different colloid concentration and solvent: **A**) pure EG, low colloid concentration, **B**) pure EG, high colloid concentration, and **C**) EG/H_2O mixture, high colloid concentration. Reproduced from ref [162] Copyright © 2013, American Chemical Society

Fang et al. prepared Pt/γ-Fe_2O_3 using a protocol similar to those of An et al. previously reported[163]. The commercial support was added to the colloidal solution of Pt and the obtained powder was washed and dried for 3 days. Using this procedure Pt NPs with an average diameter of 2.2 nm were obtained. HR-XPS spectra of Pt 4f region revealed that the Pt binding energy was very close to that of bulk Pt. The small shift of this signal was attributed to the electron transfer from Pt NPs to the iron oxide. On the other hand, no binding energy shift of Fe 2p was observed. XRD patterns confirmed the crystal structure of γ-Fe_2O_3 but no peaks related to Pt were detected due to its low content. The catalyst was used for the hydrogenation of o-chloronitrobenzene to o-chloroaniline under mild reaction conditions, reaching 99.9 % of yield. In addition, the authors found that increasing the drying temperature, the catalytic stability increased.

Wang et al. reported the synthesis of Pt/γ-Fe_2O_3 starting from an EG colloidal solution of Pt nanoclusters and a sol of ferric hydroxide[164,165]. The mixture was heated in an autoclave for 3 days at 90 °C and a Pt/γ-Fe_3O_4 magnetic precipitate was obtained. The final Pt/γ-Fe_2O_3 was obtained heating the precipitate at 90 °C. XRD analyses showed the presence of pure maghemite with a crystal size of about 15 nm. The composition was also confirmed with XPS and RAMAN spectroscopy. Pt NPs size measured with STEM gave a mean value of 2.5 nm and a homogeneous dispersion of Pt NPs was observed. The catalyst was used for

bromonitrobenzene hydrogenation giving full conversion in less than 15 min. The selectivity to bromoaniline was > 99 %, showing that the Pt/γ-Fe_2O_3 could suppress the hydrodebromination pathway as well.

A similar procedure was used by Neumann et al. increasing the temperature of the synthesis to 150 °C and varying the metal precursors[166]. This allowed preparing Pt NPs with different particle size from 1 to 4 nm. Briefly, commercial Fe_3O_4 support was added to Pt colloidal solutions and a complete deposition of Pt NPs on iron oxide was achieved. Before the reaction, the catalyst was either used as is or pre-treated in a reductive atmosphere. HR-XPS analyses of Fe 2p region were carried out after exposure to the reaction conditions (a mixture of O_2 and CO) on the bare support before and after reductive pre-treatment. Both samples showed the presence of Fe^{3+}, Fe^{2+} and Fe^0 species at 711.5 eV, 710.1 eV and 707.7 eV, respectively, with the main difference being the relative amount of these species (64.2 %, 31.0 % and 4.8 % for the reduced sample versus 76 %, 23.3 % and 0.7 % for the untreated sample, respectively). TEM images confirmed the production of Pt NPs with a narrow size distribution and with the desired average particle size (from 1 to 4 nm). The authors reported that both reduced and unreduced FeOx supports exhibited catalytic activity in the CO oxidation reaction, with a Mars van Krevelen mechanism between CO and lattice oxygen of the FeOx support. Supported Pt NPs on unreduced FeOx showed a strong metal-support interaction. For very small Pt NPs, it was found that CO adsorbed on Pt surface atoms and that the reaction took place at the periphery of Pt-FeOx, with lattice oxygen as the active species. Increasing particle surface, on the other hand, the Langmuir−Hinshelwood mechanism contribution between chemisorbed CO and O_2 on the Pt surface increased. The catalyst reduction treatment caused partial encapsulation of the Pt NPs with the FeOx layer that negatively altered the catalytic properties. However, the authors suggested that the partial coverage of the Pt NPs with the support may have a positive effect on the stability of the NPs against sintering at higher reaction temperature.

Lian et al. reported the synthesis of Pt/Fe_3O_4 by adsorption of Pt colloidal particles with an average size of 1.3 nm[167]. Fe_3O_4 support was prepared by precipitation method from a solution of glycol, urea and iron chloride. From HRTEM images the inter-fringe distances of the Pt and Fe_3O_4 were measured (0.223 nm and 0.252 nm, respectively). The XRD pattern confirmed the presence of Fe_3O_4 phase while no peaks of Pt were detected due to the low loading and the small particles size. The prepared catalyst was used for the solventless hydrogenation of chlorobenzene to chloroaniline, with a final yield > 99 % and no hydrodechlorination side-reactions.

Chen et al. reported the synthesis of amorphous Fe_2O_3 nanosheets (A-Fe_2O_3) with Pt single atoms (SA) to enhance carbon monoxide oxidation[168]. Differently from all the previous cases, no sodium hydroxide was used during the synthesis. SA Pt on Fe_2O_3 were synthesized starting from an EG solution of platinum and iron acetylacetonate. This solution was then heated at 120 °C for 42 h in an autoclave. Pt single atoms with clusters (SC) and Pt sub-nanoparticles (SN) on amorphous Fe_2O_3 nanosheets were prepared following the method used for SA, but Pt precursor amount was increased to 0.075 and 0.12 mmol, respectively (Figure 16). All these catalysts were finally annealed in furnace at 300 °C for 30 min to transform the amorphous support to crystalline (C) Fe_2O_3.

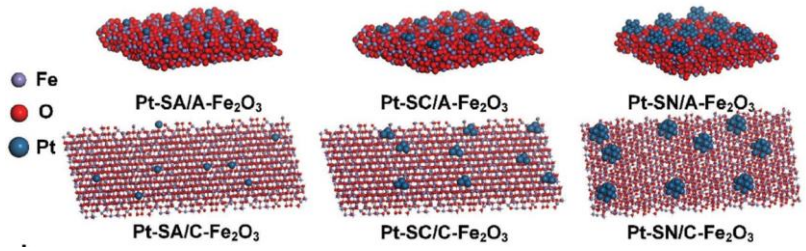

Figure 16. Schematic of the different Pt/Fe_2O_3 structures, different sizes were used to distinguish the elements Adapted from ref [168] © 2019 WILEY-VCH Verlag GmbH & Co. KGaA, Weinheim

TEM images of and Pt-SN/A-Fe_2O_3 displayed small particles on the nanosheets surface. Pt-SA/A-Fe_2O_3 showed a clean nanosheets surface, while Pt-SC/A-Fe_2O_3 exhibited a dust-like surface. HAADF-STEM and HRTEM revealed an average nanosheet thickness of about 3.1 nm. Moreover, HAADF-STEM allowed to identify heavy atoms as bright spots. The images clearly demonstrated the presence of single atoms, clusters (0.8-1.6 nm) and small NPs (2 nm) in the respective catalysts. The XPS spectra of Fe 2p region of the three catalysts exhibited two peaks of Fe $2p_{3/2}$ and Fe $2p_{1/2}$ at 711.3 eV and 724.7 eV, respectively. A small satellite peak was observed at 719.0 eV indicating the presence of Fe_2O_3. As expected, XRD pattern did not show any peaks, confirming the amorphous nature of the support. In Pt-SA/A-Fe_2O_3 and Pt-SC/A-Fe_2O_3 catalysts no Pt diffraction peaks were observed due to the small size of Pt. Instead, in Pt-SN/A-Fe_2O_3 catalyst the peaks of *fcc* Pt were clearly identified, indicating the presence of crystalline Pt NPs. SAED, HRTEM and HAADF-STEM (Figure 17) analyses were performed to validate the amorphous nature of Fe_2O_3. In all the cases no crystal lattice fringes were found.

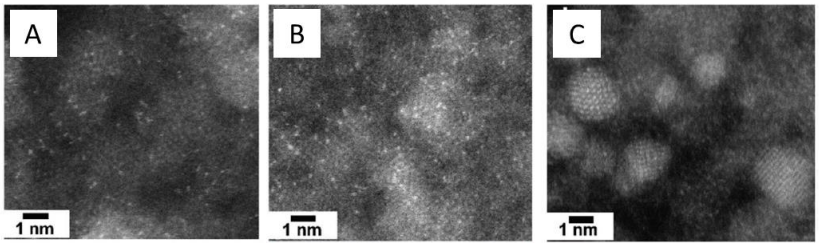

Figure 17. Magnified HAADF-STEM images of **A**) Pt-SA/A-Fe_2O_3, **B**) Pt-SC/A-Fe_2O_3, and **C**) Pt-SN/A-Fe_2O_3 Adapted from ref [168] © 2019 WILEY-VCH Verlag GmbH & Co. KGaA, Weinheim

EXAFS curve of Pt-SA/A-Fe_2O_3 indicated a Pt-O coordination that was assigned to a Pt atom coordinated with Fe_2O_3. This four-coordination structure was preferred by low-valent Pt complexes (or zerovalent Pt) and the close Pt-O bond distance respect to pure PtO_2, suggesting a strong metal-support interaction[134,169]. Pt-Pt distance appeared when Pt loading increased indicating the formation of very small Pt clusters composed by irregular Pt atoms. The annealing of these three catalysts at 300 °C transformed the amorphous Fe_2O_3 in crystalline Fe_2O_3. XRD patterns recorded after the phase transformation clearly showed the Fe_2O_3 diffraction peaks, demonstrating the crystalline structure of the support (Figure 18A). This observation was further confirmed by HAADF-STEM images which clearly showed the crystal lattice fringes of Fe_2O_3 (Figure 18B, C and D). Despite the high temperature used during the heat treatment, no Pt agglomeration occurred during the annealing process. The atomically dispersed Pt SA on ultrathin amorphous Fe_2O_3 nanosheets showed great activity in the CO oxidation reaction due to its high specific surface area, full exposed atoms sites, and the synergistic effect between the atomically dispersed Pt single atoms and the amorphous Fe_2O_3 support. In addition, the authors reported superior activity of the Pt-SA/A-Fe_2O_3 compared to the other synthesized catalysts due to several reasons, such as: 1) the strong binding and stabilization of single Pt atoms coming from the strong metal-support interaction between the in situ locally synthesized Pt atoms and Fe_2O_3 supports; 2) the weak CO adsorption on Pt and an enhanced O_2 adsorption on nearby Fe_2O_3 due to the single-atom configuration; 3) the active abundant sites to activate O provided by amorphous Fe_2O_3, which further facilitated the oxidation of adsorbed CO on the neighboring Pt or on the interface between Pt and Fe_2O_3.

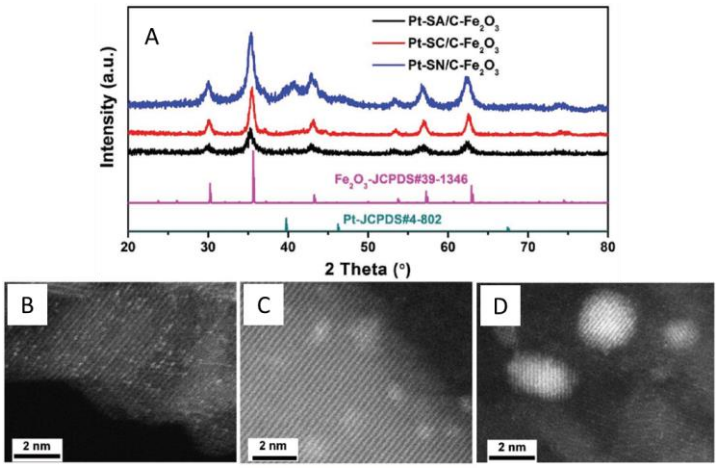

Figure 18. A) XRD pattern of annealed catalysts, and HAADF-STEM images of **B**) Pt-SA/A-Fe_2O_3, **C**) Pt-SC/A-Fe_2O_3, and **D**) Pt-SN/A-Fe_2O_3 Adapted from ref [168] © 2019 WILEY-VCH Verlag GmbH & Co. KGaA, Weinheim

Liu et al. reported the synthesis of Pt/Fe_2O_3 using EG as solvent and polyvinylpyrrolidone (PVP) as stabilizer[170]. The EG metal precursor solution, PVP and the Fe_2O_3 dispersion were separately prepared and simultaneously injected drop-by-drop in a round bottom flask; the resulting suspension was heated at 100 °C and maintained under stirring for 22 h. Finally, the catalyst was recovered, washed with ethanol and dried. SEM and TEM images showed the presence of flake-shape structures with a mean length of 50 nm belonging to cubic-phase Fe_2O_3. Well-dispersed Pt NPs with a size range of 3-6 nm were observed indicating a successful immobilization of Pt NPs on the iron oxide support. N_2 adsorption-desorption analyses revealed a mesoporous structure of the support. Moreover, the BET surface area was calculated and Pt/Fe_2O_3 catalysts exhibited a higher surface area (45 m^2 g^{-1}) than the bare support (34 m^2 g^{-1}), while the pore size did not change after Pt loading. The oxidation state of the samples was investigated by XPS analysis. XPS spectrum of Fe 2p showed two characteristic peaks at 724.4 eV and 709.7 eV which were attributed to Fe $2p_{1/2}$ and Fe $2p_{3/2}$, respectively. These two signals indicated the presence of Fe^{3+} species. Considering the Pt 4f HR spectrum, Pt $4f_{7/2}$ and Pt $4f_{5/2}$ peaks appeared at 73.1 eV and 76.3 eV, respectively. Both peaks were assigned to the presence of Pt^0. Interestingly, the binding energy of Pt 4f in the Pt/Fe_2O_3 sample was higher than that of Pt standard, suggesting an electron transfer between Pt NPs and the iron oxide. The magnetically recoverable flake-like catalyst showed good catalytic performance in the hydrogenation of various nitrobenzenes (yield > 99 %) as well as in the hydrogenation of other functional groups (carbonyl bonds and C-C double and triple bonds). Excellent recycling durability was demonstrated using nitrobenzene and phenylacetylene as substrates, showing no loss of activity over 10 reaction runs.

Differently from the above colloidal methods, Zhang et al. reported the synthesis of Pt/Fe_2O_3 micro-flower using hydrothermal method for the preparation of the support[171]. Therefore, an EG/H_2O solution was used instead of pure EG. γ-Fe_2O_3 micro-flower support (Fe_2O_3-MF) was prepared by low-temperature hydrothermal synthesis using iron chloride and urea. The mixture composed by water, EG, urea, and iron chloride was heated at 180 °C for 15 h in an autoclave. EG-reduction method was employed for loading Pt NPs on the surface of Fe_2O_3-MF. For comparison, a Pt/Fe_2O_3 catalyst was synthesized using commercial iron oxide. BET surface area of bare support and Pt supported NPs was the same in both samples and meso and micro porosity was found. XRD pattern showed the peaks associated to γ-Fe_2O_3 and after the Pt loading no changes in the crystal structure of the support occurred. The morphology of Fe_2O_3-MF was analyzed by SEM.

The images clearly showed a unique flower-like morphology with a nanosheet thickness of 52-62 nm. Pt NPs anchored on the flower-like support had a narrow particle size distribution (0.6-2.4 nm) with an average diameter of 1.5 nm. XPS analyses demonstrated that the oxidation state of Fe species was consistent to that of Fe_2O_3, while the deconvolution of Pt 4f region clearly indicated the presence of both Pt^0 and Pt^{2+} with a Pt^0/Pt^{2+} atomic ratio of 1. Besides, the calculated Pt/Fe ratio based on XPS and ICP analyses gave quite different results. In particular, Pt/Fe ratio evaluated with XPS (0.43) was one order of magnitude higher than the one calculated with ICP analysis (0.025). This meant that Pt NPs were mainly located on the surface of Fe_2O_3 MF. The large specific surface area and abundant macropores and mesopores of the MF support proved to be beneficial in the reduction of 4-nitrophenol to 4-amminophenol when compared to a conventional Pt/Fe_2O_3 catalyst of the same Pt loading, where full conversion of 4-NP is obtained within 12 min under ambient conditions. The catalytic activity of the Pt/Fe_2O_3-MF showed no apparent loss within 10 consecutive cycles, implying a very good stability.

Hong et al. reported the synthesis of Pt/Fe_2O_3 nanocables using platinum acetylacetonate and oleylamine[172]. These two chemicals were mixed at room temperature and then heated at 120 °C for 20 min in inert atmosphere. Then $Fe(CO)_5$ was injected and the temperature was raised to 160 °C for 30 min. Finally, the obtained material was washed with ethanol and dispersed in hexane. The iron oxide nanowires showed a diameter of 2.8 nm and XPS analysis confirmed the iron oxide structure (Fe_2O_3). The material was used for the selective oxidation of olefins and alcohols to ketone or aldehyde, showing promising results compared to other similar Pt-iron oxide systems.

Finally, Li et al. prepared PtFe supported on mesoporous zeolite beta (Pt/FemBETA) with a combination of ion exchange and colloidal method[173]. Fe addition into zeolite beta (mBETA) framework was performed by ion exchange. Different amount of iron nitrate was added to mBETA and the obtained Fe-mBETA material was calcined at 550 °C for 8 h. Then Pt nitrate aqueous solution was mixed with Fe-mBETA dispersed in ethylene glycol. The mixture was stirred at 40 °C for 6 h, recovered and dried for 1 day at 100 °C. XRD pattern showed the characteristic diffraction peaks of mBETA while no Pt and FeOx species were detected. Interestingly, increasing the Fe amount the diffraction peak intensity decreased, suggesting that some Fe ions entered in the zeolite framework. SEM images did not show any particles aggregation and Pt NPs size range was 2-5 nm (Figure 19 A-D). N_2-adsorption isotherm confirmed the presence of mesoporous structure and the surface area was estimated in the range of 528-590 $m^2\ g^{-1}$. XPS analyses (Figure 19E) revealed the presence of both Pt^0 (67 %) and Pt^{2+} (33 %) at 71.3 eV and 72.4 eV, respectively. Fe 2p HR spectrum exhibited two Fe species: Fe^{3+} at 714.4 eV and Fe^{2+} at 711.2 eV. The insertion of Fe atoms into the zeolite framework was also confirmed by HR spectra of O 1s. The peaks at 532.8 eV was assigned to the chemisorbed oxygen species that is related to the presence of oxygen vacancies (derived from the doping of Fe atoms). The interaction between Pt and FeOx was studied using TPR analysis, where a shift of the reduction peak of Fe_3O_4 to lower temperature suggested a synergic effect. Among the different Pt/Fe ratio tested, the sample containing 9.3 % of Fe showed excellent catalytic activity and high water resistance in the CO oxidation reaction. Complete CO conversion was obtained at a reaction temperature as low as 78 °C, with unaltered performance over 100 h working hours in the presence of H_2O. The authors ascribed the improved performance to the high surface area and pore volume of the zeolite beta, which favored the dispersion of active Fe and Pt species and the diffusion of reaction gas, as well as to the synergetic effect between Pt and Fe which greatly accelerates CO oxidation.

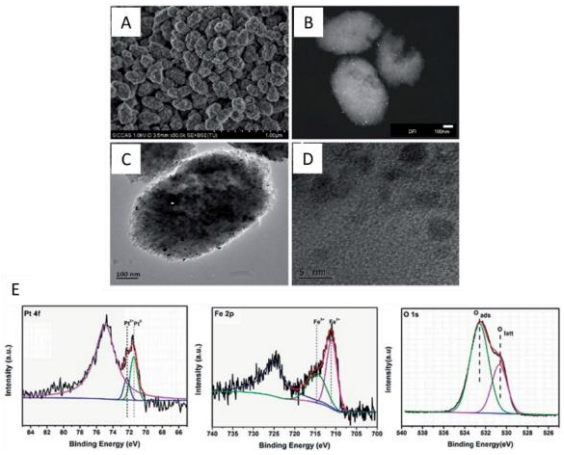

Figure 19. **A**) Typical SEM images, **B**) the DFI image and **C-D**) TEM images of Fe(3)–mBeta. **E**) XPS spectra of Pt 4f, Fe 2p and O 1s of the sample Pt/Fe(3)–mBeta. Reproduced from ref [173] Published by The Royal Society of Chemistry 2019

Among the colloidal methods, the sol-immobilization technique allows to obtain NPs with a narrow distribution and the size of NPs can be varied changing the amount of stabilizing agent, the temperature, the solvent and other experimental parameters[174]. In this case, the reduction of the metal precursor is performed using a strong reducing agent such as $NaBH_4$, and therefore high temperatures can be avoided.

Zhang et. al prepared a layered double hydroxides (LDHs) composed by Fe(II)-Fe(III) on which Pt NPs were subsequently immobilized[175]. The support was prepared mixing $FeSO_4 \cdot 7H_2O$ and $Fe_2(SO_4)_3$ in decarbonated deionized water. A NaOH solution was dropped until pH=7 and the suspension was stirred for 2 h in an ice bath. The precipitate was finally washed and dried under vacuum. Pt/Fe-Fe LDH NPs were prepared by sol-immobilization using poly(N-vinyl-2-pyrrolidone) as stabilizer and $NaBH_4$ as reducing agent. Firstly, the Pt precursor was dissolved in water and the stabilizing agent was added. Then a fresh solution of $NaBH_4$ was added under vigorous stirring for 7 h to reduce the Pt precursor to metallic Pt. Afterwards, Fe-Fe LDH support was added, and the dispersion was stirred for 2 h. The obtained catalyst was finally recovered and dried. XRD patter showed typical characteristic planes of hydrotalcite-like phase. Moreover, two diffraction peaks at low angles (8.1° and 10.0°) were attributed to presence of interlayer sulfate anions. SEM images clearly demonstrated the formation of large and uniform LDH nanosheets with a thickness of about 20 nm. Their surface area calculated from N_2 adsorption-desorption experiments was 72 $m^2\ g^{-1}$. TEM and HRTEM images did not show any NPs aggregation and uniform dispersion of 3.4 nm Pt NPs was found. The evaluation of the lattice fringes from HRTEM images and HR XPS spectra of Pt 4f region confirmed the reduction of Pt precursor to Pt^0 (Figure 20). The catalyst was applied in the selective hydrogenation of cinnamaldehyde to cinnamyl alcohol, showing higher selectivity (91 % at 90 % cinnamaldehyde conversion) compared to other Fe-containing LDHs-supported Pt catalysts. In situ IR spectra of cinnamaldehyde adsorption showed that Pt/FeFe-LDH could more easily activate the carbonyl group in cinnamaldehyde and reduce the probability of coordination of the C=C bond to the active metal sites. In addition, the introduction of Fe^{2+} into the brucite-like layers of LDHs could promote the interactions between Pt species and the LDH matrix, thus forming surface electron-rich Pt^0 species; this induced the promoted activation of the carbonyl group in cinnamaldehyde. Finally, compared with other Fe-containing LDH supports, FeFe-LDH enabled Pt species to be more tightly immobilized on the surface due to a stronger Pt-LDH interaction, thus leading to a good reusability of the catalyst.

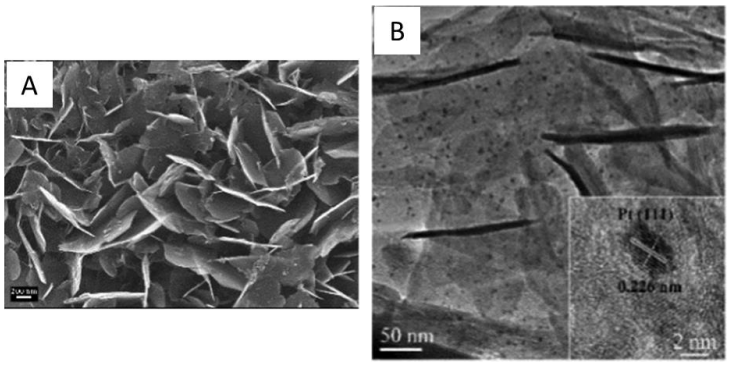

Figure 20. A) TEM images of the Pt/Fe-Fe HDL and **B**) HRTEM of Pt/Fe-Fe HDL and Pt lattice fringe evaluation Adapted from ref [175] Copyright © 2018 American Chemical Society

- Co-precipitation

Pt/FeOx catalysts can also be prepared by the traditional co-precipitation process. The oxidation state of the iron support can be controlled and regulated by varying the type of precipitating agent and the calcination conditions.

Wei et al. reported the synthesis of Pt/FeOx with a Pt NPs size of 1 nm[176]. Chloroplatinic acid and ferric nitrate were mixed with ammonia carbonate that was used as precipitating agent. The mixture was stirred for 3 h at 50 °C. After the recovery, the catalyst was calcined for 5 h at 400 °C. XRD pattern revealed that the support was only composed by Fe_3O_4 phase. No diffraction peaks of Pt were detected due to the small particle size. HAADF-STEM images showed the presence of very small Pt NPs (0.4 nm) homogeneously distributed on the iron oxide support. After the reduction, almost 100 % of Pt was found in the metallic state. The catalyst was used for the chemoselective hydrogenation of 3-nitrostyrene giving a conversion > 98 % with a selectivity of 66 %, although higher selectivity was obtained when the catalyst was doped with alkali metal cations such as Na^+.

- Other techniques

Beside the most common synthetic methods, metal vapour synthesis, redox reaction and strong electrostatic adsorption (SEA) can be applied for the synthesis of Pt/FeOx catalysts. Evangelisti et al. reported the synthesis of Pt/γ-Fe_2O_3 using metal vapor synthesis[177]. Pt vapor was generated by heating a tungsten wire coated with Pt and then condensed with mesitylene at liquid nitrogen temperature. To stabilize the mesitylene solvated Pt solution at room temperature 1,3-divinyl-1,1,3,3-tetramethyldisiloxane was added. The stabilized Pt NPs solution was finally added to γ-Fe_2O_3, thus producing Pt/γ-Fe_2O_3 catalyst. TEM images showed a narrow size distribution with small Pt NPs (1.2 nm) well dispersed on the support surface. XPS HR spectra of the Pt 4f region was deconvoluted in two peaks at 71.40 eV and 72.66 eV, which were assigned to Pt^0 and $Pt(OH)_2$, respectively. Interestingly, the biding energy of metal Pt was positively shifted respect to literature reports (71.00 eV), indicating an electron transfer from Pt NPs to the iron oxide support. The quantitative analysis revealed that Pt^0 amount was about 85 % of the total Pt. Furthermore, the HR spectrum of Fe 2p confirmed the oxidation state of iron, while O 1s spectrum suggested the presence of iron oxide (530.0 eV), OH groups bonded to $Pt(OH)_2$ (532.0 eV), and OH groups adsorbed on the catalyst surface. Therefore, the prepared catalyst displayed an interaction between Fe_2O_3 and Pt NPs, resulting in an electron-deficient state of Pt. This catalyst showed better activity towards hydrogenation of halonitrobenzenes than a Pt/γ-Al_2O_3 catalyst prepared with the same method, as well as selectivity higher than 98 % towards the corresponding haloaniline. The author ascribed the improved reactivity of the nitro group of the aromatic substrate to the

electron-deficient state of the Pt NPs. In addition, the catalyst could be used for at least 5 times without appreciable decline of its catalytic efficiency or permanent modification of its chemical and electronic structure.

Zhou et al. synthesized Pt/Fe_3O_4/reduced graphene oxide (rGO) catalysts using a two-step microwave-assisted solvothermal method[178]. Firstly, Fe_3O_4/rGO material was prepared by adding rGO support to a solution of NaOH in diethylene glycol. Then anhydrous $FeCl_3$ was added and the mixture was refluxed at 220 °C for 30 min. The Pt NPs supported on Fe_3O_4/rGO were prepared by adding H_2PtCl_6 to Fe_3O_4/rGO material. This composite was dispersed in EG and put in a microwave reactor at 165 °C for 1.5 min. The final catalyst was washed and dried at 100 °C. The Fe_3O_4 and Pt NPs were hard to separate by TEM analysis, but from HR-TEM images the lattice fringes of Pt<111> and Fe_3O_4<311> were observed. Pt and Fe_3O_4 NPs with an average diameter of 3.6 nm and 7.5 nm, respectively, were well dispersed on rGO support. XRD analysis confirmed the presence of Fe_3O_4 and Pt<111>. Moreover, the dispersion of Pt NPs was evaluated using different techniques. Firstly, the geometrical surface area was calculated considering a semi-spherical shape. The dispersion and the geometrical surface area were 11.2 % and 79 $m^2\ g^{-1}$, respectively. The electrochemical active surface area (EAS) confirmed the better dispersion of Pt in the Pt/Fe_3O_4/rGO catalyst than in a Pt/rGO composite used for comparison. All these results were further verified by H_2 chemisorption, where an active surface area of 86.2 $m^2\ g^{-1}$ and 93.2 $m^2\ g^{-1}$ was calculated for Pt/rGO and Pt/Fe_3O_4/rGO, respectively. To correlate the surface structure and the electronic effect, XPS analyses were performed (Figure 21). Pt 4f HR spectra displayed a doublet at 70.0 eV and 74.4 eV associated to metallic Pt, and other two peaks at 72.2 eV and 76.2 eV that corresponded to Pt^{2+}. The binding energies of these peaks were higher (+0.2 eV) than the ones of Pt/rGO and an inverse behavior was found for Fe species (-0.1 eV). This suggested that iron oxide might obstruct the electron transfer from rGO to Pt. Therefore, the synergistic effect of FeOx and Pt was confirmed by XPS analyses. The as synthesized Pt/Fe_3O_4/rGO was tested in the selective oxidation of HMF along with the Pt/rGO as a comparison. The authors found that the activation of alcohol and aldehyde was enhanced at the interface of Pt/Fe_3O_4, which greatly improved the catalytic performance in the studied reaction. In addition, the catalyst could be easily magnetic recycled and reused without significant loss of activity after 5 reaction cycles.

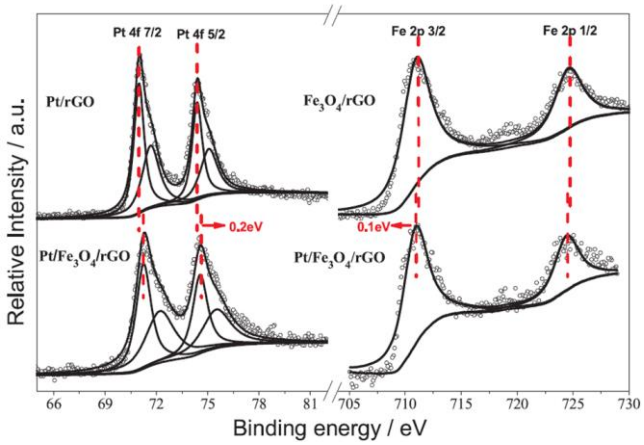

Figure 21. XPS spectra for Pt/rGO, Fe_3O_4/rGO and Pt/Fe_3O_4/rGO. Reproduced from ref [178] © 2018 Elsevier B.V.

Zhang et al. reported a flexible one-pot synthesis of Pt/Fe_3O_4 using a redox reaction which occurs from Pt(IV) and Fe(II)[179]. The reducible $FeO(OH)^{\delta+}$ can progressively attract negative $PtCl^{4-}$ ions via their mutual

electrostatic interaction in alkaline medium. The nitrogen flow used during all the synthesis excludes the possibility that Fe^{2+} could be oxidized by O_2 rather than by the Pt precursor. A solution of $FeSO_4$ was added to an aqueous solution of NaOH under N_2 flow. Then, H_2PtCl_4 solution was quickly added to the mixture under vigorous stirring. The dispersion was treated at 70 °C for 4 h and then recovered with a magnet and washed many times with ethanol and water. Finally, the catalyst was dried in a vacuum oven at 60 °C. The prepared catalysts were named $Pt/Fe_3O_4(x)$, where "x" is the molar ratio between Fe and Pt. From XRD pattern Fe_3O_4 phase was detected, as well as Pt <111> in $Pt/Fe_3O_4(50)$ and $Pt/Fe_3O_4(100)$ samples. O_2–H_2 pulse titration allowed the evaluation of Pt NPs dispersion and size. The catalysts with low loading of Pt showed poor dispersion of Pt due to inefficient H_2 adsorption, and Pt NPs size was in the range of 2.1-6.8 nm. However, increasing the Pt content, the redox reaction can offer more Pt active site, thus increasing H_2 adsorption. N_2 adsorption-desorption isotherm curves showed a IV type adsorption isotherm which denoted a mesoporous structure. TEM images showed that iron oxide NPs had a spherical shape with an average diameter of 80-100 nm. EDS mapping displayed uniform Pt NPs distribution that became more uniform and regular increasing the Pt content. This suggested that Pt content influenced the NPs morphology. Furthermore, the interaction between Pt and iron oxide was studied using XPS analysis. Pt high resolution spectrum showed two peaks at 71.3 eV and 74.6 eV, which were assigned to Pt $4f_{7/2}$ and $4f_{5/2}$, respectively. Both Pt^{2+} and Pt^0 species were found after the deconvolution. The catalysts were used for the chemoselective hydrogenation of cinnamaldehyde. The authors found that the inherent variable electron transfer of Fe_3O_4 drove electrons to metallic Pt nanocrystallites, which promote the adsorption of cinnamaldehyde on the surface of Pt metal via terminal C=O group, showing prominent catalytic activity and high selectivity to cinnamyl alcohol under mild reaction conditions. In particular, the catalyst with a Fe:Pt molar ratio of 100 was found to be the most active among the materials tested; the same catalyst could also be used for 5 cycles with only a slight activity loss.

Finally, Navas-Cardenas synthesized $Pt/FeOx/TiO_2$ catalyst using strong electrostatic adsorption method (SAD)[148]. This catalyst was used for the preferential oxidation of CO. The SAD synthesis allowed the preparation of well dispersed Pt NPs on carbon or metal oxide taking advantage of the surface charge that can be generated on the support varying the pH. Therefore, point of zero charge (PZC) analysis were employed to determine the optimal conditions for the adsorption of Pt precursor on the catalyst surface. $FeOx/TiO_2$ was prepared by incipient wetness impregnation using commercial TiO_2 (P25) and iron nitrate. Then, H_2PtCl_6 was dissolved in nitric acid solution and it was added to $FeOx/TiO_2$ support. The solid was then recovered and calcined at 200-300 °C and further reduced in-situ with H_2 for 1 h at 100 °C. The support exhibited a surface area of 45 $m^2\ g^{-1}$ with a PZC of 5.4. The Pt adsorption capacity was evaluated and $Pt/FeOx/TiO_2$ showed a maximum adsorption at pH lower than the PZC of the support. Moreover, the $FeOx/TiO_2$ support was able to adsorb a higher amount of Pt than the bare TiO_2 due the presence of higher concentration of hydroxyl groups. The highest Pt adsorption density was reached at pH 3 and 4 for TiO_2 and $FeOx/TiO_2$, respectively (Figure 22A). In these acidic conditions the surface of the support was protonated, allowing the electrostatic adsorption of Pt anionic species onto its surface. The H_2-TPR profile showed an interaction between Pt NPs and iron oxide. In fact, two reduction peaks at 280 °C and 440 °C were assigned to the reduction of Fe^{3+} to Fe^{2+} and of Fe^{2+} to Fe^0, respectively. The lower temperature of this sample in comparison to those of $FeOx/TiO_2$ suggested that Pt was able to promote the reduction of FeOx and TiO_2 by hydrogen spillover[180]. Furthermore, a reduction peak at low temperature (ca. 100 °C) was assigned to Pt-O-Fe species, which suggested a preferential deposition of Pt on the FeOx surface. The superficial oxidation state was studied by XPS analyses (Figure 22C), revealing the presence of Fe^{2+}, $Fe^{δ+}$, Fe^{3+}, and Pt-FeOx moieties at 704.9 eV, 711.1 eV, 713.1 eV, and 715.5 eV, respectively. The HR spectra of Pt 4f region showed the presence of Pt^0, Pt^{2+} and Pt^{4+} at binding energies of 71.0 eV, 72.5 eV and 74.3 eV, respectively. These binding energies were shifted to higher values than those of Pt/TiO_2, confirming the intimate contact of Pt NPs with FeOx species. TEM images of $Pt/FeOx/TiO_2$ catalysts calcined at 200 °C and 300 °C exhibited a good Pt dispersion with an average NPs size of 1.7 nm and 1.2 nm, respectively (Figure 22B). The catalyst was compared with monometallic Pt/TiO_2 and $Pt/CoOx/TiO_2$ in the preferential oxidation of CO to CO_2, showing

higher conversion at lower reaction temperature (50 % conversion at 100 °C, compared to 10 % and 20 % respectively) with 60 % of the product being CO_2. Similar performance required higher reaction temperature for the Co-based catalyst (> 150 °C).

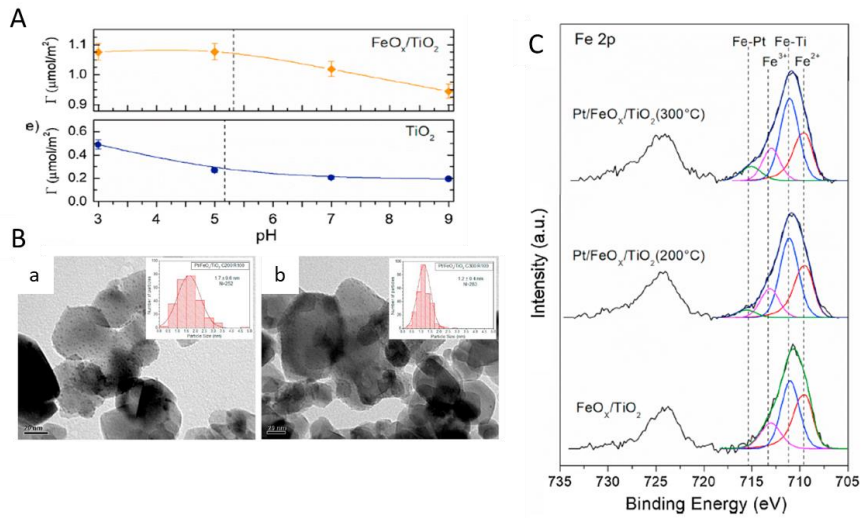

Figure 22. A) Pt adsorption capacity measurements at different pH. **B**) TEM images of $Pt/FeOx/TiO_2$ calcined at a) 200 °C and b) 300 °C. **C**) XPS HR-spectra of Fe 2p region. Adapted from ref [148] © 2019 Elsevier B.V.

2.2.2 PtFe and PtFeOx nanoparticles supported on metal oxides and carbonaceous materials

- Impregnation

Impregnation method is widely used for the synthesis of PtFe supported NPs and sometimes ultrasound assisted impregnation is used to prepare catalysts with a high metal dispersion. Saravanan et al., and Hu and co-workers prepared PtFe bimetallic NPs supported on commercial Al_2O_3 using impregnation technique[181,182]. Saravanan et al. prepared ordered intermetallic $PtFe/\gamma\text{-}Al_2O_3$ catalysts by wet impregnation from H_2PtCl_6 and iron(III) 2,4-pentanedoinate[181]. The powder was reduced at 800 °C for 8 h under H_2 flow. Two different intermetallic Pt-Fe systems were synthesized: Pt_3Fe and $PtFe_3$. XRD profiles showed characteristic peaks of $\gamma\text{-}Al_2O_3$ and cubic ordered intermetallic Pt_3Fe (or $PtFe_3$), while no peaks associated to iron oxide or platinum oxide were detected. TEM images of Pt_3Fe NPs of about 4 nm showed NPs with a semi-spherical shape and homogeneously dispersed on the support. HRTEM of the same NPs displayed atomic fringes corresponding to <200> plane of Pt_3Fe. Analogous results were obtained for $PtFe_3$ NPs which exhibited slightly larger mean particle size (6 nm). Moreover, ICP-OES experiments confirmed the composition of the intermetallic Pt-Fe systems which was very close to the calculated value. Both catalysts were used for CO oxidation, where the intermetallic $PtFe_3$ NPs showed higher activity compared to Pt_3Fe (81 % conversion at 75 °C, compared to 9 % at the same reaction temperature). Despite having the same Pt-mass loading, the higher activity of the $PtFe_3/Al_2O_3$ was ascribed to a larger extent of <200> intermetallic surface plane and the presence of larger particles as well. On the other hand, both catalysts displayed similar activity when applied in the benzene oxidation reaction at different temperatures (from room temperature to 250 °C). Catalyst reusability was demonstrated for both intermetallic structures, in terms of crystallographic structure and particle morphology.

Hu et al. prepared $PtFe/Al_2O_3$ catalysts by impregnating Pt/Al_2O_3 prepared by atomic layer deposition[182]. Pt/Al_2O_3 was impregnated with iron nitrate at pH=3 and dried at 110 °C. Moreover, the sample was calcined at 500 °C for 2 h in air and reduced for 3 h at 400 °C in H_2/Ar atmosphere. Different catalysts were prepared varying the amount of Fe from 0.5% to 5 %wt. TEM images showed a homogeneous distribution of PtFe NPs on the spherical support. The NPs possessed an average diameter of 2.9 nm with a size range within 1-7 nm. The lattice fringes measurement of 0.225 nm was assigned to Pt <111> plane. XRD analysis was also performed, but only peaks associated to Al_2O_3 were detected. The surface electronic properties were evaluated by XPS measurements. The HR spectrum of Pt 4d region showed the presence of Pt^0 and Pt^{4+} species at 314.3 eV and 318.1 eV, respectively and the Pt^0 amount was higher than that of Pt^{4+}. The catalyst prepared with impregnation method exhibited lower activity in cinnamaldehyde hydrogenation than the same catalyst prepared by atomic layer deposition of Fe onto Pt/Al_2O_3.

Pan et al. co-impregnated an Al_2O_3@SBA-15 support (15AS) with iron nitrate and H_2PtCl_6[141]. SBA-15 is an interesting mesoporous silica material having highly ordered nanopores and a large surface area, which is widely employed as catalyst support. The impregnated support was calcined for 3 h at 500 °C and reduced with H_2 at the same operating conditions. The synthesized PtFe/15AS catalysts were prepared varying the amount of iron, thus the Fe/Pt molar ratio was changed in the range of 0.1-1. N_2-adsorption measurements showed the characteristic IV type hysteresis, indicating that the mesoporous structure of SBA was maintained after the impregnation. Moreover, the surface area did not change increasing the amount of Fe (409-425 m^2 g^{-1}). XRD patterns displayed the diffraction peak of Pt <111> at 39.8°, which was considerably suppressed by decreasing the Pt/Fe molar ratio. This meant that the addition of low amount of iron had a strong impact both on the dispersion of Pt NPs and their size. To further characterize the NPs size, HAADF-STEM electron microscopy was used (Figure 23A). The images showed that Fe atoms were well distributed on the support, while Pt NPs formed some aggregations. Nevertheless, the signal of Pt and Fe were overlapped, suggesting that Pt NPs are closely related to Fe entities. HRTEM images were also recorded and lattice fringe of Pt<111> was detected (Figure 23B). Moreover, to better study the electronic properties, DRIFT analyses were carried out. For all the catalysts, only one adsorption mode of CO was detected at about 2073-2081 cm^{-1} that indicated a lack in the electron density respect to the monometallic Pt catalysts. XPS spectroscopy was performed to evaluate the oxidation states of Pt and Fe species (Figure 23C). The dominant species was $Pt^{\delta+}$ that indicated an electron-deficient state of Pt NPs, possibly due to electron transfer from Pt atoms to FeOx species. Finally, TPR analyses were performed to confirm the interaction between Pt and Fe. Two main adsorption peaks were detected at 104 °C and 399 °C. These values were about 44 °C higher than those of monometallic Pt/15AS, thus confirming a strong and intimate Pt-FeOx interaction. The different PtFex/15AS catalysts were used for the selective hydrogenation of cinnamaldehyde, demonstrating good activity and selectivity to cinnamyl alcohol even under mild reaction conditions. In particular, the reaction rate of the PtFex/15AS catalysts varied with the Fe amount, and a volcano-like curve between the reaction rate and the Fe/Pt molar fraction was observed; maximum mass-specific rate was obtained with an Fe/Pt molar ratio of 0.25, with a selectivity to COL of 77 %. According to the authors, the Pt species with positive charges are beneficial for the preferential adsorption and activation of terminal C=O groups, while FeOx species assisted the adsorption of the same functional group.

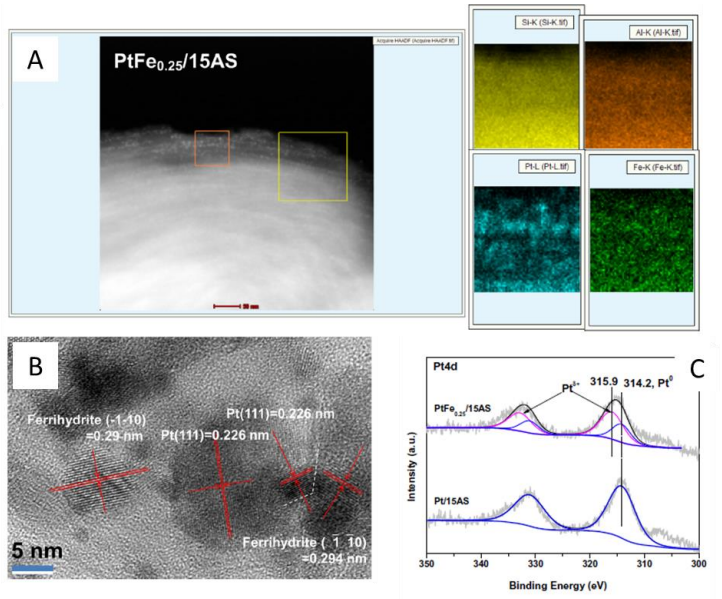

Figure 23. A) HAADF-STEM with relative element mapping of $PtFe_{0.25}$/15AS. **B**) HRTEM and lattice fringe evaluation of $PtFe_{0.25}$/15AS. **C**) HR-XPS spectra of Pt 4d species of Pt/15As and $PtFe_{0.25}$/15AS. Adapted from ref [141] © 2017 Elsevier Inc.

Wang et al. used impregnation method for the preparation of PtFe/HPZSM-5[183]. The support was synthesized by partial desilication of zeolite ZSM-5. Pt and Fe were impregnated on the support using an ethanolic solution of ferric trichloride and chloroplatinic acid, giving a final Pt content of 5 wt% and a Fe:Pt molar ratio of 0.25. The catalyst was dried and then calcined at 400 °C for 4 h in static air and reduced for 2 h at 400 °C with a hydrogen flow. XRD analysis of PtFe systems did not reveal any intense peak of Pt species, demonstrating that the addition of Fe helps the dispersion of Pt NPs. In fact, HRTEM images showed a good dispersion of Pt NPs with an average size of 3 nm. N_2-adsorption isotherm displayed a typical behavior belonging to mesoporous structure. Moreover, FT-IR spectroscopy was performed to study the surface geometry using CO as probe molecule. Two linear CO bands were observed at 2089 cm^{-1} and 2062 cm^{-1} which were attributed to CO adsorbed on Pt<111> and Pt<110>, respectively[184]. Furthermore, the surface properties of PtFe/HPZSM-5 were studied by XPS analysis. The bimetallic catalyst showed a Pd^0 amount (82.2 %), which was higher than the monometallic catalyst (7.9 %). This suggested a strong interaction between Pt and Fe NPs as well as an electron transfer from Fe to Pt. Finally, TPR measurements confirmed that behavior since a much higher reduction temperature of PtFe catalysts was detected respect to the monometallic catalyst. The bimetallic catalyst showed excellent activity towards the selective hydrogenation of cinnamaldehyde to cinnamyl alcohol, with a selectivity of 87.6 % calculated at 97.9 % of cinnamaldehyde conversion. The authors ascribed the enhanced activity compared to a standard monometallic Pt/ZSM-5 catalyst to Fe doping, which provided electron transfer from Fe species to Pt atoms, as well as to partial desilication of ZSM-5 which altered the surface geometry of Pt NPs. In addition, good stability was reported with no obvious loss in activity or selectivity after 9 recycles.

PtFe bimetallic NPs can be also prepared using carbon as support. Chen et al. prepared PtFe/activated carbon (AC) by a two steps impregnation technique for the selective hydrogenation of *p*-chloronitrobenzene[185]. Firstly, iron nitrate solution was added to the support and stirred for 24 h. Then, H_2PtCl_6 was added dropwise

to the mixture and the dispersion was stirred for an additional 24 h. Finally, the impregnated sample was reduced with an aqueous solution of $NaBH_4$. The obtained catalyst was then dried and calcined in air flow. As reported in previous works, XRD analysis did not show any characteristic peaks of metallic Pt, while a peak at 44.4° was assigned to Fe<110> plane. TEM images revealed a well distribution of Pt and Fe NPs with an average diameter of 4.5 nm and a size distribution from 3 to 7 nm. Moreover, HR spectra of Fe 2p region revealed the presence of Fe^{3+}, $Fe^{8/3+}$ and Fe^{2+} which corresponded to Fe_2O_3, Fe_2O_4 and FeO, respectively. The HR spectra of Pt 4f region exhibited a higher binding energy than metallic Pt, indicating the electron transfer between Pt^0 and Fe_2O_3 species formed on the surface of the NPs during the calcination step. The authors reported full conversion of *p*-chloronitrobenzene to the corresponding aniline, with the catalytic performance unaltered after 4 consecutive ~~reaction~~reactions.

Xu et al. prepared PtFe NPs supported on carbon black (CB) using co-impregnation method by adding iron nitrate and H_2PtCl_6 to the CB support[52]. The obtained catalyst was reduced in pure H_2 for 2 h at 450 °C. Differently from other preparations, the reduced sample was added to dilute HNO_3 at room temperature for a leaching treatment. After the leaching, the sample was either analyzed as is or calcined in air for 1 h at different temperatures. XRD pattern of the un-leached sample showed the characteristic peak of cubic *fcc* Pt<111> at 40.0°, which is higher than that of pure Pt (39.8°) indicating inward diffusion of Fe into the Pt lattice upon high temperature treatment in reductive atmosphere and therefore formation of a PtFe alloy. After leaching treatment and calcination, an inverse behavior was noticed, with partial Fe diffusion towards the outermost layer of the NPs. During the leaching step only iron was removed in a percentage in a 15-18 % range as confirmed by ICP analyses. TEM images confirmed the presence of *fcc* Pt lattice and the alloyed NPs were dominated by Pt. The particle size range was 1-3 nm and it slightly increased after leaching (1-4 nm). XPS analyses were also performed to study the surface composition. The leached PtFe/CB catalyst that did not undergo calcination showed the presence of a small peaks at 711.3 eV and one at 708.4 eV with higher intensity, corresponding to Fe_2O_3 and metallic Fe respectively; this indicated that the leaching step preserved and exposed the internal alloyed structure composed mainly of Fe^0 species and Fe^{3+} in lesser extent. As expected, upon calcination at 250 °C no surface Fe^0 species were detected. The authors observed low activity towards the complete CO oxidation reaction due to the presence of superficial Fe_2O_3 species formed after the calcination step. These fully oxidized species could however be reduced into reactive FeO species under preferential CO oxidation reaction conditions (excess of H_2) showing increased activity (Figure 24).

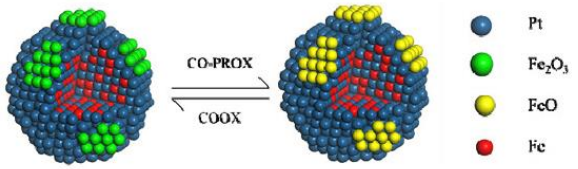

Figure 24. Schematic diagram of the active structures of leached PtFe NPs oxidized at 250 °C under complete CO oxidation (COOX) and preferential CO oxidation (CO-PROX) reaction conditions. Adapted from ref [52] © 2017 Elsevier Inc.

Commentato [S1]: Ask permission

Liu et al. prepared Pt-Fe NPs deposited on multi wall carbon nanotubes (MWNTs)[186]. The catalyst was prepared by co-impregnating iron nitrate and H_2PtCl_6 for 24 h and then dried at 400 °C for 4 h with H_2. TPR profile showed a reduction peak at higher temperature than the monometallic Pt, suggesting an alloy phase which was further confirmed by HR-TEM analysis. The alloy phase was also confirmed by XPS analysis where a shift of Pt signal toward lower binding energy in comparison of monometallic catalyst was detected. Therefore, an electron transfer from iron to platinum was hypothesized. The catalyst was used for furfural hydrogenation giving full conversion and high yield (92 %) towards furfuryl alcohol, as well as good stability over 5 reaction cycles.

Shesterkina et al. prepared $FePt/SiO_2$ catalyst for the hydrogenation of phenylacetylene[57]. The supported bimetallic $PtFe/SiO_2$ was prepared by co-incipient wetness impregnation. Iron nitrate and H_2PtCl_4 aqueous solution was added to the support and then the sample was dried at 110 °C and calcined in air for 3 h at 300 °C. Finally, the sample was reduced at 480 °C for 3 h in hydrogen flow. TEM images showed a good NPs distribution with an average size of 4-5 nm. The reducibility of the calcined samples was studied using TPR analysis. The bimetallic $PtFe/SiO_2$ TPR profiles exhibited two peaks at 100 °C and 160 °C, which were associated to the reduction of Pt oxide to metallic Pt. These temperatures are lower than the respective peak of Pt reduction in monometallic Pt/SiO_2. As already mentioned, the presence of iron oxide helps the reduction of Pt decreasing the reduction temperature. Moreover, other 3 peaks were observed at 230 °C, 360 °C, and 510 °C which were assigned to the reduction of Fe_2O_3 to Fe_3O_4, of Fe_3O_4 to FeO, and FeO to Fe^0, respectively. Furthermore, the metal oxidation state of the calcined sample was estimated using CO-DRIFTS spectroscopy. The band at 2351 cm^{-1} indicated the CO oxidation to CO_2 on Fe^{3+} species, the peak at 2127 cm^{-1} was assigned to CO adsorbed on divalent iron cations (Fe^{2+}-CO), while the band at 2097 cm^{-1} was attributed to linear Pt^0-CO bond[187]. In order to confirm these results, XPS spectroscopy was used and it proved the presence of both Fe and Pt on the support surface. Moreover, a core(Pt)-shell(Fe) structure was hypothesized for the reduced catalysts. The catalytic performance of the catalyst was compared with monometallic Pt/SiO_2 and Fe/SiO_2; highest phenylacetylene hydrogenation rate was obtained with the monometallic Pt catalyst, although selectivity towards styrene decreased drastically at high conversion (reaching selectivity < 10 % over 90 % of conversion). On the other hand, the strong contact interaction between Pt and Fe and the charge transfer from Fe to Pt in the bimetallic particles led to high styrene selectivity (> 70 %) throughout the whole duration of the reaction.

- Colloidal method

PtFe systems can also be prepared by colloidal method. Colloidal method is a well-established synthetic technique for the production of colloidal NPs. Commonly, the colloidal solution can be prepared either at room temperature or at high temperatures (solvothermal/hydrothermal method). Therefore, the reduction process is often initialized by increasing the temperature above the atmospheric boiling point of the solvent (water, alcohol, glycols, polymers, polyamine…) at higher pressures. Cui et al. prepared $PtFe/Al_2O_3$ catalysts for the complete oxidation of formaldehyde[188]. The PtFe colloids were synthesized via a two-steps solvothermal synthesis. Firstly, a glycol solution of NaOH was added to a glycol solution of H_2PtCl_6 and heated at 140 °C. Then a $FeCl_2$ glycol solution was added and Al_2O_3 was inserted when the colloidal solution reached 80 °C. The solid was finally dried and calcined at 200 °C for 2 h. Different catalysts were prepared varying the Fe/Pt atomic ratio. XRD patterns of the catalysts showed the presence of the peaks associated to the support (γ-Al_2O_3) while no peaks related to Pt or Fe species appeared. This means that Fe and Pt species were highly dispersed on the support surface. HRTEM, HAADF-STEM and EDX mapping were performed to investigate the morphology of the NPs. Pt NPs were homogeneously dispersed on Al_2O_3 and the lattice fringes of Pt<111> (0.224 nm) and Al_2O_3<311> (0.239 nm) were detected. Pt NPs mean diameter was 2.2 nm and no evident agglomerations of Pt and iron oxide NPs were observed; EDX maps indicated the presence of finely dispersed iron oxide on the support. H_2-O_2 titration was performed to determine the Pt dispersion. The catalysts with low amount of iron displayed a Pt dispersion of 39 %, while increasing the amount of iron the dispersion decreased. The lower dispersion was attributed to an excess of FeOx species that are covering the Pt NPs. The oxidation state of Pt species was investigated by XPS spectroscopy. The HR spectra of Pt 4d region exhibited two peaks at 314.7 eV and 317.3 eV which were assigned to Pt^0 and Pt^{2+} species, respectively. Interestingly, the Pt species were mainly in the metallic form due to the reduction of the metal precursor in the glycol solution at high temperature. The intensity of the recorded spectra gradually decreases increasing the amount of Fe, confirming that FeOx is covering the Pt NPs surfaces. On the contrary, the HR spectra of Fe 2p region showed an increase in the intensity increasing the amount of Fe. Only Fe^{3+} species were detected in a binding energy range of 709-713 eV. Interestingly, the Fe 2p binding energy of the catalysts prepared with the lowest amount of Fe shifted towards lower values. This behaviour was associated to the interaction

between FeOx and Pt NPs which was established at Pt-FeOx interfaces. The H_2-TPR profile confirmed this interaction since for the Pt-rich samples a peak at about 120 °C appeared. This peak was assigned to the reduction of Pt^{2+} to metallic Pt and to the reduction of FeOx in close contact with Pt. Increasing the Fe amount the peak shifted to 90 °C and its intensity increased. The author hypothesized that this behaviour was due to the formation of more easily reduced FeOx placed at the boundary of Pt. The relatively strong interactions between FeOx and Pt species were able to adjust the redox properties of the $PtFe/Al_2O_3$ catalyst. In particular, by selecting appropriate Fe/Pt molar ratios, highly active $PtFe/Al_2O_3$ catalyst (Fe/Pt molar ratio of 1:1) could be obtained, which achieved complete formaldehyde oxidation at ambient reaction conditions. The authors attributed the excellent catalytic property of this catalyst to the formation of more accessible active sites located at the boundaries between Pt NPs and FeOx species.

Jin et al. reported the synthesis of $PtFe/CeO_2$ catalysts by solvothermal method using dimethyl formamide (DMF) as solvent[147]. One-pot wet chemistry approach was applied to a DMF solution of $Pt(acac)_2$ and $Fe(acac)_3$ mixed with CeO_2. The synthesis occurred at 200 °C and 10 bar of nitrogen varying the Fe/Pt atomic ratio. Moreover, the bimetallic samples were reduced with pure H_2 at 400 °C and denoted as $PtFe_x$-a. TEM images of the not reduced samples evidenced an anisotropic growth of the bimetallic clusters. This behavior was explained hypothesizing an interference of Fe^{3+} species that influence the reduction kinetic via galvanic displacement. Therefore, highly disordered PtFe structures were synthesized after the solvothermal process. Interestingly, the annealed catalyst reduced at 400 °C exhibited an ordered layer-by-layer structure and the particle size of PtFe-a catalysts decreased. The authors hypothesized that the smaller particle size was due to a greater Ostwald ripening effect which occurred in the presence of H_2[189]. EDS maps of fresh catalysts showed an important fraction of Fe species dispersed on PtFe surfaces. This denoted that core-shell structures were facilitated increasing the Fe/Pt atomic ratio (>1). On the contrary, TEM images of annealed samples displayed an ordered *fct* structure, confirming the change in the NPs crystalline structure. To reveal the possible interaction between Fe and Pt, XPS analyses were performed on monometallic Pt/CeO_2 (used as reference) and on the reduced samples. A red shift of the Pt 4f species towards lower binding energy and a split orbital was observed. This behavior derived from the *fct* distortion due to strained Pt and Fe[190]. Furthermore, DFT calculation performed on disordered and ordered PtFe bimetallic samples confirmed that Pt-Fe interaction was crucial for the electronic configuration of the surface. Therefore, the authors demonstrated that thermal annealing led to significant phase transformation from disordered *fcc* to ordered *fct* structure of the bimetallic PtFe NPs. This phase transformation was induced by Pt and Fe interdiffusion phenomena. Despite changes in surface composition of the Pt and Fe elements were considered insignificant before and after annealing, the catalytic activity, selectivity and stability of the bimetallic $PtFe/CeO_2$ catalysts were enhanced with the *fct* structure during aqueous-phase oxidation of glycerol to tartronic acid. The same $PtFe/CeO_2$ catalyst was synthesized by Shi et al. and applied in the liquid-phase oxidation of ethylene glycol[191]. Also in this case, the bimetallic catalyst revealed an initial turnover frequency ca. 17 times higher than that observed on the monometallic Pt/CeO_2 catalyst (19.1 s^{-1} versus 1.1 s^{-1} respectively), with 100 % conversion of ethylene glycol and 62 % glycolic acid selectivity obtained after 4 h of reaction. The alloyed PtFe structure, in particular, enables efficient electron transfer from Fe to Pt that favored dissociative O_2 adsorption on the catalyst surface and its participation in the ethylene glycol oxidation reaction.

Miligal et al. firstly prepared Pt NPs using a colloidal method[53]. Tetradecyltrimethylammonium bromide (TTAB) was dissolved in water and K_2PtCl_4 was added. The solution was heated at 50 °C for 25 minutes to allow the complete solubilization of the TTAB. Then the metal precursor was reduced with $NaBH_4$ and the dispersion was stirred for 1 day at 50 °C. The Pt NPs were then coated with mesoporous SiO_2 ($Pt@mSiO_2$) using tetraethyl orthosilicate (TEOS) as precursor. Furthermore, the surfactant (TTAB) was removed from the surface using concentrated HCl at 90 °C. Lastly, the final $Pt\text{-}Fe@mSiO_2$ catalysts were prepared by solvothermal method using different Pt/Fe ratios. $Fe(acac)_3$ was added to an acetone dispersion of $Pt@mSiO_2$ and then tetraethylene glycol was added. The solution was heated for 28 min at 170 °C and then 2 h at 200 °C. Finally, the catalysts were calcined in air for 6 h at 550 °C and reduced for 6 h at 700 °C. The XRD pattern

of the reduced PtFe@SiO_2 catalysts showed the characteristic peaks of the Pt_3Fe alloy at 23° ad 32°. The addition of small amounts of Fe contracted the *fcc* lattice due to the smaller atomic ratio of Fe than Pt. This was reflected in a shift towards higher angles of the peaks at about 40° and 47°. Increasing the amount of Fe the peak at 40° considerably shifted to higher angle due to the formation of ordered Pt_3Fe alloy phase. TEM images of the reduced sample showed that the mesoporous SiO_2 had an average thickness of 9.1 nm while the metallic core was about 15 nm. The mesoporosity of the SiO_2 was confirmed by N_2-physysorption and a BET surface area of 550-580 $m^2\ g^{-1}$ was calculated. Furthermore, the surface properties of the catalysts were studied by XPS analyses. The Pt-rich catalysts (Pt_5Fe_1@$mSiO_2$ and Pt_5Fe_2@$mSiO_2$) showed an increase in the binding energy of Pt respect to the Pt@$mSiO_2$ and the authors found that Pt was mainly in the metallic state. Moreover, Fe 2p HR spectra showed a peak related to Fe_2O_3 (710-710.6 eV) and its amount was higher for Pt_5Fe_2@$mSiO_2$ catalyst than for $PtFe_1$@$mSiO_2$, indicating that when Fe is loaded in high amount, the iron in excess remains as iron oxide. The authors elucidated the role of Fe content on cinnamaldehyde hydrogenation as a model reaction over the Pt_5Fe_1@$mSiO_2$ catalyst. The selectivity to cinnamyl alcohol during cinnamaldehyde hydrogenation was enhanced by adding Fe to the monometallic Pt catalyst. Vapor-phase hydrogenation of furfural selectively to furfuryl alcohol further confirmed the beneficial aspects of adding Fe to the Pt@$mSiO_2$ NPs, with higher selectivity to furfuryl alcohol being observed with greater Fe content.

Da Silva and co-workers synthesized a core-shell Pt/Fe_3O_4@SiO_2 by oxidation of core-shell FePt@SiO_2 nanoflowers[60]. The PtFe NPs were prepared by polyol solvothermal synthesis using oleylamine and oleic acid as capping agents. Firstly, $PtCl_2$, oleylamine and oleic acid were mixed and heated at 60 °C until complete dissolution. Then, $Fe(acac)_3$ was added and the mixture was heated at 180 °C for 20 min. The temperature was further increased to 240 °C and kept constant for 20 min and then increased again at 300 °C for 1 h. The FePt NPs were coated with SiO_2 by a microemulsion method (FePt@SiO_2)[192,193]. The final catalyst was divided and calcined at different temperatures for 2 h and then reduced in H_2 flow at 350 °C (Pt/Fe_3O_4@SiO_2). TEM images showed that the PtFe NPs had a flower-like shape with an average size of 20-40 nm, while the silica thickness of the silica-coated FePt nanoflowers (FePt@SiO_2) was about 5 nm. XRD pattern of the un-calcined sample exhibited the peaks typical of the *fcc* FePt phase. The calcined samples instead displayed a shift towards lower angles and the higher the calcination temperature the higher the shift. Moreover, Fe_3O_4 phase appeared at 35.6° in the sample calcined at the highest temperature (550 °C). This suggested that for high calcination temperatures the iron atoms migrated on the surface thus forming the iron oxide phase. The presence of Fe_3O_4 phase was also confirmed by HRTEM images where an interplanar distance of 0.25 nm was observed, corresponding to the *fcc* Fe_3O_4 phase (<311> plane). The silica layer covering the Pt/Fe_3O_4 layer proved to be effecting in avoiding large Pt sintering during the heat treatments. The catalyst was used in the preferential CO oxidation reaction, confirming the beneficial role of Fe_3O_4 in promoting the reaction; higher CO conversion was in fact obtained with the Pt/Fe_3O_4/SiO_2 catalyst compared to the bimetallic FePt@SiO_2.

- Other techniques

The PtFe based systems can be also prepared by galvanic displacement, modified adsorption technique, controlled surface reaction and via microemulsion.

The controlled surface reaction (CSR) represents an alternative to the colloidal method, where the presence of capping molecules can sometimes reduce the activity of the catalyst. CSR can be used to selectively deposit a commercial organometallic complex on the surface of the support without using capping agent. Ro et al. synthesized PtFe/SiO_2 catalyst with different Pt/Fe molar ratios and studied their performance in the CO oxidation reaction[194]. The catalysts were prepared using Schlenck line techniques and a glove box. Firstly, Pt/SiO_2 was synthesized by IWI and the obtained material was reduced at 260 °C for 3 h under H_2 flow. Pt/SiO_2 was then added to a pentane solution of (cyclohexadiene)iron tricarbonyl and the dispersion was stirred for 2 h, followed by a drying and reduction step carried out at 300 °C. Finally, the catalyst was passivated or re-reduced. Several CSR cycles were performed until reaching the target Fe loading. TEM images and EDS analyses revealed that the real Pt/Fe ratio was very close to the nominal one, but a divergence between EDS

and ICP method values increased increasing the Fe amount. UV-Vis spectroscopy revealed the deposition of Fe, since the absorbance of the Fe solution decreased during the deposition. The selective deposition of Fe on Pt was studied using CO chemisorption. The analysis revealed that the amount CO uptake decreased when the Fe loading increased[195]. Moreover, XPS spectra were collected for the *in-situ* reduced catalyst and after its exposure to the reactant mixture. HR spectra of Pt 4f showed two peaks at 71.5 eV and 74.8 eV which were assigned to Pt $4f_{7/2}$ and Pt $4f_{5/2}$, respectively. Both peaks were related to presence of Pt^0 species, which remained also in zero valent state during the reaction conditions. The HR spectra of Fe 2p exhibited three peaks related to Fe^0, Fe^{2+} and Fe^{3+} at 706.9 eV, 710.2 eV and 711.7 eV, respectively. After reduction, the main contribution was assigned to the presence of metallic Fe. On the other hand, the Fe^0 contribution became lower after exposing the catalyst to the reactant mixture; Fe can therefore be oxidized during the reaction. XANES and EXAFS spectra revealed that the iron species were mainly in the form of Fe^{3+} before the reduction step. After the reduction, Fe^{2+} and Fe^0 appeared. The Fe-Pt coordination distance was 2.58 Å, related to the formation of a Fe-Pt alloy. The addition of Fe onto Pt/SiO_2 increased the turnover frequency for CO oxidation at 40 °C by up to two orders of magnitude. The authors calculated the number of Pt and Pt-FeOx sites through experimental CO chemisorption data, and calculated their respective intrinsic activities; Pt-FeOx sites were found to be approximately 700 times more active than the Pt site. In addition, through kinetic analysis the authors established that the rate determining step was O_2 adsorption on the metal surface for both mono- and bimetallic catalyst, while the surface of Pt was saturated with CO; the enhanced activity over $PtFe/SiO_2$ catalysts compared to Pt/SiO_2 was therefore attributed to a decreased barrier for O_2 activation over Pt-FeOx interfacial sites.

Lou and co-workers synthesized $PtFe/\gamma\text{-}Al_2O_3$ by modified-adsorption method for the preferential CO oxidation in excess of H_2[196]. Hexachloroplatinic acid and iron nitrate nonahydrate where dissolved in water and pumped into a commercial $\gamma\text{-}Al_2O_3$ dispersion. The mixture was left 2 h at room temperature. Then the synthesized catalyst was washed, dried, and calcined in air for 4 h at 300 °C. The catalyst was reduced at 300 °C for 2 h in hydrogen before the reaction. TEM images of the reduced sample showed that Pt NPs of 1.8 nm average size were finely dispersed on the support. Moreover, HAADF-STEM images confirmed the absence of agglomerations and the presence of isolated Fe and Pt atoms. HR spectra of Fe 2p collected during XPS analysis on the reduced catalyst displayed only the peak of Fe^{2+}, indicating that the reduction conditions were not enough to completely reduced iron species. The as synthesized $PtFe/\gamma\text{-}Al_2O_3$ catalyst, containing 0.43 and 0.34 %wt of Pt and Fe respectively, exhibited high catalytic activity and selectivity in a 25-200 °C temperature range, as well as good stability in the reaction conditions used. In addition, the provided the highest specific rate for the preferential CO oxidation among all Pt-based catalysts tested. The authors ascribed the enhanced activity to Pt clusters decorated with isolated FeOx species, which efficiently enhanced O_2 activation.

Shi et al. prepared $PtFeOx/SiO_2$ catalyst using galvanic displacement reaction which spontaneously occurs in a solution of Fe^0 and Pt^{2+}[197]. Firstly, Fe/SiO_2 with different Fe loadings were prepared by deposition precipitation method with urea starting from commercial SiO_2 (200 $m^2\ g^{-1}$) and a solution of iron nitrate. The obtained samples were reduced at 700 °C. The reduced samples were then added to a solution of $Pt(NH_3)_4(NO_3)_2$ under bubbling Ar to protect the sample from air passivation. The obtained solid was washed and dried at 110 °C. HAADF-STEM images did not clearly show the presence of Pt NPs, although EDS mapping showed the presence of both Pt and Fe. In particular, the signals of Pt were closely associated with the Fe signals, revealing that the two metals were in close contact. Moreover, TPR profiles exhibited a peak at 250 °C associated to the reduction of Pt and FeOx in close interaction with Pt. The peak at 80-160 °C was, on the other hand, attributed to the reduction of PtOx. Hydrogen consumption below 350 °C was quantified in order to calculate H/Pt ratios; these can give an indication on the presence and extent of interaction between Pt and Fe species. The authors found H/Pt ratios significantly larger than that for the same catalyst prepared by impregnation (16.2 versus 6.2, respectively) and larger than the theoretical H/Pt (2.0) assuming that all Pt was in the +2 oxidation state. The high H/Pt ratio for the catalyst prepared by galvanic displacement indicated that the preferential deposition of Pt on Fe/SiO_2 generated far more intimate Pt–FeOx interactions than those

in the reference catalyst from conventional impregnation preparation. The oxidation state of the surface was analyzed by XPS. HR spectra of Pt 4f region showed the presence of $Pt^{\delta+}$ and Pt^{2+} at 72.3 eV and 74.0 eV, respectively. Therefore, the galvanic displacement method allowed to form small Pt NPs on the surface of FeOx and a strong interaction between the two metals can be established. The catalyst showed high activity and selectivity in the hydrogenation of cinnamaldehyde, with 92 % selectivity towards cinnamyl alcohol at 41 % conversion. The same catalyst prepared by impregnation showed only 63 % cinnamyl alcohol selectivity and 21 % conversion.

Finally, $PtFe/Al_2O_3$ was prepared by Li et al. using microemulsion technique[198] which allowed synthesizing metal NPs with different size by regulating the size of the reversed micelles. The microemulsion was prepared using cetyltrimethylammonium bromide and n-butanol as surfactant and co-surfactant, respectively. An aqueous solution of H_2PtCl_6 and $FeCl_3$ was added to the surfactant and co-surfactants mixture and cyclohexane was added as oil phase. Then N_2H_4 was added and the emulsion was stirred. The commercial support was finally added, and tetrahydrofuran was dripped to break the microemulsion. TEM and SAED images did not show any aggregations and a polycrystalline structure was detected. Both monometallic Fe and Pt NPs and bimetallic PtFe NPs were present on the catalyst surface. The close contact of Pt and Fe was confirmed by XPS analysis where a lower binding energy of Pt^0 was observed in respect to the monometallic Pt/Al_2O_3. This indicated that Pt^0 received electrons and therefore it is electron rich. In fact, HR spectra of Fe 2p region exhibited a high amount of Fe^{3+} species (710 eV), underlining the donation of electrons to Pt. According to the authors, this electron transfer was responsible to the enhanced activity in the hydrogenation of m-chloronitrobenzene, as well as for the inhibition of the dechlorination pathway.

5. Conclusions and Outlook

Supported noble metal nanoparticles are well established active materials in many catalytic processes. Their scarce abundance on the Earth crust, along with the efforts by the governments of all the countries spread around the globe towards more sustainable and environmentally friendly processes, has driven scientists to find more viable and greener solutions in catalysis. In this regard, Fe-based catalysts are an emerging class of materials which can be potentially used in a wide range of hydrogenation and oxidation reactions. In particular, Fe has shown in the last few decades to be extremely versatile as a support for noble metal NPs (such as Pd and Pt) when present in one of its many oxidized ~~form~~forms (commonly referred as FeOx). This is due to its unique physical-chemical properties that can be modulated by several parameters, such as the synthetic procedure, heat treatments or chemical attacks. In addition, due the different oxidation states that Fe can assume (Fe^0, Fe^{II}, and Fe^{III}) it is possible to modify the crystallinity as well as its allotropic form. In addition, the magnetic properties of some iron oxides (such as Fe_3O_4) make these materials very suitable for catalysis due to their simple recovery after use, which in turn leads to more economic reactions and environmentally sustainable processes. Another way to implement the use of Fe into active catalysts is by adding Fe to the active noble metal (Pd and Pt) in a similar molar amount in order to create bimetallic systems that are mainly composed of M-Fe or M-FeOx entities (where M is either Pd or Pt) present as small NPs and supported on a wide range of materials such as metal oxides or carbonaceous materials.

In this review we presented both the simplest synthetic methods (impregnation, colloidal synthesis…) as well as the not so common routes to prepare bimetallic catalysts. Beside the description of the synthetic methods, we reported the physico-chemical characterization (XRD, TEM, BET, TPR, XAS, XANES, SEM…), emphasizing the role of iron in the considered catalyst. In all the described systems, iron plays a key role to enhance the activity or to stabilize the noble metal NPs, whether it is used mainly as a support or as a co-active element in bimetallic systems.

One of the most important parameters in catalysis is the interaction between the active metal and the substrate. Most of the catalytic steps, in fact, happen at the interface between the active site on the catalyst

surface and the functional group of the substrate. In order to optimize this interaction, the catalyst must have specific geometric and electronic properties which can be modulated in several ways, as previously mentioned, such as by modifying the synthetic procedure, adding heat treatments in oxidative or reductive atmosphere or by selective chemical leaching. In this regard, Fe proved to be fundamental in either modifying the electron transfer (from or to the active metal) or in creating anchoring sites for other species to adsorb and react.

Recent studies highlighted that when Fe is used as a support, the Fe oxidation state plays a key role in determining the electron transfer between the active metal and the FeOx species; TPR and XPS analyses help obtaining information in this regard. In particular, a reduction peak in TPR analyses at temperatures between the reduction temperature of FeOx and M oxide appears when there is an interaction between M and FeOx, indicating that the presence of intimate contact helps the reduction of iron oxide species[57]. High resolution XPS analyses, on the other hand, highlight the presence and the direction of electron transfer. When the noble metal is supported onto high oxidation state Fe oxide (such as Fe_2O_3), an electron transfer from the electron rich M towards the electron deficient support is often detected (Figure 25A); as a result, the binding energy of the M shifts towards higher potentials[95,170,177]. On the contrary, when the noble metal is supported onto low oxidation state Fe oxide (such as Fe_3O_4), an electron transfer from the support towards M is detected (Figure 25B), which results in a decrease in the binding energy of M[175,179]. A similar behavior is observed when Fe is present as a co-active metal in alloyed MFe NPs; electron transfer from Fe towards M is often observed in XPS analyses (Figure 25C)[147,183,186]. In this latter case, however, the electronic properties of the material are always hard to effectively evaluate due to the tendency of zero valent Fe to easily oxidize when exposed to air. Another particular case is when M nanoparticles are anchored to the FeOx support through a ligand, such as a functionalized polymer; in this case, the electron transfer can be mediated by the strong interactions between the NPs and the ligand surface functionalities[92].

The electronic and geometric effects induced by the presence of Fe species proved to be beneficial in a wide range of catalytic reactions, as synthetically reported in Tables 1-X. In particular, Fe-based systems are often capable of enhancing not only the overall activity of the reaction, but also the selectivity towards specific products of interest. Catalyst stability is also frequently improved by formation of strong M-FeOx or M-Fe interactions that prevent noble metal leaching during reaction, a problem that oftentimes affects monometallic Pt and Pd catalysts[75,155].

Commentato [S2]: Add

In conclusion, Pd-Fe and Pt-Fe materials are proving to be very versatile systems where chemo-physical properties can be easily tuned simply by modifying the synthetic parameters. An accurate choice of the system is necessary and it strictly depends on the active phase required for a specific reaction. However, a lot of effort is still required to fully understand their behavior in specific situations. For example, a specific theoretical and experimental study about the influence of Fe/FeOx particle size and its oxidation state on the properties of noble metal NPs is still missing. Moreover, the mechanism on the basis of the different catalytic behaviors is not completely clear, therefore theoretical studies and characterizations aimed at the understanding of electronic modification will improve our knowledge about these unique catalysts.

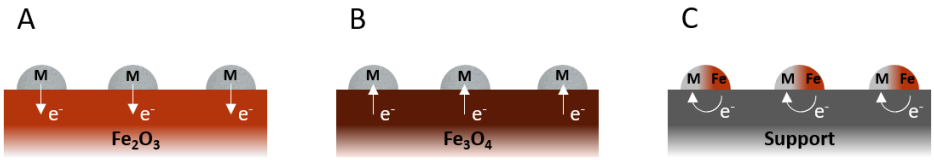

Figure 25. Electron transfer behavior in **A)** M/Fe_2O_3, **B)** M/Fe_3O_4 and **C)** MFe/Support systems

Conflicts of Interest: The authors declare no conflict of interest.

References

[1] A.A. Yaroshevsky, Abundances of chemical elements in the Earth's crust, Geochemistry Int. (2006). doi:10.1134/S001670290601006X.

[2] S. Milisauskas, European Prehistory, 1st ed., Springer US, 2002. doi:10.2307/2801682.

[3] R.L. Milford, S. Pauliuk, J.M. Allwood, D.B. Müller, The roles of energy and material efficiency in meeting steel industry CO2 targets, Environ. Sci. Technol. (2013). doi:10.1021/es3031424.

[4] B.S. Taranath, Steel Buildings, in: Tall Build. Des., 2016. doi:10.1201/9781315374468-13.

[5] C. Hardness, H. Treatment, Standard Specification for Automotive Malleable Iron Castings 1, Current. (2004). doi:10.1520/A0159-83R11.2.

[6] O. Maluf, M.T. Milan, Development of Materials for Automotive Disc Brakes, Minerva. (2004).

[7] B.R. Linter, G.T. Burstein, Reactions of pipeline steels in carbon dioxide solutions, Corros. Sci. (1999). doi:10.1016/S0010-938X(98)00104-8.

[8] A. Vojvodic, A.J. Medford, F. Studt, F. Abild-Pedersen, T.S. Khan, T. Bligaard, J.K. Nørskov, Exploring the limits: A low-pressure, low-temperature Haber-Bosch process, Chem. Phys. Lett. (2014). doi:10.1016/j.cplett.2014.03.003.

[9] J. Van de Loosdrecht, F.G. Botes, I.M. Ciobica, A. Ferreira, P. Gibson, D.J. Moodley, A.M. Saib, J.L. Visagie, C.J. Weststrate, J.W. Niemantsverdriet, Fischer-Tropsch Synthesis: Catalysts and Chemistry, in: Compr. Inorg. Chem. II (Second Ed. From Elem. to Appl., 2013. doi:10.1016/B978-0-08-097774-4.00729-4.

[10] N. Yahya, P. Puspitasari, K. Koziol, P. Guiseppe, Ammonia synthesis, Adv. Struct. Mater. (2011). doi:10.1007/8611_2010_25.

[11] Y. Li, Z. Li, A. Ahsen, L. Lammich, G.J.A. Mannie, J.W.H. Niemantsverdriet, J. V Lauritsen, Atomically Defined Iron Carbide Surface for Fischer–Tropsch Synthesis Catalysis, ACS Catal. 9 (2019) 1264–1273. doi:10.1021/acscatal.8b03684.

[12] D.R. Milburn, K.V.R. Chary, B.H. Davis, Promoted iron Fischer-Tropsch catalysts: Characterization by nitrogen sorption, Appl. Catal. A Gen. (1996). doi:10.1016/0926-860X(96)00128-7.

[13] V.R.R. Pendyala, G. Jacobs, M.K. Gnanamani, Y. Hu, A. Maclennan, B.H. Davis, Selectivity control of Cu promoted iron-based Fischer-Tropsch catalyst by tuning the oxidation state of Cu to mimic K, Appl. Catal. A Gen. (2015). doi:10.1016/j.apcata.2015.01.027.

[14] F. Meemken, A. Baiker, Recent Progress in Heterogeneous Asymmetric Hydrogenation of C═O and C═C Bonds on Supported Noble Metal Catalysts, Chem. Rev. 117 (2017) 11522–11569. doi:10.1021/acs.chemrev.7b00272.

[15] J. Zhong, X. Yang, Z. Wu, B. Liang, Y. Huang, T. Zhang, State of the art and perspectives in heterogeneous catalysis of CO2 hydrogenation to methanol, Chem. Soc. Rev. 49 (2020) 1385–1413. doi:10.1039/c9cs00614a.

[16] M.J. Ndolomingo, N. Bingwa, R. Meijboom, Review of supported metal nanoparticles: synthesis methodologies, advantages and application as catalysts, J. Mater. Sci. 55 (2020) 6195–6241. doi:10.1007/s10853-020-04415-x.

[17] C. Megías-Sayago, S. Navarro-Jaén, R. Castillo, S. Ivanova, Recent advances in selective oxidation of biomass-derived platform chemicals over gold catalysts, Curr. Opin. Green Sustain. Chem. 21 (2020) 50–55. doi:https://doi.org/10.1016/j.cogsc.2019.12.001.

[18] S. Dey, G.C. Dhal, Property and structure of various platinum catalysts for low-temperature carbon monoxide oxidations, Mater. Today Chem. 16 (2020) 100228. doi:https://doi.org/10.1016/j.mtchem.2019.100228.

[19] J. Guo, C. Lin, C. Jiang, P. Zhang, Review on noble metal-based catalysts for formaldehyde oxidation at room temperature, Appl. Surf. Sci. 475 (2019) 237–255. doi:https://doi.org/10.1016/j.apsusc.2018.12.238.

[20] X. Tong, H. Zhang, D.Y. Li, Effect of Annealing Treatment on Mechanical Properties of Nanocrystalline α-iron: An Atomistic Study, Sci. Rep. (2015). doi:10.1038/srep08459.

[21] A. V Anupama, W. Keune, B. Sahoo, Thermally induced phase transformation in multi-phase iron oxide nanoparticles on vacuum annealing, J. Magn. Magn. Mater. 439 (2017) 156–166. doi:https://doi.org/10.1016/j.jmmm.2017.04.094.

[22] X.N. Xu, Y. Wolfus, A. Shaulov, Y. Yeshurun, I. Felner, I. Nowik, Y. Koltypin, A. Gedanken, Annealing study of Fe2O3 nanoparticles: Magnetic size effects and phase transformations, J. Appl. Phys. 91 (2002) 4611–4616. doi:10.1063/1.1457544.

[23] A. Šutka, S. Lagzdina, T. Käämbre, R. Pärna, V. Kisand, J. Kleperis, M. Maiorov, A. Kikas, I. Kuusik, D. Jakovlevs, Study of the structural phase transformation of iron oxide nanoparticles from an Fe2+ ion source by precipitation under various synthesis parameters and temperatures, Mater. Chem. Phys. 149–150 (2015) 473–479. doi:https://doi.org/10.1016/j.matchemphys.2014.10.048.

[24] J.W. Geus, Preparation and properties of iron oxide and metallic iron catalysts., Appl. Catal. 25 (1986) 313–333. doi:https://doi.org/10.1016/S0166-9834(00)81249-X.

[25] S.M. Rodulfo-Baechler, S.L. González-Cortés, J. Orozco, V. Sagredo, B. Fontal, A.J. Mora, G. Delgado, Characterization of modified iron catalysts by X-ray diffraction, infrared spectroscopy, magnetic susceptibility and thermogravimetric analysis, Mater. Lett. 58 (2004) 2447–2450. doi:https://doi.org/10.1016/j.matlet.2004.02.032.

[26] F. Kallmeier, T. Irrgang, T. Dietel, R. Kempe, Highly Active and Selective Manganese C=O Bond Hydrogenation Catalysts: The Importance of the Multidentate Ligand, the Ancillary Ligands, and the Oxidation State, Angew. Chemie Int. Ed. 55 (2016) 11806–11809. doi:10.1002/anie.201606218.

[27] G.S. Parkinson, Iron oxide surfaces, Surf. Sci. Rep. 71 (2016) 272–365. doi:https://doi.org/10.1016/j.surfrep.2016.02.001.

[28] M. Munoz, Z.M. de Pedro, J.A. Casas, J.J. Rodriguez, Preparation of magnetite-based catalysts and their application in heterogeneous Fenton oxidation - A review, Appl. Catal. B Environ. (2015). doi:10.1016/j.apcatb.2015.04.003.

[29] Y. Liu, F. Yang, P.L. Yue, G. Chen, Catalytic dechlorination of chlorophenols in water by palladium/iron, Water Res. (2001). doi:10.1016/S0043-1354(00)00463-2.

[30] H. Lu, J. Wang, M. Stoller, T. Wang, Y. Bao, H. Hao, An Overview of Nanomaterials for Water and Wastewater Treatment, Adv. Mater. Sci. Eng. (2016). doi:10.1155/2016/4964828.

[31] R.A. Crane, T.B. Scott, Nanoscale zero-valent iron: Future prospects for an emerging water treatment technology, J. Hazard. Mater. (2012). doi:10.1016/j.jhazmat.2011.11.073.

[32] C. Xu, S. Sun, New forms of superparamagnetic nanoparticles for biomedical applications, Adv. Drug Deliv. Rev. (2013). doi:10.1016/j.addr.2012.10.008.

[33] L. Mohammed, H.G. Gomaa, D. Ragab, J. Zhu, Magnetic nanoparticles for environmental and biomedical applications: A review, Particuology. (2017). doi:10.1016/j.partic.2016.06.001.

[34] A.K. Gupta, M. Gupta, Synthesis and surface engineering of iron oxide nanoparticles for biomedical applications, Biomaterials. (2005). doi:10.1016/j.biomaterials.2004.10.012.

[35] C. Adán, A. Bahamonde, M. Fernández-García, A. Martínez-Arias, Structure and activity of nanosized iron-doped anatase TiO2 catalysts for phenol photocatalytic degradation, Appl. Catal. B Environ. (2007). doi:10.1016/j.apcatb.2006.09.018.

[36] M. Nolan, Electronic coupling in iron oxide-modified TiO2 leads to a reduced band gap and charge separation for visible light active photocatalysis, Phys. Chem. Chem. Phys. (2011). doi:10.1039/c1cp21418g.

[37] W. Wu, C. Jiang, V.A.L. Roy, Recent progress in magnetic iron oxide-semiconductor composite nanomaterials as promising photocatalysts, Nanoscale. (2015). doi:10.1039/c4nr04244a.

[38] M. Sander, T.B. Hofstetter, C.A. Gorski, Electrochemical analyses of redox-active iron minerals: A review of nonmediated and mediated approaches, Environ. Sci. Technol. (2015). doi:10.1021/acs.est.5b00006.

[39] A. Boddien, B. Loges, F. Gärtner, C. Torborg, K. Fumino, H. Junge, R. Ludwig, M. Beller, Iron-catalyzed hydrogen production from formic acid, J. Am. Chem. Soc. (2010). doi:10.1021/ja100925n.

[40] L. Guo, Q. Huang, X.Y. Li, S. Yang, Iron nanoparticles: Synthesis and applications in surface enhanced Raman scattering and electrocatalysis, Phys. Chem. Chem. Phys. (2001). doi:10.1039/b0099511.

[41] A. Fürstner, A. Leitner, M. Méndez, H. Krause, Iron-catalyzed cross-coupling reactions, J. Am. Chem. Soc. (2002). doi:10.1021/ja027190t.

[42] D. Gärtner, A.L. Stein, S. Grupe, J. Arp, A.J. Von Wangelin, Iron-Catalyzed Cross-Coupling of Alkenyl Acetates, Angew. Chemie - Int. Ed. (2015). doi:10.1002/anie.201504524.

[43] A. Piontek, E. Bisz, M. Szostak, Iron-Catalyzed Cross-Couplings in the Synthesis of Pharmaceuticals: In Pursuit of Sustainability, Angew. Chemie - Int. Ed. (2018). doi:10.1002/anie.201800364.

[44] S.-F. Jiang, K.-F. Xi, J. Yang, H. Jiang, Biochar-supported magnetic noble metallic nanoparticles for the fast recovery of excessive reductant during pollutant reduction, Chemosphere. 227 (2019) 63–71. doi:https://doi.org/10.1016/j.chemosphere.2019.04.044.

[45] G. Kozma, A. Rónavári, Z. Kónya, Á. Kukovecz, Environmentally Benign Synthesis Methods of Zero-Valent Iron Nanoparticles, ACS Sustain. Chem. Eng. (2016). doi:10.1021/acssuschemeng.5b01185.

[46] Y. Zhuang, S. Ahn, A.L. Seyfferth, Y. Masue-Slowey, S. Fendorf, R.G. Luthy, Dehalogenation of polybrominated diphenyl ethers and polychlorinated biphenyl by bimetallic, impregnated, and nanoscale zerovalent iron, Environ. Sci. Technol. (2011). doi:10.1021/es104312h.

[47] J. Blotevogel, R.J. Giraud, T. Borch, Reductive defluorination of perfluorooctanoic acid by zero-valent iron and zinc: A DFT-based kinetic model, Chem. Eng. J. (2018). doi:10.1016/j.cej.2017.10.131.

[48] N.J. Van Eck, L. Waltman, Software survey: VOSviewer, a computer program for bibliometric mapping, Scientometrics. 84 (2010) 523–538. doi:10.1007/s11192-009-0146-3.

[49] N.J. Van Eck, L. Waltman, Visualizing bibliometric networks, in: Y. Ding, R. Rousseau, D. Wolfram (Eds.), Meas. Sch. Impact Methods Pract., Berlin: Springer, 2014.

[50] G.L. Dimas-Rivera, J. Rivera De la Rosa, C.J. Lucio-Ortiz, D.X. Martínez-Vargas, L. Sandoval-Rangel, D.I. García Gutiérrez, C. Solis Maldonado, Bimetallic Pd-Fe supported on γ-Al2O3 catalyst used in the ring opening of 2-methylfuran to selective formation of alcohols, Appl. Catal. A Gen. 543 (2017) 133–140. doi:https://doi.org/10.1016/j.apcata.2017.06.019.

[51] Y. Cheng, H. Pham, J. Huo, R. Johnson, A.K. Datye, B. Shanks, High activity Pd-Fe bimetallic catalysts for aqueous phase hydrogenations, Mol. Catal. 477 (2019) 110546. doi:https://doi.org/10.1016/j.mcat.2019.110546.

[52] H. Xu, K. Ni, X. Li, S. Zhu, G. Fan, Comparative studies of leached Pt-Fe and Pt-Co catalysts for CO oxidation reactions, Chinese J. Catal. 38 (2017) 1261–1269. doi:https://doi.org/10.1016/S1872-2067(17)62838-9.

[53] R. V Maligal-Ganesh, K. Brashler, X. Luan, T.W. Goh, J. Gustafson, J. Wu, W. Huang, Enhanced Chemoselectivity in Pt–Fe@mSiO2 Bimetallic Nanoparticles in the Absence of Surface Modifying Ligands, Top. Catal. 61 (2018) 940–948. doi:10.1007/s11244-018-0933-2.

[54] C. Lin, K. Tao, D. Hua, Z. Ma, S. Zhou, Transformation of Au3M/SiO2 (M = Ni, Co, Fe) into Au–MOx/SiO2 Catalysts for the Reduction of p-Nitrophenol, Catal. Letters. 144 (2014) 1001–1008. doi:10.1007/s10562-014-1224-6.

[55] J. Sun, A.M. Karim, H. Zhang, L. Kovarik, X.S. Li, A.J. Hensley, J.-S. McEwen, Y. Wang, Carbon-supported bimetallic Pd–Fe catalysts for vapor-phase hydrodeoxygenation of guaiacol, J. Catal. 306 (2013) 47–57. doi:https://doi.org/10.1016/j.jcat.2013.05.020.

[56] A. Feng, J. Bai, W. Shao, W. Hong, Z. Tian, Z. Xiao, Surfactant-free Pd–Fe nanoparticles supported on reduced graphene oxide as nanocatalyst for formic acid oxidation, Int. J. Hydrogen Energy. 42 (2017) 15196–15202. doi:https://doi.org/10.1016/j.ijhydene.2017.04.278.

[57] A.A. Shesterkina, O.A. Kirichenko, L.M. Kozlova, G.I. Kapustin, I. V Mishin, A.A. Strelkova, L.M. Kustov, Liquid-phase hydrogenation of phenylacetylene to styrene on silica-supported Pd–Fe nanoparticles, Mendeleev Commun. 26 (2016) 228–230. doi:https://doi.org/10.1016/j.mencom.2016.05.002.

[58] V.K. Gupta, N. Atar, M.L. Yola, Z. Üstündağ, L. Uzun, A novel magnetic Fe@Au core–shell nanoparticles anchored graphene oxide recyclable nanocatalyst for the reduction of nitrophenol compounds, Water Res. 48

(2014) 210–217. doi:https://doi.org/10.1016/j.watres.2013.09.027.

[59] V. Papaefthimiou, F. Tournus, A. Hillion, G. Khadra, D. Teschner, A. Knop-Gericke, V. Dupuis, S. Zafeiratos, Mixing Patterns and Redox Properties of Iron-Based Alloy Nanoparticles under Oxidation and Reduction Conditions, Chem. Mater. 26 (2014) 1553–1560. doi:10.1021/cm403172a.

[60] T.L. da Silva, A.H.M. da Silva, J.M. Assaf, Preparation of core-shell Pt@Fe3O4@SiO2 nanostructures by oxidation of core-shell FePt@SiO2 nanoflowers and their performance in preferential CO oxidation reaction, Mater. Res. Express. 6 (2019) 015042.

[61] S. Carrettin, Y. Hao, V. Aguilar-Guerrero, B.C. Gates, S. Trasobares, J.J. Calvino, A. Corma, Increasing the Number of Oxygen Vacancies on TiO2 by Doping with Iron Increases the Activity of Supported Gold for CO Oxidation, Chem. – A Eur. J. 13 (2007) 7771–7779. doi:10.1002/chem.200700472.

[62] J. Zhu, S.A.C. Carabineiro, D. Shan, J.L. Faria, Y. Zhu, J.L. Figueiredo, Oxygen activation sites in gold and iron catalysts supported on carbon nitride and activated carbon, J. Catal. 274 (2010) 207–214. doi:https://doi.org/10.1016/j.jcat.2010.06.018.

[63] S. Capelli, A. Rosengart, A. Villa, A. Citterio, A. Di Michele, C.L. Bianchi, L. Prati, C. Pirola, Bio-adipic acid production by catalysed hydrogenation of muconic acid in mild operating conditions, Appl. Catal. B Environ. 218 (2017). doi:10.1016/j.apcatb.2017.06.060.

[64] M. V Rajashekharam, D.D. Nikalje, R. Jaganathan, R. V Chaudhari, Hydrogenation of 2,4-Dinitrotoluene Using a Pd/Al2O3 Catalyst in a Slurry Reactor: A Molecular Level Approach to Kinetic Modeling and Nonisothermal Effects, Ind. Eng. Chem. Res. 36 (1997) 592–604. doi:10.1021/ie9603651.

[65] W.-J. Shen, M. Okumura, Y. Matsumura, M. Haruta, The influence of the support on the activity and selectivity of Pd in CO hydrogenation, Appl. Catal. A Gen. 213 (2001) 225–232. doi:https://doi.org/10.1016/S0926-860X(01)00465-3.

[66] S. Alijani, S. Capelli, S. Cattaneo, M. Schiavoni, C. Evangelisti, K.M.H. Mohammed, P.P. Wells, F. Tessore, A. Villa, Capping Agent Effect on Pd-Supported Nanoparticles in the Hydrogenation of Furfural, Catalysts. 10 (2020) 1–16. doi:10.3390/catal10010011.

[67] S. Cattaneo, F.J.S. Trujillo, N. Dimitratos, A. Villa, The Effect of Carbon Nanofibers Surface Properties in Hydrogenation and Dehydrogenation Reactions, Appl. Sci. 9 (2019) 1–14.

[68] A.S. Berenblyum, T.A. Podoplelova, R.S. Shamsiev, E.A. Katsman, V.Y. Danyushevsky, On the mechanism of catalytic conversion of fatty acids into hydrocarbons in the presence of palladium catalysts on alumina, Pet. Chem. 51 (2011) 336. doi:10.1134/S0965544111050069.

[69] P. Mäki-Arvela, M. Snåre, K. Eränen, J. Myllyoja, D.Y. Murzin, Continuous decarboxylation of lauric acid over Pd/C catalyst, Fuel. (2008). doi:10.1016/j.fuel.2008.07.004.

[70] I. Simakova, O. Simakova, P. Mäki-Arvela, D.Y. Murzin, Decarboxylation of fatty acids over Pd supported on mesoporous carbon, Catal. Today. (2010). doi:10.1016/j.cattod.2009.07.064.

[71] R. Easterday, C. Leonard, O. Sanchez-Felix, Y. Losovyj, M. Pink, B.D. Stein, D.G. Morgan, N.A. Lyubimova, L.Z. Nikoshvili, E.M. Sulman, W.E. Mahmoud, A.A. Al-Ghamdi, L.M. Bronstein, Fabrication of Magnetically Recoverable Catalysts Based on Mixtures of Pd and Iron Oxide Nanoparticles for Hydrogenation of Alkyne Alcohols, ACS Appl. Mater. Interfaces. 6 (2014) 21652–21660. doi:10.1021/am5067223.

[72] C. Espro, B. Gumina, E. Paone, F. Mauriello, Upgrading Lignocellulosic Biomasses: Hydrogenolysis of Platform Derived Molecules Promoted by Heterogeneous Pd-Fe Catalysts, Catalysts. 7 (2017) 78. doi:10.3390/catal7030078.

[73] J. Liu, B. Sun, J. Hu, Y. Pei, H. Li, M. Qiao, Aqueous-phase reforming of ethylene glycol to hydrogen on Pd/Fe3O4 catalyst prepared by co-precipitation: Metal–support interaction and excellent intrinsic activity, J. Catal. 274 (2010) 287–295. doi:https://doi.org/10.1016/j.jcat.2010.07.014.

[74] R. Easterday, O. Sanchez-Felix, Y. Losovyj, M. Pink, B.D. Stein, D.G. Morgan, M. Rakitin, V.Y. Doluda, M.G. Sulman, W.E. Mahmoud, A.A. Al-Ghamdi, L.M. Bronstein, Design of ruthenium/iron oxide nanoparticle mixtures for hydrogenation of nitrobenzene, Catal. Sci. Technol. 5 (2015) 1902–1910. doi:10.1039/C4CY01277A.

[75] T. Jiang, S. Du, T. Jafari, W. Zhong, Y. Sun, W. Song, Z. Luo, W.A. Hines, S.L. Suib, Synthesis of mesoporous γ-

Fe2O3 supported palladium nanoparticles and investigation of their roles as magnetically recyclable catalysts for nitrobenzene hydrogenation, Appl. Catal. A Gen. 502 (2015) 105–113. doi:10.1016/J.APCATA.2015.05.013.

[76] A. Schätz, O. Reiser, W.J. Stark, Nanoparticles as Semi-Heterogeneous Catalyst Supports, Chem. – A Eur. J. 16 (2010) 8950–8967. doi:10.1002/chem.200903462.

[77] B. Han, C. Xu, Nanoporous PdFe alloy as highly active and durable electrocatalyst for oxygen reduction reaction, Int. J. Hydrogen Energy. 39 (2014) 18247–18255. doi:https://doi.org/10.1016/j.ijhydene.2014.09.006.

[78] E. Paone, C. Espro, R. Pietropaolo, F. Mauriello, Selective arene production from transfer hydrogenolysis of benzyl phenyl ether promoted by a co-precipitated Pd/Fe3O4 catalyst, Catal. Sci. Technol. 6 (2016) 7937–7941. doi:10.1039/c6cy01626j.

[79] Y. Tang, S. Cao, Y. Chen, T. Lu, Y. Zhou, L. Lu, J. Bao, Effect of Fe state on electrocatalytic activity of Pd–Fe/C catalyst for oxygen reduction, Appl. Surf. Sci. 256 (2010) 4196–4200. doi:https://doi.org/10.1016/j.apsusc.2010.01.124.

[80] C. Milone, C. Crisafulli, R. Ingoglia, L. Schipilliti, S. Galvagno, A comparative study on the selective hydrogenation of ??,?? unsaturated aldehyde and ketone to unsaturated alcohols on Au supported catalysts, Catal. Today. 122 (2007) 341–351. doi:10.1016/j.cattod.2007.01.011.

[81] F. Pinna, M. Selva, M. Signoretto, G. Strukul, F. Boccuzzi, A. Benedetti, P. Canton, G. Fagherazzi, Pd-Fe/SiO2 Catalysts in the Hydrogenation of 2,4-Dinitrotoluene, J. Catal. 150 (1994) 356–367. doi:https://doi.org/10.1006/jcat.1994.1354.

[82] J. Ge, Z. Zeng, F. Liao, W. Zheng, X. Hong, S.C.E. Tsang, Palladium on iron oxide nanoparticles: the morphological effect of the support in glycerol hydrogenolysis, Green Chem. 15 (2013) 2064–2069. doi:10.1039/C3GC40712H.

[83] H. Elazab, S. Moussa, K. Brinkley, B. Gupton, M.S. El-Shall, The continuous synthesis of Pd supported on Fe3O4 nanoparticles: A highly effective and magnetic catalyst for CO oxidation, Green Process. Synth. 6 (2017). doi:10.1515/gps-2016-0168.

[84] Y. Tuo, G. Liu, B. Dong, J. Zhou, A. Wang, J. Wang, R. Jin, H. Lv, Z. Dou, W. Huang, Microbial synthesis of Pd/Fe3O4, Au/Fe3O4 and PdAu/Fe3O4 nanocomposites for catalytic reduction of nitroaromatic compounds, Sci. Rep. 5 (2015) 13515. doi:10.1038/srep13515.

[85] M. Campanati, G. Fornasari, A. Vaccari, Fundamentals in the preparation of heterogeneous catalysts, Catal. Today. 77 (2003) 299–314. doi:https://doi.org/10.1016/S0920-5861(02)00375-9.

[86] C.-H. Pélisson, A. Denicourt-Nowicki, C. Meriadec, J.-M. Greneche, A. Roucoux, Magnetically Recoverable Palladium(0) Nanocomposite Catalyst for Hydrogenation Reactions in Water, ChemCatChem. 7 (2015) 309–315. doi:10.1002/cctc.201402761.

[87] M. Farrag, Preparation of mesoporous palladium nanoclusters supported over hematite (α-Fe2O3) for selective catalytic hydrogenation of α,β-unsaturated aldehydes, Microporous Mesoporous Mater. 257 (2018) 110–117. doi:10.1016/j.micromeso.2017.08.022.

[88] F. Mauriello, H. Ariga, M.G. Musolino, R. Pietropaolo, S. Takakusagi, K. Asakura, Exploring the catalytic properties of supported palladium catalysts in the transfer hydrogenolysis of glycerol, Appl. Catal. B Environ. 166–167 (2015) 121–131. doi:10.1016/J.APCATB.2014.11.014.

[89] G. Neri, G. Rizzo, L. De Luca, A. Donato, M.G. Musolino, R. Pietropaolo, Supported Pd catalysts for the hydrogenation of campholenic aldehyde: Influence of support and preparation method, Appl. Catal. A Gen. 356 (2009) 113–120. doi:10.1016/j.apcata.2008.12.027.

[90] L. Bartolome, M. Imran, K.G. Lee, A. Sangalang, J.K. Ahn, D.H. Kim, Superparamagnetic γ-Fe2O3 nanoparticles as an easily recoverable catalyst for the chemical recycling of PET, Green Chem. 16 (2014) 279–286. doi:10.1039/C3GC41834K.

[91] F.J. Caparrós, L. Soler, M.D. Rossell, I. Angurell, L. Piccolo, O. Rossell, J. Llorca, Remarkable Carbon Dioxide Hydrogenation to Ethanol on a Palladium/Iron Oxide Single-Atom Catalyst, ChemCatChem. 10 (2018) 2365–2369. doi:10.1002/cctc.201800362.

[92] M. Li, X. Zhou, J. Sun, H. Fu, X. Qu, Z. Xu, S. Zheng, Highly effective bromate reduction by liquid phase catalytic hydrogenation over Pd catalysts supported on core-shell structured magnetites: Impact of shell properties, Sci. Total Environ. 663 (2019) 673–685. doi:https://doi.org/10.1016/j.scitotenv.2019.01.392.

[93] Y. Matsumura, M. Okumura, Y. Usami, K. Kagawa, H. Yamashita, M. Anpo, M. Haruta, Low-temperature decomposition of methanol to carbon monoxide and hydrogen with low activation energy over Pd/ZrO2 catalyst, Catal. Letters. 44 (1997) 189–191.

[94] V. Hajdu, Á. Prekob, G. Muránszky, I. Kocserha, Z. Kónya, B. Fiser, B. Viskolcz, L. Vanyorek, Catalytic activity of maghemite supported palladium catalyst in nitrobenzene hydrogenation, React. Kinet. Mech. Catal. 129 (2020) 107–116. doi:10.1007/s11144-019-01719-1.

[95] A.J.R. Hensley, Y. Hong, R. Zhang, H. Zhang, J. Sun, Y. Wang, J.-S. McEwen, Enhanced Fe2O3 Reducibility via Surface Modification with Pd: Characterizing the Synergy within Pd/Fe Catalysts for Hydrodeoxygenation Reactions, ACS Catal. 4 (2014) 3381–3392. doi:10.1021/cs500565e.

[96] R. Burch, M.J. Hayes, The Preparation and Characterisation of Fe-Promoted Al2O3-Supported Rh Catalysts for the Selective Production of Ethanol from Syngas, J. Catal. 165 (1997) 249–261. doi:https://doi.org/10.1006/jcat.1997.1482.

[97] B. Gumina, F. Mauriello, R. Pietropaolo, S. Galvagno, C. Espro, Hydrogenolysis of sorbitol into valuable C3-C2 alcohols at low H2 pressure promoted by the heterogeneous Pd/Fe3O4 catalyst, Mol. Catal. 446 (2018) 152–160. doi:10.1016/j.mcat.2017.12.038.

[98] C.-T. Wu, K.M.K. Yu, F. Liao, N. Young, P. Nellist, A. Dent, A. Kroner, S.C.E. Tsang, A non-syn-gas catalytic route to methanol production, Nat. Commun. 3 (2012) 1050. doi:10.1038/ncomms2053.

[99] M.G. Musolino, C. Busacca, F. Mauriello, R. Pietropaolo, Aliphatic carbonyl reduction promoted by palladium catalysts under mild conditions, Appl. Catal. A Gen. 379 (2010) 77–86. doi:10.1016/j.apcata.2010.03.008.

[100] M.G. Musolino, L.A. Scarpino, F. Mauriello, R. Pietropaolo, Glycerol Hydrogenolysis Promoted by Supported Palladium Catalysts, ChemSusChem. 4 (2011) 1143–1150. doi:10.1002/cssc.201100063.

[101] T. Yamashita, P. Hayes, Analysis of XPS spectra of Fe2+ and Fe3+ ions in oxide materials, Appl. Surf. Sci. 254 (2008) 2441–2449. doi:https://doi.org/10.1016/j.apsusc.2007.09.063.

[102] M. Muhler, R. Schlögl, G. Ertl, The nature of the iron oxide-based catalyst for dehydrogenation of ethylbenzene to styrene 2. Surface chemistry of the active phase, J. Catal. 138 (1992) 413–444. doi:https://doi.org/10.1016/0021-9517(92)90295-S.

[103] K. Sun, W. Lu, M. Wang, X. Xu, Characterization and catalytic performances of La doped Pd/CeO2 catalysts for methanol decomposition, Appl. Catal. A Gen. 268 (2004) 107–113. doi:https://doi.org/10.1016/j.apcata.2004.03.020.

[104] D. Scholz, C. Aellig, I. Hermans, Catalytic Transfer Hydrogenation/Hydrogenolysis for Reductive Upgrading of Furfural and 5-(Hydroxymethyl)furfural, ChemSusChem. 7 (2014) 268–275. doi:10.1002/cssc.201300774.

[105] K. Noack, H. Zbinden, R. Schlogl, Identification of the state of palladium in various hydrogenation catalysts by XPS, Catal. Letters. 4 (1990) 145–156.

[106] S.L. Zhang, J.R. Zhang, Photoemission and Mossbauer-effect studies of sputter-deposited Fe-Pd alloys, Phys. Status Solidi B. 182 (1994) 42–427.

[107] A. Shukla, R.K. Singha, T. Sasaki, V.V.D.N. Prasad, R. Bal, Synthesis of Highly Active Pd Nanoparticles Supported Iron Oxide Catalyst for Selective Hydrogenation and Cross-Coupling Reactions in Aqueous Medium, ChemistrySelect. 4 (2019) 5019–5032. doi:10.1002/slct.201900358.

[108] H. Xie, Y. Li, S. Jin, J. Han, X. Zhao, Facile Fabrication of 3D-Ordered Macroporous Nanocrystalline Iron Oxide Films with Highly Efficient Visible Light Induced Photocatalytic Activity, J. Phys. Chem. C. 114 (2010) 9706–9712. doi:10.1021/jp102525y.

[109] S. Lian, E. Wang, Z. Kang, Y. Bai, L. Gao, M. Jiang, C. Hu, L. Xu, Synthesis of magnetite nanorods and porous hematite nanorods, Solid State Commun. 129 (2004) 485–490. doi:https://doi.org/10.1016/j.ssc.2003.11.043.

[110] X. Hu, J.C. Yu, Continuous Aspect-Ratio Tuning and Fine Shape Control of Monodisperse α-Fe2O3 Nanocrystals

by a Programmed Microwave–Hydrothermal Method, Adv. Funct. Mater. 18 (2008) 880–887. doi:10.1002/adfm.200700671.

[111] A.L. Cappelletti, P.M. Uberman, S.E. Martín, M.E. Saleta, H.E. Troiani, R.D. Sánchez, R.E. Carbonio, M.C. Strumia, Synthesis, Characterization, and Nanocatalysis Application of Core–Shell Superparamagnetic Nanoparticles of Fe3O4@Pd, Aust. J. Chem. 68 (2015) 1492–1501.

[112] R.Y. Hong, T.T. Pan, H.Z. Li, Microwave synthesis of magnetic Fe3O4 nanoparticles used as a precursor of nanocomposites and ferrofluids, J. Magn. Magn. Mater. 303 (2006) 60–68. doi:https://doi.org/10.1016/j.jmmm.2005.10.230.

[113] C. Biglione, A.L. Cappelletti, M.C. Strumia, S.E. Martín, P.M. Uberman, Magnetic Pd nanocatalyst Fe3O4@Pd for C–C bond formation and hydrogenation reactions, J. Nanoparticle Res. 20 (2018) 127. doi:10.1007/s11051-018-4233-3.

[114] B.-W. Zhu, T.-T. Lim, Catalytic Reduction of Chlorobenzenes with Pd/Fe Nanoparticles: Reactive Sites, Catalyst Stability, Particle Aging, and Regeneration, Environ. Sci. Technol. 41 (2007) 7523–7529. doi:10.1021/es0712625.

[115] D.W. Elliott, W. Zhang, Field Assessment of Nanoscale Bimetallic Particles for Groundwater Treatment, Environ. Sci. Technol. 35 (2001) 4922–4926. doi:10.1021/es0108584.

[116] B. Huang, T. Wang, Z. Yang, W. Qian, J. Long, G. Zeng, C. Lei, Iron-Based Bimetallic Nanocatalysts for Highly Selective Hydrogenation of Acetylene in N,N-Dimethylformamide at Room Temperature, ACS Sustain. Chem. Eng. 5 (2017) 1668–1674. doi:10.1021/acssuschemeng.6b02413.

[117] J.-H. Lee, Y. Roh, H.-G. Hur, Microbial production and characterization of superparamagnetic magnetite nanoparticles by Shewanella sp. HN-41, J. Microbiol. Biotechnol. 18 (2008) 1572–1577.

[118] N. Pino, S. Sitthisa, Q. Tan, T. Souza, D. López, D.E. Resasco, Structure, activity, and selectivity of bimetallic Pd-Fe/SiO2 and Pd-Fe/γ-Al2O3 catalysts for the conversion of furfural, J. Catal. 350 (2017) 30–40. doi:https://doi.org/10.1016/j.jcat.2017.03.016.

[119] M.P. Felicissimo, O.N. Martyanov, T. Risse, H.J. Freund, Characterization of a Pd-Fe bimetallic model catalyst, Surf. Sci. 601 (2007) 2105–2116.

[120] R.J. Farrauto, J.K. Lampert, M.C. Hobson, E.M. Waterman, Thermal decomposition and reformation of PdO catalysts; support effects, Appl. Catal. B Environ. 6 (1995) 263–270. doi:https://doi.org/10.1016/0926-3373(95)00015-1.

[121] A. Barrera, M. Viniegra, S. Fuentes, G. Díaz, The role of lanthana loading on the catalytic properties of Pd/Al2O3-La2O3 in the NO reduction with H2, Appl. Catal. B Environ. 56 (2005) 279–288. doi:https://doi.org/10.1016/j.apcatb.2004.09.015.

[122] V.D. Stytsenko, D.P. Mel'nikov, O.P. Tkachenko, E. V Savel'eva, A.P. Semenov, L.M. Kustov, Selective Hydrogenation of Acetylene and Physicochemical Properties of Pd–Fe/Al2O3 Bimetallic Catalysts, Russ. J. Phys. Chem. A. 92 (2018) 862–869. doi:10.1134/S0036024418050308.

[123] A.U. Nilekar, A. V Ruban, M. Mavrikakis, Surface segregation energies in low-index open surfaces of bimetallic transition metal alloys, Surf. Sci. 603 (2009) 91–96. doi:https://doi.org/10.1016/j.susc.2008.10.029.

[124] A.H. Rojas, L.G. Zendri, L. Lafuente, A. Ponzinibbio, V. Vetere, Synthesis of Potentially Bioactive Carbohydrate Derivatives by Chemoslective Hydrogenation with PdFe Catalyst, ChemistrySelect. 4 (2019) 14228–14232. doi:10.1002/slct.201903853.

[125] D. Wang, J. Liu, J. Xi, J. Jiang, Z. Bai, Pd-Fe dual-metal nanoparticles confined in the interface of carbon nanotubes/N-doped carbon for excellent catalytic performance, Appl. Surf. Sci. 489 (2019) 477–484. doi:https://doi.org/10.1016/j.apsusc.2019.06.039.

[126] M. Liao, Q. Hu, J. Zheng, Y. Li, H. Zhou, C.-J. Zhong, B.H. Chen, Pd decorated Fe/C nanocatalyst for formic acid electrooxidation, Electrochim. Acta. 111 (2013) 504–509. doi:https://doi.org/10.1016/j.electacta.2013.08.102.

[127] W. Zhang, W. Wu, Y. Long, J. Qin, F. Wang, J. Ma, Promoting Role of Iron Series Elements Modification on Palladium/Nitrogen Doped Carbon for the Semihydrogenation of Phenylacetylene, ChemCatChem. 11 (2019) 1510–1517. doi:10.1002/cctc.201801946.

[128] X. Chen, L. Zhang, B. Zhang, X. Guo, X. Mu, Highly selective hydrogenation of furfural to furfuryl alcohol over Pt nanoparticles supported on g-C3N4 nanosheets catalysts in water, Sci. Rep. (2016). doi:10.1038/srep28558.

[129] S. Kattel, B. Yan, J.G. Chen, P. Liu, CO2 hydrogenation on Pt, Pt/SiO2 and Pt/TiO2: Importance of synergy between Pt and oxide support, J. Catal. (2016). doi:10.1016/j.jcat.2015.12.019.

[130] A. Jouve, S. Cattaneo, D. Delgado, N. Scotti, C. Evangelisti, J.M. López Nieto, L. Prati, Furfural Hydrogenation on Modified Niobia, Appl. Sci. (2019) 2287.

[131] P.J.S. Prieto, A.P. Ferreira, P.S. Haddad, D. Zanchet, J.M.C. Bueno, Designing Pt nanoparticles supported on CeO2-Al 2O3: Synthesis, characterization and catalytic properties in the steam reforming and partial oxidation of methane, J. Catal. (2010). doi:10.1016/j.jcat.2010.09.025.

[132] X. Ning, H. Yu, F. Peng, H. Wang, Pt nanoparticles interacting with graphitic nitrogen of N-doped carbon nanotubes: Effect of electronic properties on activity for aerobic oxidation of glycerol and electro-oxidation of CO, J. Catal. (2015). doi:10.1016/j.jcat.2015.02.010.

[133] X. Liu, Z.D. Hood, Q. Zheng, T. Jin, G.S. Foo, Z. Wu, C. Tian, Y. Guo, S. Dai, W. Zhan, H. Zhu, M. Chi, Optimizing the structural configuration of FePt-FeOx nanoparticles at the atomic scale by tuning the post-synthetic conditions, Nano Energy. 55 (2019) 441–446. doi:https://doi.org/10.1016/j.nanoen.2018.10.066.

[134] B. Qiao, A. Wang, X. Yang, L.F. Allard, Z. Jiang, Y. Cui, J. Liu, J. Li, T. Zhang, Single-atom catalysis of CO oxidation using Pt1/FeOx, Nat. Chem. 3 (2011) 634–641. doi:10.1038/nchem.1095.

[135] M. de. C. Aguirre, P. Reyes, M. Oportus, I. Melián-Cabrera, J.L.G. Fierro, Liquid phase hydrogenation of crotonaldehyde over bimetallic Rh-Sn/SiO2 catalysts: Effect of the Sn/Rh ratio, Appl. Catal. A Gen. 233 (2002) 183–196. doi:https://doi.org/10.1016/S0926-860X(02)00141-2.

[136] K. Inomata, T. Sawa, S. Hashimoto, Effect of large boron additions to magnetically hard Fe-Pt alloys, J. Appl. Phys. 64 (1988) 2537–2540. doi:10.1063/1.341638.

[137] S. Sun, C.B. Murray, D. Weller, L. Folks, A. Moser, Monodisperse FePt Nanoparticles and Ferromagnetic FePt Nanocrystal Superlattices, Science. 287 (2000) 1989 LP – 1992. doi:10.1126/science.287.5460.1989.

[138] S. Okamoto, N. Kikuchi, O. Kitakami, T. Miyazaki, Y. Shimada, K. Fukamichi, Chemical-order-dependent magnetic anisotropy and exchange stiffness constant of FePt (001) epitaxial films, Phys. Rev. B. 66 (2002) 24413. doi:10.1103/PhysRevB.66.024413.

[139] T. Shima, K. Takanashi, Y.K. Takahashi, K. Hono, Coercivity exceeding 100kOe in epitaxially grown FePt sputtered films, Appl. Phys. Lett. 85 (2004) 2571–2573. doi:10.1063/1.1794863.

[140] S. Maenosono, S. Saita, Theoretical assessment of FePt nanoparticles as heating elements for magnetic hyperthermia, IEEE Trans. Magn. 42 (2006) 1638–1642. doi:10.1109/TMAG.2006.872198.

[141] H. Pan, J. Li, J. Lu, G. Wang, W. Xie, P. Wu, X. Li, Selective hydrogenation of cinnamaldehyde with PtFex/Al2O3@SBA-15 catalyst: Enhancement in activity and selectivity to unsaturated alcohol by Pt-FeOx and Pt-Al2O3@SBA-15 interaction, J. Catal. 354 (2017) 24–36. doi:https://doi.org/10.1016/j.jcat.2017.07.026.

[142] S. Kobayashi, S. Kaneko, M. Ohshima, H. Kurokawa, H. Miura, Effect of iron oxide on isobutane dehydrogenation over Pt/Fe2O3-Al2O3 catalyst, Appl. Catal. A Gen. 417–418 (2012) 306–312. doi:https://doi.org/10.1016/j.apcata.2012.01.007.

[143] S.-W. Chou, Y.-H. Shau, P.-C. Wu, Y.-S. Yang, D.-B. Shieh, C.-C. Chen, In Vitro and in Vivo Studies of FePt Nanoparticles for Dual Modal CT/MRI Molecular Imaging, J. Am. Chem. Soc. 132 (2010) 13270–13278. doi:10.1021/ja1035013.

[144] P. Reyes, C. Rodríguez, G. Pecchi, J.L.G. Fierro, Promoting effect of Mo on the selective hydrogenation of cinnamaldehyde on Rh/SiO2 catalysts, Catal. Letters. 69 (2000) 27–32. doi:10.1023/A:1019041100128.

[145] G. Neri, L. Mercadante, A. Donato, A.M. Visco, S. Galvagno, Influence of Ru precursor, support and solvent in the hydrogenation of citral over ruthenium catalysts, Catal. Letters. 29 (1994) 379–386. doi:10.1007/BF00807117.

[146] N. An, P. Wu, S. Li, M. Jia, W. Zhang, Catalytic oxidation of formaldehyde over Pt/Fe2O3 catalysts prepared by different method, Appl. Surf. Sci. 285 (2013) 805–809. doi:https://doi.org/10.1016/j.apsusc.2013.08.132.

[147] X. Jin, H. Yan, C. Zeng, P.S. Thapa, B. Subramaniam, R. V Chaudhari, Phase Transformed PtFe Nanocomposites Show Enhanced Catalytic Performances in Oxidation of Glycerol to Tartronic Acid, Ind. Eng. Chem. Res. 56 (2017) 13157–13164. doi:10.1021/acs.iecr.7b01473.

[148] C. Navas-Cárdenas, N. Benito, E.E. Wolf, F. Gracia, Effect of Pt-MOx (M = Fe, Co) interaction on the preferential oxidation of CO over Pt/MOx/TiO2 catalysts prepared by selective electrostatic adsorption, Appl. Catal. A Gen. 576 (2019) 11–19. doi:https://doi.org/10.1016/j.apcata.2019.02.030.

[149] V.R. Stamenkovic, B.S. Mun, M. Arenz, K.J.J. Mayrhofer, C.A. Lucas, G. Wang, P.N. Ross, N.M. Markovic, Trends in electrocatalysis on extended and nanoscale Pt-bimetallic alloy surfaces, Nat. Mater. 6 (2007) 241–247. doi:10.1038/nmat1840.

[150] A. Kirkeminde, S. Ren, Interdiffusion Induced Exchange Coupling of L10-FePd/α-Fe Magnetic Nanocomposites, Nano Lett. 14 (2014) 4493–4498. doi:10.1021/nl502167m.

[151] H.L. Nguyen, L.E.M. Howard, G.W. Stinton, S.R. Giblin, B.K. Tanner, I. Terry, A.K. Hughes, I.M. Ross, A. Serres, J.S.O. Evans, Synthesis of Size-Controlled fcc and fct FePt Nanoparticles, Chem. Mater. 18 (2006) 6414–6424. doi:10.1021/cm062127e.

[152] R.D. Rutledge, W.H. Morris, M.S. Wellons, Z. Gai, J. Shen, J. Bentley, J.E. Wittig, C.M. Lukehart, Formation of FePt Nanoparticles Having High Coercivity, J. Am. Chem. Soc. 128 (2006) 14210–14211. doi:10.1021/ja0633868.

[153] M. Podgórny, Electronic structure of the ordered phases of Pt-Fe alloys, Phys. Rev. B. 43 (1991) 11300–11318. doi:10.1103/PhysRevB.43.11300.

[154] Z. Ji, G. Zhu, X. Shen, H. Zhou, C. Wu, M. Wang, Reduced graphene oxide supported FePt alloy nanoparticles with high electrocatalytic performance for methanol oxidation, New J. Chem. 36 (2012) 1774–1780. doi:10.1039/C2NJ40133A.

[155] G.-Y. Fan, W.-J. Huang, Solvent-Free Hydrogenation of Nitrobenzene Catalyzed by Magnetically Recoverable Pt Deposited on Multiwalled Carbon Nanotubes, Synth. React. Inorganic, Met. Nano-Metal Chem. 45 (2015) 1819–1825. doi:10.1080/15533174.2013.872139.

[156] F. Hoxha, B. Schimmoeller, Z. Cakl, A. Urakawa, T. Mallat, S.E. Pratsinis, A. Baiker, Influence of support acid–base properties on the platinum-catalyzed enantioselective hydrogenation of activated ketones, J. Catal. 271 (2010) 115–124. doi:https://doi.org/10.1016/j.jcat.2010.02.012.

[157] K. Thomas, C. Binet, T. Chevreau, D. Cornet, J.-P. Gilson, Hydrogenation of Toluene over Supported Pt and Pd Catalysts: Influence of Structural Factors on the Sulfur Tolerance, J. Catal. 212 (2002) 63–75. doi:https://doi.org/10.1006/jcat.2002.3780.

[158] W. Rachmady, M.A. Vannice, Acetic acid hydrogenation over supported platinum catalysts, J. Catal. 192 (2000) 322–334. doi:https://doi.org/10.1006/jcat.2000.2863.

[159] C.-J. Jia, F. Schüth, Colloidal metal nanoparticles as a component of designed catalyst, Phys. Chem. Chem. Phys. 13 (2011) 2457–2487. doi:10.1039/c0cp02680h.

[160] N. An, Q. Yu, G. Liu, S. Li, M. Jia, W. Zhang, Complete oxidation of formaldehyde at ambient temperature over supported Pt/Fe2O3 catalysts prepared by colloid-deposition method, J. Hazard. Mater. 186 (2011) 1392–1397. doi:https://doi.org/10.1016/j.jhazmat.2010.12.018.

[161] F.-W. Chang, L.S. Roselin, T.-C. Ou, Hydrogen production by partial oxidation of methanol over bimetallic Au–Ru/Fe2O3 catalysts, Appl. Catal. A Gen. 334 (2008) 147–155. doi:https://doi.org/10.1016/j.apcata.2007.10.003.

[162] N. An, S. Li, P.N. Duchesne, P. Wu, W. Zhang, J.-F. Lee, S. Cheng, P. Zhang, M. Jia, W. Zhang, Size Effects of Platinum Colloid Particles on the Structure and CO Oxidation Properties of Supported Pt/Fe2O3 Catalysts, J. Phys. Chem. C. 117 (2013) 21254–21262. doi:10.1021/jp404266p.

[163] Y. Fang, H. Xiao, N. Sui, M. Liu, W.W. Yu, Hydrogenation of o-chloronitrobenzene to o-chloroaniline over a Pt/γ-Fe2O3 catalyst under ambient conditions, RSC Adv. 4 (2014) 11788–11793. doi:10.1039/C4RA00657G.

[164] X. Wang, M. Liang, H. Liu, Y. Wang, Selective hydrogenation of bromonitrobenzenes over Pt/γ-Fe2O3, J. Mol. Catal. A Chem. 273 (2007) 160–168. doi:https://doi.org/10.1016/j.molcata.2007.04.004.

[165] Y. Wang, J. Ren, K. Deng, L. Gui, Y. Tang, Preparation of Tractable Platinum, Rhodium, and Ruthenium Nanoclusters with Small Particle Size in Organic Media, Chem. Mater. 12 (2000) 1622–1627. doi:10.1021/cm0000853.

[166] S. Neumann, H.H. Doebler, S. Keil, A.J. Erdt, C. Gutsche, H. Borchert, J. Kolny-Olesiak, J. Parisi, M. Bäumer, S. Kunz, Effects of Particle Size on Strong Metal–Support Interactions Using Colloidal "Surfactant-Free" Pt Nanoparticles Supported on Fe3O4, ACS Catal. 10 (2020) 4136–4150. doi:10.1021/acscatal.9b04367.

[167] C. Lian, H. Liu, C. Xiao, W. Yang, K. Zhang, Y. Liu, Y. Wang, Solvent-free selective hydrogenation of chloronitrobenzene to chloroaniline over a robust Pt/Fe3O4 catalyst, Chem. Commun. 48 (2012) 3124–3126. doi:10.1039/C2CC16620H.

[168] W. Chen, Y. Ma, F. Li, L. Pan, W. Gao, Q. Xiang, W. Shang, C. Song, P. Tao, H. Zhu, X. Pan, T. Deng, J. Wu, Strong Electronic Interaction of Amorphous Fe2O3 Nanosheets with Single-Atom Pt toward Enhanced Carbon Monoxide Oxidation, Adv. Funct. Mater. 29 (2019) 1904278. doi:10.1002/adfm.201904278.

[169] Z. Zhang, Y. Zhu, H. Asakura, B. Zhang, J. Zhang, M. Zhou, Y. Han, T. Tanaka, A. Wang, T. Zhang, N. Yan, Thermally stable single atom Pt/m-Al2O3 for selective hydrogenation and CO oxidation, Nat. Commun. 8 (2017) 16100. doi:10.1038/ncomms16100.

[170] Y. Liu, J. Chung, Y. Jang, S. Mao, B.M. Kim, Y. Wang, X. Guo, Magnetically Recoverable Nanoflake-Shaped Iron Oxide/Pt Heterogeneous Catalysts and Their Excellent Catalytic Performance in the Hydrogenation Reaction, ACS Appl. Mater. Interfaces. 6 (2014) 1887–1892. doi:10.1021/am404904p.

[171] P. Zhang, X. Yang, H. Peng, D. Liu, H. Lu, J. Wei, J. Gui, Magnetically recoverable hierarchical Pt/Fe2O3 microflower: Superior catalytic activity and stability for reduction of 4-nitrophenol, Catal. Commun. 100 (2017) 214–218. doi:https://doi.org/10.1016/j.catcom.2017.06.047.

[172] H. Hong, L. Hu, M. Li, J. Zheng, X. Sun, X. Lu, X. Cao, J. Lu, H. Gu, Preparation of Pt@Fe2O3 Nanowires and their Catalysis of Selective Oxidation of Olefins and Alcohols, Chem. – A Eur. J. 17 (2011) 8726–8730. doi:10.1002/chem.201003429.

[173] Q. Li, X. Zhou, W. Zhao, C. Peng, H. Wu, H. Chen, Pt/Fe co-loaded mesoporous zeolite beta for CO oxidation with high catalytic activity and water resistance, RSC Adv. 9 (2019) 28089–28094. doi:10.1039/C9RA04599F.

[174] S. Capelli, D. Motta, C. Evangelisti, N. Dimitratos, L. Prati, C. Pirola, A. Villa, Effect of Carbon Support, Capping Agent Amount, and Pd NPs Size for Bio-Adipic Acid Production from Muconic Acid and Sodium Muconate, Nanomaterials. 10 (2020) 505. doi:10.3390/nano10030505.

[175] Y. Zhang, S. Wei, Y. Lin, G. Fan, F. Li, Dispersing Metallic Platinum on Green Rust Enables Effective and Selective Hydrogenation of Carbonyl Group in Cinnamaldehyde, ACS Omega. 3 (2018) 12778–12787. doi:10.1021/acsomega.8b02114.

[176] H. Wei, Y. Ren, A. Wang, X. Liu, X. Liu, L. Zhang, S. Miao, L. Li, J. Liu, J. Wang, G. Wang, D. Su, T. Zhang, Remarkable effect of alkalis on the chemoselective hydrogenation of functionalized nitroarenes over high-loading Pt/FeOx catalysts, Chem. Sci. 8 (2017) 5126–5131. doi:10.1039/C7SC00568G.

[177] C. Evangelisti, L.A. Aronica, M. Botavina, G. Martra, C. Battocchio, G. Polzonetti, Chemoselective hydrogenation of halonitroaromatics over γ-Fe2O3-supported platinum nanoparticles: The role of the support on their catalytic activity and selectivity, J. Mol. Catal. A Chem. 366 (2013) 288–293. doi:https://doi.org/10.1016/j.molcata.2012.10.007.

[178] C. Zhou, W. Shi, X. Wan, Y. Meng, Y. Yao, Z. Guo, Y. Dai, C. Wang, Y. Yang, Oxidation of 5-hydroxymethylfurfural over a magnetic iron oxide decorated rGO supporting Pt nanocatalyst, Catal. Today. 330 (2019) 92–100. doi:https://doi.org/10.1016/j.cattod.2018.05.037.

[179] Y. Zhang, C. Chen, W. Gong, J. Song, Y. Su, H. Zhang, G. Wang, H. Zhao, One-pot redox synthesis of Pt/Fe3O4 catalyst for efficiently chemoselective hydrogenation of cinnamaldehyde, RSC Adv. 7 (2017) 21107–21113. doi:10.1039/C7RA02898A.

[180] S. Huang, K. Hara, A. Fukuoka, Green catalysis for selective CO oxidation in hydrogen for fuel cell, Energy Environ. Sci. 2 (2009) 1060–1068. doi:10.1039/B910696K.

[181] G. Saravanan, K.P. Jayasree, Y. Divya, M. Pallavi, L. Nitin, Ordered intermetallic Pt-Fe nano-catalysts for carbon

monoxide and benzene oxidation, Intermetallics. 94 (2018) 179–185. doi:https://doi.org/10.1016/j.intermet.2018.01.008.

[182] Q. Hu, S. Wang, Z. Gao, Y. Li, Q. Zhang, Q. Xiang, Y. Qin, The precise decoration of Pt nanoparticles with Fe oxide by atomic layer deposition for the selective hydrogenation of cinnamaldehyde, Appl. Catal. B Environ. 218 (2017) 591–599. doi:https://doi.org/10.1016/j.apcatb.2017.06.087.

[183] G. Wang, H. Xin, Q. Wang, P. Wu, X. Li, Efficient liquid-phase hydrogenation of cinnamaldehyde to cinnamyl alcohol with a robust PtFe/HPZSM-5 catalyst, J. Catal. 382 (2020) 1–12. doi:https://doi.org/10.1016/j.jcat.2019.12.004.

[184] B. Gil, Ł. Mokrzycki, B. Sulikowski, Z. Olejniczak, S. Walas, Desilication of ZSM-5 and ZSM-12 zeolites: Impact on textural, acidic and catalytic properties, Catal. Today. 152 (2010) 24–32. doi:https://doi.org/10.1016/j.cattod.2010.01.059.

[185] H. Chen, D. He, Q. He, P. Jiang, G. Zhou, W. Fu, Selective hydrogenation of p-chloronitrobenzene over an Fe promoted Pt/AC catalyst, RSC Adv. 7 (2017) 29143–29148. doi:10.1039/C7RA04700B.

[186] L. Liu, H. Lou, M. Chen, Selective hydrogenation of furfural over Pt based and Pd based bimetallic catalysts supported on modified multiwalled carbon nanotubes (MWNT), Appl. Catal. A Gen. 550 (2018) 1–10. doi:10.1016/j.apcata.2017.10.003.

[187] A. Davydov Alexandrovitch., N. Sheppard, Molecular spectroscopy of oxide catalyst surfaces, J. Wiley, Chichester (Grande-Bretagne), 2003.

[188] W. Cui, X. Yuan, P. Wu, B. Zheng, W. Zhang, M. Jia, Catalytic properties of γ-Al2O3 supported Pt–FeOx catalysts for complete oxidation of formaldehyde at ambient temperature, RSC Adv. 5 (2015) 104330–104336. doi:10.1039/C5RA19151C.

[189] L. Gan, R. Yu, J. Luo, Z. Cheng, J. Zhu, Lattice Strain Distributions in Individual Dealloyed Pt–Fe Catalyst Nanoparticles, J. Phys. Chem. Lett. 3 (2012) 934–938. doi:10.1021/jz300192b.

[190] A.L. Walter, F. Schiller, M. Corso, L.R. Merte, F. Bertram, J. Lobo-Checa, M. Shipilin, J. Gustafson, E. Lundgren, A.N.X. Bribón-Ríos, P. Cabrera-Sanfelix, D. Sánchez-Portal, J.E. Ortega, X-ray photoemission analysis of clean and carbon monoxide-chemisorbed platinum(111) stepped surfaces using a curved crystal, Nat. Commun. 6 (2015) 8903. doi:10.1038/ncomms9903.

[191] H. Shi, X. Yin, B. Subramaniam, R. V. Chaudhari, Liquid-Phase Oxidation of Ethylene Glycol on Pt and Pt-Fe Catalysts for the Production of Glycolic Acid: Remarkable Bimetallic Effect and Reaction Mechanism, Ind. Eng. Chem. Res. 58 (2019) 18561–18568. doi:10.1021/acs.iecr.9b03419.

[192] M. Zhang, B.L. Cushing, C.J. O'Connor, Synthesis and characterization of monodisperse ultra-thin silica-coated magnetic nanoparticles, Nanotechnology. 19 (2008) 85601. doi:10.1088/0957-4484/19/8/085601.

[193] D.C. Lee, F. V Mikulec, J.M. Pelaez, B. Koo, B.A. Korgel, Synthesis and Magnetic Properties of Silica-Coated FePt Nanocrystals, J. Phys. Chem. B. 110 (2006) 11160–11166. doi:10.1021/jp060974z.

[194] I. Ro, I.B. Aragao, J.P. Chada, Y. Liu, K.R. Rivera-Dones, M.R. Ball, D. Zanchet, J.A. Dumesic, G.W. Huber, The role of Pt-FexOy interfacial sites for CO oxidation, J. Catal. 358 (2018) 19–26. doi:https://doi.org/10.1016/j.jcat.2017.11.021.

[195] I. Ro, I.B. Aragao, Z.J. Brentzel, Y. Liu, K.R. Rivera-Dones, M.R. Ball, D. Zanchet, G.W. Huber, J.A. Dumesic, Intrinsic activity of interfacial sites for Pt-Fe and Pt-Mo catalysts in the hydrogenation of carbonyl groups, Appl. Catal. B Environ. 231 (2018) 182–190. doi:https://doi.org/10.1016/j.apcatb.2018.02.058.

[196] Y. Lou, J. Liu, A highly active Pt–Fe/γ-Al2O3 catalyst for preferential oxidation of CO in excess of H2 with a wide operation temperature window, Chem. Commun. 53 (2017) 9020–9023. doi:10.1039/C7CC03787B.

[197] Y.-S. Shi, Z.-F. Yuan, Q. Wei, K.-Q. Sun, B.-Q. Xu, Pt–FeOx/SiO2 catalysts prepared by galvanic displacement show high selectivity for cinnamyl alcohol production in the chemoselective hydrogenation of cinnamaldehyde, Catal. Sci. Technol. 6 (2016) 7033–7037. doi:10.1039/C6CY01340F.

[198] F. Li, J. Liang, K. Wang, B. Cao, H. Song, Fe-Promoted Pt-Fe/Al2O3 Catalyst Prepared by Microemulsion Technique for m-Chloronitrobenzene Hydrogenation, Russ. J. Phys. Chem. A. 92 (2018) 1279–1284.

doi:10.1134/S0036024418070117.